A Genetic Algorithm Matched Filtered Optimization for Blood Vessels Detection of Digital Retinal Images

By

Huda Abdel-Rahim Karajeh

Supervisor

Dr. Mohammed Al-Rawi

This Thesis is Submitted in Partial Fulfillment of the Requirements for the Master's Degree of Science in Computer Science

Faculty of Graduate Studies

The University of Jordan

May, 2006

All Rights Reserved - Library of University of Jordan - Center of Thesis Deposit

المنارة للاستشارات

www.manaraa.com

i

This Thesis/Dissertation (A Genetic Algorithm Matched Filtered Optimization for Blood Vessels Detection of Digital Retinal Images) was successfully defended and approved on 18-5-2006:

Examination Committee:	**Signature**
Dr. Mohammed Al-Rawi, Supervisor Assistant Prof. in Intelligence Systems and Pattern Recognition	----------
Dr. Ahmad Sharieh, Member Associate Prof. in Parallel Processing	----------
Dr. Amjad Hudaib, Member Assistant Prof. in Software Engineering	----------
Dr. Abdellatif Abu-dalhoum, Member Assistant Prof. in Genetic Algorithms and Complex Systems	----------
Dr. Hussein Al-Omari, External Associate Prof. in Electrical and Computer Engineering (Applied Science University)	----------

تعتمد كلية الدراسات العليا
هذه النسخة من الرسالة
التوقيع.....التاريخ.....

All Rights Reserved - Library of University of Jordan - Center of Thesis Deposit

المنارة للاستشارات
www.manaraa.com

DEDICATION

- I dedicate my work to my great parents, to all my brothers and sisters especially, Dr. Mohammed, Dr. Mahmoud, Nuha and Ola for their love, inspiration, patience, and support through the development of my thesis.
- To my special Friends Hutaf, Safa'a, Hama, Doa'a, and Samar.

All Rights Reserved - Library of University of Jordan - Center of Thesis Deposit

المنارة للاستشارات
www.manaraa.com

ACKNOWLEDGEMENT

Firstly, all thanks for Allah who gave me the ability to finish this work successfully. Then, I would like to thank my supervisor, Dr. Mohammed Al-Rawi, for giving me the guidance and motivation that was needed to lead me in the correct direction and a special thank to A. Hoover and J. Staal for making their databases publicly available.

All Rights Reserved - Library of University of Jordan - Center of Thesis Deposit

www.manaraa.com

TABLE OF CONTENTS

Committee Decision……...i

Dedication……ii

Acknowledgment……iii

Table of Contents……iv

List of Tables ……..vii

List of Figures……...x

List of Abbreviations and Symbols..……xiii

List of Algorithms……xiv

Abstract……..xv

INDRODUCTION 1

1. Problem Overview……...2
2. System Structure……..3
3. System Objectives……5

LITERATURE REVIEW 7

1. Detection of Retinal Vessels……8
   1.1. Extraction of the Vessel Edges……..8
   1.2. Extraction of the core of vessels……9
2. Two Dimensional Gaussian Matched Filter (GMF)……10
3. Amplitude-Modified Second Order Gaussian Matched Filter……..11
4. Retina Detection Systems……11
5. Genetic Algorithms ……20

All Rights Reserved - Library of University of Jordan - Center of Thesis Deposit

المنارة للاستشارات

www.manaraa.com

THEORY AND IMPLEMENTATION 22

1. Gaussian Matched Filter (GMF)……23

1.1. Design & Implementation of GMF……..23

1.2. Detection of Blood Vessels using GMF……..27

1.2.1. Preprocessing Stage……..28

1.2.2. Vessel Segmentation……28

1.2.3. Post Processing Stage……28

2. Amplitude Modified Second Order GMF……28

3. Genetic Algorithms……...31

3.1. Objective Function……..32

3.2. Population diversity……32

3.3. Population Size……32

3.4. Encoding……..32

3.5. Elitism……33

3.6. Selection……33

3.7. Crossover……34

3.8. Mutation……37

4. Optimization of the Matched Filter by using Genetic Algorithms……..38

4.1. Implementation of the Optimized Matched Filter……53

5. Optimization of the Second Order GMF using Genetic Algorithms……57

5.1. Implementation of the Optimized Second Order GMF……58

DISCUSSION AND ANALYSIS OF RESULTS 59

1. Materials……..60

All Rights Reserved - Library of University of Jordan - Center of Thesis Deposit

www.manaraa.com

2. Hardware and Software…….....61

3. Experimental Results……..61

4. Result of the GAMF Optimization ……63

5. Results of the Second Order GMF Optimization……88

6. A Comparison with Other Detection Techniques……91

CONCLUSIONS AND FUTURE WORKS 98

1. Conclusions…… 99

2. Future Works……..100

REFERENCES 102

APPENDIX A 107

APPENDIX B 121

APPENDIX C 129

Abstract in Arabic……137

All Rights Reserved - Library of University of Jordan - Center of Thesis Deposit

www.manaraa.com

LIST OF TABLES

Table No	Table Caption	Page
1	The new proposed filter parameters for the GMF that found by Genetic Algorithm	63
2	True and false ratio for the first image using Filter 1	64
3	Comparison of GAMF filters with the GMF and OGMF filters on a test set of the DRIVE database.	67
4	Area under the ROC and the MAA for the 40 image in the DRIVE database	67
5	Area under the ROC and the MAA for the Hoover database	68
6	The area under the ROC for the 20 image in the test set of the DRIVE database using Filter 6 via different degree of rotations.	73
7	The area under the ROC for the 20 image in the test set of the DRIVE database using Filter 3 via different degree of rotations.	74
8	The MA for the 20 image in the test set of the DRIVE database using Filter 6 via different degree of rotations.	75
9	Average area under the ROC for the 20 retinal images of the DRIVE under different bands using Filter 6	82
10	Average area under the ROC for filters that result from genetic algorithm experiments on a Red and Blue band on a test set of the DRIVE database	82
11	Differences in the average area under the ROC and MAAs that result from smoothing the green band for the test set of the DRIVE database.	83
12	Determining the average threshold of the matched filter with Filter 6 for the test set of the DRIVE database.	84
13	The difference in MAA between thresholding at the optimum threshold and thresholding at the average threshld.	85
14	The new proposed filter parameters for the second order GMF that	88

All Rights Reserved - Library of University of Jordan - Center of Thesis Deposit

www.manaraa.com

	found by Genetic Algorithm	
15	are σ New parameters for $\{L, T\}$ while t = 3. 5 and the values of $\{0.5, 1, 1.5, 2.5\}$ for the second order GMF on the test set of the DRIVE database.	**90**
16	Comparison of different methods with the improved matched filter and its second order derivative using 20 images in the test set of the DRIVE database.	**93**
17	Comparison of GAMF filters with the GMF and OGMF filters on a test set of the DRIVE database (JPEG images).	**109**
18	Area under the ROC and the MAA for the 40 image in the DRIVE database (JPEG images).	**109**
19	The area under the ROC for the 20 image in the test set of the DRIVE database (JPEG images) using Filter 6 via different degree of rotations.	**110**
20	The area under the ROC for the 20 image in the test set of the DRIVE database (JPEG images) using Filter 3 via different degree of rotations.	**111**
21	The MA for the 20 image in the test set of the DRIVE database (JPEG images) using Filter 6 via different degree of rotations.	**112**
22	Average area under the ROC for the 20 retinal images of the DRIVE (JPEG images) under different bands using Filter 6.	**116**
23	Average area under the ROC for filters that result from genetic algorithm experiments on a Red and Blue band on a test set of the DRIVE database (JPEG images).	**116**
24	Differences in the average area under the ROC and MAAs that result from smoothing the green band for the test set of the DRIVE database (JPEG images).	**116**
25	Determining the average threshold of the matched filter with Filter 6 for the test set of the DRIVE database (JPEG images).	**117**
26	The difference in MAA between thresholding at the best threshold and	**118**

All Rights Reserved - Library of University of Jordan - Center of Thesis Deposit

www.manaraa.com

	thresholding at the average threshold.	
27	The new proposed filter parameters for the second order GMF that found by Genetic Algorithm using JPEG images.	**119**
28	are σ New parameters for $\{L, T\}$ while t = 3. 5 and the values of $\{0.5, 1, 1.5, 2.5\}$ for the second order GMF on the test set of the DRIVE database (JPEG images).	**120**

All Rights Reserved - Library of University of Jordan - Center of Thesis Deposit

www.manaraa.com

LIST OF FIGURES

Figure Number	Figure Captions	Page
1	The green band of a digital retinal image and a cross section profile at a row number 110 of the retinal image.	24
2	The segmental image from the green band of the original image in Figure 1 that obtain the small vessels and a cross section profile at the row number 25 of the segmental image.	25
3	Block diagram to calculate the fitness function for one individual of the population	44
4	Block diagram for genetic algorithm to find the best matched filter parameters	46
5	Block Diagram for the GAMF optimization	56
6	The ROC area for the first image in the DRIVE database using Filter 1 under20 thresholds	65
7	The ROC area for the first image in the DRIVE database using Filter 1 under 1000 thresholds	65
8	Average ROC area for 20 images in the test set of the DRIVE database using Filter 1	66
9	The matched output image using Filter 1 and the corresponding thresholded image at the best threshold for the 7^{th} image in Hoover database	68
10	Two kernels produced from Filter 1 at zero and 60 degree of rotations.	69
11	Two kernels produced from Filter4 at 45 and 90 degree of rotations.	70
12	A 3-D graph for the kernels produced from Filter 1 at zero and 60 degrees of rotation which shown in Figure 10	71
13	The average area under the ROC for the 20 retinal images of the DRIVE database under different rotations using Filter 6.	76
14	The average area under the ROC for the 20 retinal images of the DRIVE	77

All Rights Reserved - Library of University of Jordan - Center of Thesis Deposit

www.manaraa.com

	database under different rotations using Filter 3.	
15	The results of applying the optimized GMF with Filter 6 under different degree of rotations and Filter 7 with the corresponding thresholded images at the best threshold for the first image in the DRIVE database.	**78-80**
16	The Difference between thresholding the matched output images at the optimum threshold and at the average threshold (0.2575) of the Filter 1 for the first five images in the DRIVE database.	**86-87**
17	Average ROC area for 20 images in the test set of the DRIVE database using Filter 10.	**89**
18	Result of applying the optimized second order GMF using Filter 10 and the corresponding thresholded image at the best threshold.	**89**
19	Average area under the ROC for 20 images in the test set of the DRIVE database for nine different methods.	**92**
20	The output image from different segmentation methods and the corresponding thresholded ones .	**94-96**
21	The ROC area for the first image in the DRIVE database that has JPEG extension using Filter 1 under 1000 thresholds	**108**
22	Average ROC area for 20 JPEG images in the test set of the DRIVE database using Filter 1.	**108**
23	The results of applying the optimized GMF with Filter 6 under different degree of rotations and Filter 7 with the corresponding thresholded images at the best threshold for the first image in the DRIVE database (JPEG).	**113-115**
24	Average ROC area for 20 images in the test set of the DRIVE database (JPEG images) using Filter 10.	**119**
25	Result of applying the optimized second order GMF using Filter 10 and the corresponding thresholded image at the best threshold.	**120**
26	The 20 original images in the test set of the DRIVE database	**122**
27	The hand labeled images the segmented images using GMF, OGMF, and GAMF(Filter 1) where each image is thresholded at the best threshold for the test set of the DRIVE database.	**123-126**

All Rights Reserved - Library of University of Jordan - Center of Thesis Deposit

www.manaraa.com

28	The segmented images by GAMF(Filter 6) at the best thresholds, and at the best average threshold (0.315) for the test set of the DRIVE database.	**127-128**
29	The 20 original images in the Hoover database.	**130**
30	The hand labeled images and the segmented images using GMF, OGMF, and GAMF(Filter 1) where each image is thresholded at the best threshold for the 20 image in the Hoover database.	**131-134**
31	The segmented images by GAMF(Filter 6) at the best thresholds, and at the best average threshold (0.4125) for the Hoover database.	**135-136**

All Rights Reserved - Library of University of Jordan - Center of Thesis Deposit

www.manaraa.com

LIST OF ABBREVIAVIONS AND SYMBOLS

Abbreviation	Meaning
DRIVE	Digital Retinal Images for Vessel Extraction
Hoover	Hoover Database
FOV	Field Of View
MAA	Maximum Average Accuracy
GMF	Gaussian Matched Filter
OGMF	Optimized Gaussian Matched Filter
ROC	Receiver Operating Curve
GAMF	Genetic Algorithm Matched Filter
STARE	Structured Analysis of the Retina
NOK	Number of Kernels
L	Length of the blood vessels segment
σ	The spread of the intensity profile
T	The position where the Gaussian curve trails will cut

All Rights Reserved - Library of University of Jordan - Center of Thesis Deposit

www.manaraa.com

LIST OF ALGORITHMS

Algorithm Number	Algorithm Title	Page
1	The basic steps for the genetic algorithms	38
2	The general steps of GAMF procedure	47
3	The steps to construct 12 kernels for GAMF	48
4	The image-filter procedure	49
5	The steps required to evaluate the fitness function for one individual from the population.	50
6	The steps needed to evaluate an area under the ROC	51
7	The steps required to calculate the MA to different thresholded images	52
8	The steps required to calculate the accuracy for one image	53
9	The steps required after finding the best parameter by genetic algorithm	57

All Rights Reserved - Library of University of Jordan - Center of Thesis Deposit

www.manaraa.com

A Genetic Algorithm Matched Filtered Optimization for Blood Vessels Detection of Digital Retinal Images

By

Huda Abdel-Rahim Karajeh

Supervisor

Dr. Mohammed Al-Rawi

ABSTRACT

Automated diagnoses for retinal images have become an important and necessary procedure in the ophthalmology. There are large efforts and researches to automate this process. Retinal blood vessels segmentation is considered an initial and important task for diagnoses of retinal images. Thus, a reliable method of vessel detection that preserves appropriate measurements of the blood vessels is needed. Many techniques have evolved for detection of blood vessels from retinal images. Two-dimensional Gaussian Matched Filter (GMF) is the most widely used technique for this purpose and has been deployed by many systems. Therefore, improving its response is highly desirable. Second order derivative of the GMF is also used for detection of the blood vessels. The GMF and its

All Rights Reserved - Library of University of Jordan - Center of Thesis Deposit

www.manaraa.com

second order derivative may vary in many ways depending on parameters governing its response.

In this thesis, an optimization system for the GMF and its second order derivative are proposed for the purpose of increasing the detection rate to blood vessels. This optimization is achieved by proposing better filter parameters. This is carried out using genetic algorithm, since its form an effective solution for optimization problems and it depends on a natural selection through a large search space. The area under the Receiver Operating Curve (ROC) and the Maximum Accuracy (MA) are used as fitness functions for the genetic algorithms. Also they are considered as an evaluation measures for the enhanced matched filter, where only the first image from the DRIVE database are used as input to genetic algorithms. Then, the enhanced matched filter and its second order derivative are tested on the two publicly available databases: DRIVE and Hoover databases. The evaluation measures are calculated on all the test images in DRIVE database, which achieves an average area under the ROC of 0.9609 and the Maximum Average Accuracy (MAA) of 0.943.

In conclusion, the results are superior to the previous described parameters. Also it is comparable to the other existing described techniques for automated vessels detection, even to those requires many steps and complex algorithms in contrast to the matched filter. Since till now no one automated segmentation technique could achieve accurate results as those of the manual one, room is still open for further improvements. So, we recommend further modification to the matched filter to detect smaller vessels.

All Rights Reserved - Library of University of Jordan - Center of Thesis Deposit

www.manaraa.com

Introduction

All Rights Reserved - Library of University of Jordan - Center of Thesis Deposit

www.manaraa.com

Introduction

1. Problem Overview

Automated Diagnosis for retinal images have become an important and necessary procedure in ophthalmology and there are large efforts and researches to automat this process. Pathological changes in the retinal blood vessels can lead to many forms of blindness, in particular, diabetic retinopathy (Banumathi et al., 2003), (Hoover et al., 2000), and (Zhou et al., 1994). These pathological processes cause characteristic changes in the color and shape of retinal vessels, such as narrowing or widening of some vessels, growth of new vessels, or developing irregular edges. For example, arteriosclerosis can cause the blood vessels to acquire a copper or silver color, diabetes can generate new blood vessels, hypertension may result in focal constriction of retinal arteries, and central retinal artery occlusion usually causes generalized constriction of retinal arteries while central vein occlusion typically produces dilated tortuous veins.

In general, retinal complication of some diseases (e.g. diabetes) can't be prevented but can be moderated if early intercepted after periodic screening of retinal images to detect the early signs of such diseases (Singer et al., 1992). Due to the large number of patients undergoing regular screening, and of the vessels in the image to be screened, physicians, with a manual segmentation of the blood vessels, have a hard and repetitive work to analyze and diagnose these images. This is time and cost-inefficient resulting in unreliable task. Because such segmentation is considered an

All Rights Reserved - Library of University of Jordan - Center of Thesis Deposit

www.manaraa.com

initial and important task for diagnoses of such a huge number of retinal images, automating this procedure (taking digital retinal images by a special camera and let the computer analyze and diagnose it) will reduce these efforts and be time and cost-saving.

Because retinal vasculature are considered the most stable structure appearing in the retinal images, the vascular tree represent the most appropriate measurement for the many applications (Zana and Klien, 1999). The position, size, and shape of the vasculature provides information which can be used to locate the optic disk and fovea (Hoover et al., 2003). Another important application is detecting and revealing the status of a number of eye lesions. Finally, the vascular tree is used in image registration via monitoring the progression of such lesions by investigating serial images (Zana and Klien, 1999) and (Goatman et al., 2003). Thus, a reliable method of vessel detection that preserves appropriate measurements of the retinal blood vessels is needed.

2. System Structure

Improvements on the response of the Two-dimensional Gaussian Matched Filter (GMF) and on its second order derivative are proposed in this thesis. The GMF forms a basis of many detection techniques that exist in the literature and improving its response is highly desirable. So, by this we will improve the response of all other detection techniques that use it. The effectiveness of the GMF in highlighting the low contrast and

All Rights Reserved - Library of University of Jordan - Center of Thesis Deposit

www.manaraa.com

narrow vessels and producing a complete and continuous map of blood vessels motivate us to improve the response of the GMF.

Based on the optical and spatial properties of objects to be recognized, two dimensional GMF is used (Chaudhuri et al., 1989). The idea of the GMF can be briefly described by the following steps: Firstly, a number of samples for a cross section of the blood vessels of the retina are taken, and the grey level profiles of these samples are approximated by a Gaussian shaped curve. Then, from this approximation an equation for filter coefficients is built. After that, a set of twelve kernels are derived from this equation and applied to the image for all twelve directions. Finally, the corresponding responses from all kernels are compared, and for each pixel only the maximum response of the convolution process is to be retained.

The GMF has some parameters governing its response and the values of these parameters have been proposed by (Chaudhuri et al., 1989). By second order derivative of GMF, (Gang et al., 2002) have added an additional valued parameter that helped to control the width of the blood vessel diameter. Many detection methods use the GMF with its old parameters. Because these parameters are found by empirical measurements (Chaudhuri et al., 1989), we believe that these parameters are not the optimum. So, in this thesis the genetic algorithms are used for optimization of the parameters used by (Chaudhuri et al., 1989) and (Gang et al., 2002) and subsequently enhance its performance. The area under the Receiver Operating Curve (ROC) is used as a fitness

All Rights Reserved - Library of University of Jordan - Center of Thesis Deposit

www.manaraa.com

function for genetic algorithms by comparing each edge-detected image to a referenced hand labeled-image to judge filter parameters.

Many authors (Chaudhuri et al., 1989) and (Banumathi et al., 2003) found that rotating the GMF by an amount of 15˚ is adequate to detect vessels with an acceptable amount of accuracy (which result of 12 kernels in a different orientations). So, experiments in this thesis are done on different amounts of rotation via genetic algorithms to find the best degree that enables the detection of vessels in all directions over 180˚ and subsequently maximizing the accuracy.

The optimized GMF and its second order derivative are tested on the DRIVE and Hoover databases which consist of 40 and 20 images respectively; for comparison purposes with other detection algorithms that use the same databases.

3. System Objectives

This study is conducted to satisfy number of objectives which are:

- Improving the response of the GMF and its second order derivative, by proposing new filter parameters.
- Use genetic algorithms to find these parameters.
- Verifying that rotating the GMF by an amount of 15˚ is the best or not. If not, what is the best.
- Comparing the optimized GMF with the original GMF (Chaudhuri et al., 1989) and other detection algorithms which implemented in the literature.

All Rights Reserved - Library of University of Jordan - Center of Thesis Deposit

www.manaraa.com

This thesis is organized as follows. A problem overview, the structure of the optimized system, and the objectives from this system are introduced in this chapter. In the next chapter, we will present the other existing methods in the literature for the blood vessel segmentation. The description of the GMF and the implementation of the optimized system using the genetic algorithms will be illustrated in the theory and implementation chapter. Experiments and the analysis of the results for the optimized systems are given in the discussion and analysis of results chapter, and the thesis is concluded in the conclusions and future work chapter.

All Rights Reserved - Library of University of Jordan - Center of Thesis Deposit

www.manaraa.com

LITERATURE REVIEW

All Rights Reserved - Library of University of Jordan - Center of Thesis Deposit

www.manaraa.com

Literature Review

Edge detection plays an important role in a number of image processing applications such as scene analysis and object recognition (Chaudhuri et al., 1989). An edge is defined as set of connected pixels lies between boundary of two regions (Gonzalez and Woods, 2002), so it represents a local change or a discontinuity in image illumination (Chaudhuri et al., 1989). The edges in an image provide useful structural information about object boundaries, as the edges are caused by changes in some physical properties of surfaces being photographed, such as illumination, geometry, and reflectance. Thus, edge detection is an essential task in computer vision.

1. Detection of Retinal Vessels

Because the extraction of the blood vessels is not a straightforward under the complex nature of retinal images, many researches and studies have been conducted in detection of these vessels from these images (Chaudhuri et al., 1989),(Li and Chutatape, 2000) and (Cree et al., 2005). These studies can be classified into two main categories: detection of blood vessels edges (Gozalez and Woods, 2002) and (Haralick et al., 1987), and extraction of the core of vessels (Chaudhuri et al., 1989).

1.1 Extraction of the Vessel Edges

The aim of edge detection is to extract the left and right edges of blood vessels. An example of edge detectors are Sobel operator, Prewitt operator (Gonzalez and Woods, 2002) and Canny operator (Canny, 1986), which are consist of two kernels each one is 3 × 3 that convolve with image and the maximum of their responses are retained at each

All Rights Reserved - Library of University of Jordan - Center of Thesis Deposit

www.manaraa.com

pixel in the resulted image. But these methods were limited by producing of unconnected parallel edges that yield unsatisfactory results. These techniques have good results only when the edges are sharp and distinct. However, retinal vessels are usually thin with low local contrast and they almost never have ideal step edges. Mathematical morphological operations such erosion and dilation operations can also be considered as edge detector (Haralick et al., 1989). However, all of these edge detection techniques are not reliable, especially when there is a noise or abnormalities in the image (Chaudhuri et al., 1989).

1.2 Extraction of the core of vessels

The aim of this blood vessel detection technique is to extract the core of the blood vessels to design special edge detectors. This category can also be divided into two sub-categories in respect to the different processing manner: scanning (Chaudhuri et al., 1989) and (Li and Chutatape, 2000) and tracking (Chutatape et al., 1998) and (Cree et al., 2005). Scanning is two pass operations; extraction of edge pixels of blood vessels and segmentation by a certain thresholding method. Extraction of edge pixels is done by an enhancement process, where the desirable image feature points are first enhanced by techniques such as convolving a mask processing with the entire image and then the segmentation is performed. Whereas, a tracking operation begins at a prior known positions in the image.

Scanning and tracking approaches have their advantages and drawbacks, scanning approach make complete segmentation for the image but it needs more time and it may not work well in noisy environment (Chutatape et al., 1998). In contrast, tracking

All Rights Reserved - Library of University of Jordan - Center of Thesis Deposit

www.manaraa.com

approach is efficient in computation but may not work well in the case the blood vessels fade away, and usually needs operator to specify starting parameters interactively to initiate the tracking process (Chutatape et al., 1998).

Chaudhuri et al., (1989) proposed a method to extract the core features of blood vessels by matching the image by two dimensional GMF based on the observation that the cross section of blood vessels is approximated by Gaussian-shaped curve.

2. Two Dimensional Gaussian Matched Filter (GMF)

Two-dimensional GMF is one of the template matching algorithms that is used in the detection of the blood vessels in retinal images and other applications as well (O'Gorman and Nickerson, 1988). It is based on the spatial properties of the object to be recognized. The idea of GMF is introduced by taking a number of samples for a cross section of retinal blood vessels, then the gray level profile of these samples is approximated by a Gaussian shaped curve. The GMF was implemented by a set of templates consist of 12 kernels applied on the retina image, and the maximum response of 12 kernels represent the resulted image. Then, the resulted image is thresholded by optimum threshold where any pixel exceeds this threshold, labeled as part of vascular tree of retina (Chaudhuri et al., 1989).

All Rights Reserved - Library of University of Jordan - Center of Thesis Deposit

www.manaraa.com

3. Amplitude-Modified Second Order Gaussian Matched Filter

It has the same idea of the GMF but instead of using the Gaussian filter, it uses the second derivative of the GMF to construct the 12 kernels that convolve with the cross section of the blood vessel in the retina image (Gang et al., 2002). But these filters include an additional factor that measures the vessel's width to give an accurate detection of the blood vessels.

4. Retina Detection Systems

There has already been some work on detection of blood vessels by other researchers, but not to the level of performance required for robust automatic detection of the entire network of blood vessels. There has also been quite a lot of work by other researchers showing that blood vessels measurements are important indicators of retinopathy and related conditions, and more detailed study of some measurements for retinopathy is required.

Goldbaum et al., (1996) developed a great system for managing the retinal images which designed to perform many operations on them such as diagnoses, searching, comparing, and classification. This system called STARE system (structured analysis of the retina). The first step in STARE system is the image acquisition. Then, a preprocessing step is required to prepare a high contrast image for segmentation algorithms. After that, the blood vessels are segmented by the GMF as in (Chaudhuri et al., 1989). The location of the optic disk is found according to its brightness, convergence

All Rights Reserved - Library of University of Jordan - Center of Thesis Deposit

www.manaraa.com

of the blood vessels at the nerve and the large vessels entering the nerve from above and below. Blue band is used to identify the fovea which appears as a dark spot on this band. Final step is the classification and recognition using appropriate classifiers to classify input features of a specific object.

Chutatape et al., (1998) developed detection and tracking algorithms of blood vessels network in the retinal images. This algorithm depends on the GMF and Kalman filters. In the tracking operation, the optic disk is considered as initial points, which are convolved with the GMF and record the maximum response in the source list, which in turn contains the initial tracking position of one blood vessel. In tracking approach, the next possible location is estimated by Kalman filter where the GMF is applied to locate the center point and width of the blood vessels. A branching detection technique is used to locate the bifurcation points in the vessels network during tracking approach.

A new thresholding technique for segmentation of blood vessel in retina images was developed by (Hoover et al., 2000). This technique works on the GMF response images which segmented by propping technique. The prop take each piece to test the region–based properties if it's a vessel or not. By this method, a false detection is reduced by 15 times over of the basic thresholding of the GMF response.

Two efficient algorithms for blood vessel detection of retinal images using entropy thresholding are developed by (Chanwimaluang et al., 2003) and (HongQing, 2004). The algorithm of (Chanwimaluang et al., 2003) consists of four steps: match

All Rights Reserved - Library of University of Jordan - Center of Thesis Deposit

www.manaraa.com

filtering, local entropy thresholding, length filtering, and vascular intersection detection. The GMF is used to highlight blood vessel detection, and then a blood vessel is distinguished from the background by entropy thresholding. Length filtering approach is used to eliminate the false detection vessels.

The algorithm developed by (Hongqing, 2004) is consists of two steps: image enhancement process and entropy thresholding. The GMF is applied to enhance the blood vessels and entropy thresholding technique is used to automatically thresholding the image based on grey level-gradient co-occurrence matrix. This algorithm works well in normal or abnormal retinal images.

A new likelihood ratio test that combines a multiscale of the GMF response, confidence measures and vessel boundary measures is proposed by Sofka et al.,(2005). A multiscale of the GMF is used to detect the vessel with different widths. The GMF gives a high response to low contrast and small vessels but its disadvantages of false detection to the objects other than blood vessels such as optic disk require using another measure to distinguish between false responses from true vessels. Vessel confidence and boundary measures are used for this purpose, which are measure how close an image region is to an ideal vessel profile. From all these measures, a six dimensional vector for each pixel location in the image is produced. Then, a learning technique is used to convert this vector to the new Likelihood Ratio Vesselness (LRV) that measure if this pixel is a true vessel or not.

All Rights Reserved - Library of University of Jordan - Center of Thesis Deposit

www.manaraa.com

Due to the response of the GMF to the false objects such as lesions and optic disk, a post-processing step is required to eliminate these false responses. Abedel-Azeem et al., (2002) proposed a new post processing step to locate and eliminate such these problems. This algorithm works after applying certain detection technique, where each detected object is checked to determine it is a true vessel or not. Objects are classified to a true vessel upon two criteria: piecewise linearity and anti parallel edges, otherwise, classified as a non-vessel.

A fast method for automated detection of blood vessels in retinal images is developed by (Wang et al., 1997). This method is a combination of two basic approaches of edges detection; the enhancement/thresholding method and the edge fitting method that yield an improvement on the accuracy and the quality of the vessel detection. In the enhancement/thresholding method, a Sobel operator are applied to detect the edges of the vessel, the edges are thinned to preserve one seed point at each cross section of the vessels which are converted to a binary map using local windowing and local thresholding. In the edge fitting method, a twelve 15 × 15 binary GMF are constructed to search for a vessel segments of all possible directions. A single-linkage region growing technique with locally adaptive thresholds is used to produce the final vascular tree.

An improvement on the response of the GMF (Chaudhuri et al., 1989) for blood vessels detection of digital retinal images is proposed by (Al-Rawi et al., 2006). The response of the GMF is improved by changing its parameters, where these new parameters are found by an optimization program based on an exhaustive search. A new

All Rights Reserved - Library of University of Jordan - Center of Thesis Deposit

www.manaraa.com

thresholding technique is also proposed by the (Al-Rawi et al., 2006) that based on a morphological operations. The area under ROC and the MAA are used as an evaluation measures on a DRIVE and Hoover database and used for comparison purpose with other detection techniques. Although (Al-Rawi et al.,2006) found new parameters for the GMF, but these parameters might not be the optimal, because the optimization program that used is a simple program; based on the exhaustive search and the search space are not vary large.

Li and Chutatape (2000) developed a system that analyzes the fundus images to facilitate diagnosis procedure. In which, different algorithms developed to detect optic disc, blood vessels, and exudates. The detection of optic disk is performed in a red component by three steps; identification of the candidate area, applying Sobel operator to detect the edges, and the LSR is used to get the estimated circle. The blood vessels and exudates are detected using kirsches method in different color bands of the retinal image. Kirsches method is used to detect the blood vessels from the green band, because the blood vessels have high contrast on it. The resulted image is computed by convolving the green component with the eight templates, each one is 3 × 3 size via different directions. The maximum responses from the convolution represent the resulted image. This resulted image contains the blood vessels and the exudates that can be separated by morphological operator. But if the Kirsches filters are applied on the red component, only the exudates will be detected.

All Rights Reserved - Library of University of Jordan - Center of Thesis Deposit

www.manaraa.com

The comparative study analysis of three different templates matching algorithms for detection of blood vessels in grey level and colored retina images presented in (Banumathi et al., 2003). This study shows that the GMF in (Chaudhuri et al, 1989) gives the complete and continuous vessels map, but can't detect the small vessels compared with binary GMF. It can perform seven times faster than GMF. The third algorithm is the Kirsches template matching which used to detect blood vessels in both grey-level and color images and produce a continuous vessels map but it can't detect small vessels and can't remove the noise.

Comparative study for different number of segmentation methods for retinal vessels is performed by (Neimeijer et al., 2003). Also, anew supervised technique which called pixel classification is developed to segment blood vessel from retinal images. Pixel classification method is compared with other methods from the literature; one of these methods is the GMF. Neimeijer et al., (2003) used the area under the ROC and the MAA as an evaluation measures in his comparison. The study show the pixel classification methods got higher ROC but the second observer still perform better, while the lowest ROC is achieved by GMF which implemented as in (Chaudhuri et al. 1989).

Another comparison is performed by (Cree et al, 2005) between wavelet approach which developed by (Cornforth et al, 2004) and other algorithm from the literature. As an example for these algorithms: GMF (Chaudhuri et al., 1989) and Morphological tophat and curvature estimation (Zana and Klien, 2001). This comparison is conducted on a

All Rights Reserved - Library of University of Jordan - Center of Thesis Deposit

www.manaraa.com

STARE database and the efficiency of these vessel detection methods is evaluated using Free-response Receiver Operating Characteristic (FROC) analysis.

Zana and Klien, (2001) presented an algorithm to segment a vessel-like profile patterns using morphological operation and curvature evaluation. This algorithm starts by noise reduction, then detection using morphological operations and removal of undesirable pattern. Properties of blood vessels such, brightness, piece-wise connectivity, and linearity make using the morphological operation is convenient for blood vessel segmentation, but other patterns will respond to the morphological operations. Thus a cross–curvature evaluation is performed to distinguish a vessel from the background patterns. Zana and Klien, (2001) made a comparison between their algorithm and other detection algorithms from four criteria: detection of the largest vessels, the ratio of false detection, the accuracy of bifurcation points that identified in the vascular structure, and the continuity of the segmented structure.

A segmentation of blood vessels in color retina images by tracking of vessels is proposed by (Cree et al., 2005). A two-dimensional model of the vessel profile to a local region of the vessels is used to measure the diameter and the orientation of this local vessel segment. These measurements are computed accurately to proceed the tracking algorithm. This model is modified to enable tracking a tortuouse vessel, and also a method to detect vessel branches is also presented in this paper.

All Rights Reserved - Library of University of Jordan - Center of Thesis Deposit

www.manaraa.com

Tolias et al., (1998) presented an unsupervised fuzzy algorithm for vessel tracking to detect the blood vessels in retinal images. This algorithm distinguishes between vessel and non-vessel regions along a vessel profile by using the fuzzy C-means clustering algorithm which provided by a preprocessed images. Tolias et al., (1998) also used other methods to check the correctness of the detected vessels and handing junctions and forks.

Ridge-based vessel segmentation of retina images is presented by (Staal et al. 2004). This supervised method based on extraction of image ridges, which grouped into sets that approximate straight line elements. These sets used to partition the retina image into patches by assigning each pixel of the images to the nearest set. For each pixel, a feature vectors are computed depending on the properties of patches and line elements. A KNN classifier is constructed using selected features by sequential forward selection matched with the training data to detect vessel pixels. The ROC area is used as an evaluation measure of this new technique under new two databases; The DRIVE and the Hoover database for comparison purpose with other techniques used for vessel detection.

Soares et al., (2004) used a 2-D Morlet wavelet and a supervised classification to segment retinal blood vessel. Each pixel in retinal images is represented by a vector which consists of the intensity of the pixel and the response of a continuous two-dimensional Morlet wavelet transform at a multiple scale. A preprocessing step is required to eliminate a noise and enhance a vessel because the Morlet wavelet is able of tuning to specific frequencies. Fast classification for a complex decision surface produced by Bayesian classifier with a Gaussian mixture model as a class likelihoods. The DRIVE

All Rights Reserved - Library of University of Jordan - Center of Thesis Deposit

www.manaraa.com

and the Hoover database are used to evaluate the performance of this method. The training data for the classifier is provided by the training images. Joao et al., (2004) plotted the ROC between the fractions of true positive and false positive to compute the area under the curve to evaluate their algorithm and to compare it with other algorithms reported in the literature.

A new algorithm is proposed to detect large and small blood vessels in retinal images by (Wu et al., 2006). This algorithm begins by taking the green band of color retina images for preprocessing steps which consist from illumination equalization and adaptive histogram equalization for contrast enhancement. Then, features of small vessels are extracted using standard deviation of Gabor filter response via different orientation. Finally, a tracing algorithm is used to find a final vessels map which consists from small and large vessels. The tracing of vascular network consist of three procedures: forward detection, backward verification and bifurcation detection. Wu et al., (2006), use a false and true positive ratio pair as an evaluation measure on Hoover database.

Many researchers apply the GMF as enhancement procedure before applying their main algorithms (Hoover et al, 2000), (Chanwimaluang et al., 2003), and (HongQing, 2004). So, efforts for maximizing the efficiency of this procedure are highly desirable. Hence, the optimized GMF alone gives good results; surely the accuracy of other algorithms that use the GMF will increase in parallel with improvement on GMF.

All Rights Reserved - Library of University of Jordan - Center of Thesis Deposit

www.manaraa.com

5. Genetic Algorithms

Genetic Algorithms form effective solution for optimization problems (Goldberg, 1989) and (Mitchell, 1997). They can be considered as probabilistic search algorithms and efficiently search a large and a complex space to find nearly optimal solution. The genetic algorithms are introduced in 1970s by John Holland (Holland, 1970).

Genetic algorithms can be used for parameter optimization and feature selection (Goldberg, 1989). Joint parameter optimization is an optimization problem which consists of searching the space of all possible parameter settings to identify the combination that is optimal or near-optimal since exhaustive search in large space is not effective. The genetic algorithms are more realistic approach to search the space, where they explore different areas of the search space in parallel.

There is many works in the literature that used the genetic algorithms to search for the best combination of certain parameters for optimization purpose. Silva et al., (2002) used a genetic algorithm to optimize image clustering using unsupervised Artificial Neural Network (ANN). The clustering optimization is achieved by optimizing the neural network training parameters. The genetic algorithms also used by (Simunic et al., 1998) to search for transformation parameters space and distance transform to compute the effectiveness of the match measure in global matching of partial view images.

All Rights Reserved - Library of University of Jordan - Center of Thesis Deposit

www.manaraa.com

An improvement obtained by applying a distributed genetic algorithm to a problem of parameter optimization in medical images is proposed by (Bevilacqua et al., 2001). Otobe et al., (1998) developed an optimization procedure for enhancing a specific component in the digital images based on the genetic algorithms. The fitness is evaluated to find appropriate filtering operations and their parameters based on the reference image given by the user as a standard image.

A very popular problem in image segmentation is active contours which have a problem in setting of many sensitive parameters. The genetic algorithms are used by (Rousselle et al., 2003) to find an appropriate setting for these parameters. Ahrens, (2005) used the genetic algorithms to determine the registration and the point spread function parameters for superresolution which is the process of producing a highly resolution image from a collection of low resolution images. Superresolved image is produced by genetic algorithm optimization of the previous superresolution method.

All Rights Reserved - Library of University of Jordan - Center of Thesis Deposit

www.manaraa.com

THEORY AND IMPLEMETATION

All Rights Reserved - Library of University of Jordan - Center of Thesis Deposit

www.manaraa.com

Theory and Implementation

1. Gaussian Matched Filter (GMF)

The GMF is one of the template matching algorithms that can be used in the detection of the blood vessels in retinal images. It is based on the spatial properties of the object to be recognized. The idea of GMF is introduced by taking a number of samples for a cross section of retinal blood vessels, then the gray level profile of these samples is approximated by a Gaussian shaped curve. Figure 1.a shows the green band of original image of the retina and Figure 1.b shows the gray level cross section profile at row number 110 for the retinal image shown in a. Figure 2.a shows a magnified segmental image from Figure 1 that contains small vessels and Figure 2.b shows the gray level cross section profile of one row on it (25) to demonstrate the shape of small vessels.

1.1 Design and Implementation of GMF

The GMF designing is based on a number of properties for blood vessels, which are useful for vessels analysis (Chaudhuri et al., 1989).

Properties of Retinal Blood Vessels:

- Vessels can be approximated as anti-parallel segments.
- Vessels have lower reflectivity than other retinal surfaces, so it appears darker relative to the background.
- Vessel size may be decreases when moving away from the optic disc, the width of the vessel is 2 – 10 pixels depending on the resolution.
- The intensity profile varies by small amounts from vessel to vessel.

All Rights Reserved - Library of University of Jordan - Center of Thesis Deposit

www.manaraa.com

- The intensity profile has a Gaussian shape.

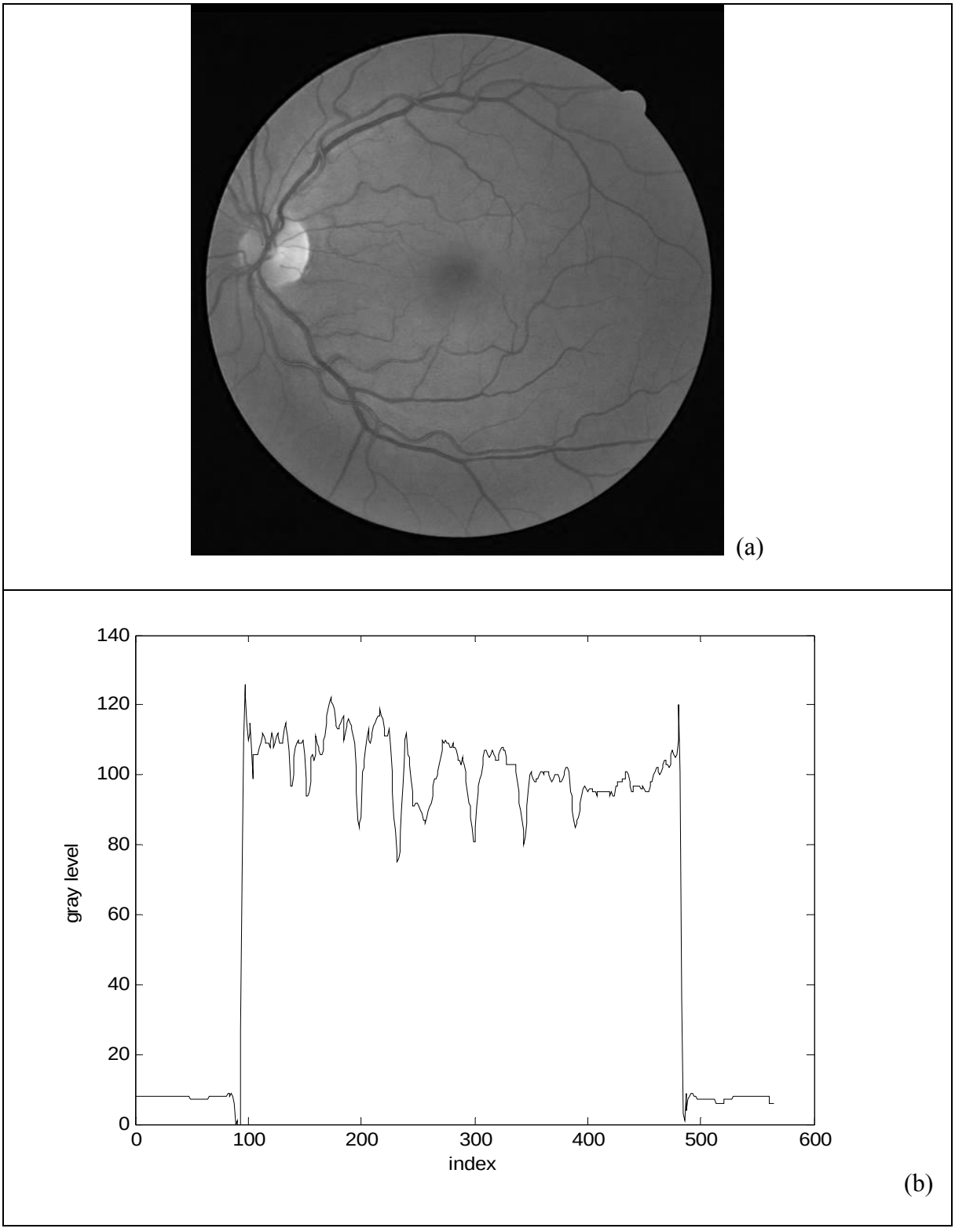

Figure1 (a) *The green band of a digital retinal image* **(b)** *A cross section profile at a row number 110 of the retinal image shown in a.*

All Rights Reserved - Library of University of Jordan - Center of Thesis Deposit

www.manaraa.com

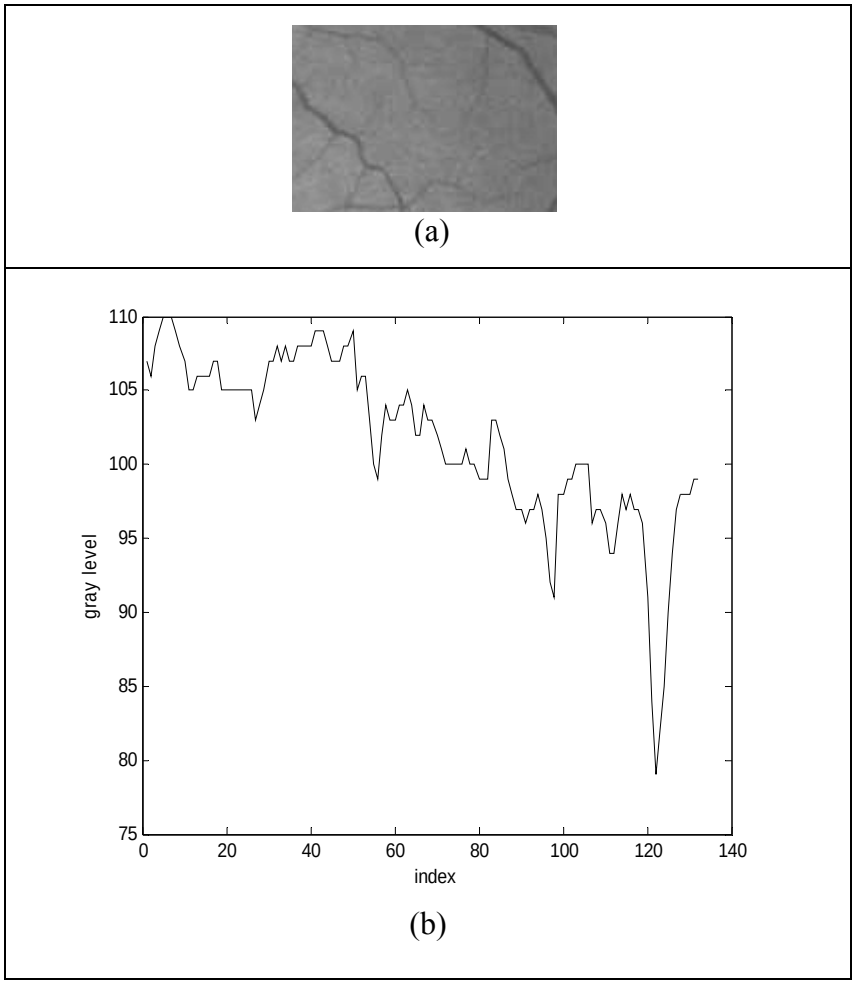

Figure 2 (a) *The segmental image from Figure 1*(a) *that obtain the small vessels.* ***(b)*** *A cross section profile at the row number 25 of the segmental image shown in a.*

The GMF kernel as given in (Chaudhuri et al., 1989) may be expressed by Equation (1):

$$k(x, y) = -\exp(-x^2 / 2\sigma^2) \qquad \forall \mid y \mid \leq L/2 \qquad (1)$$

Where L is the length of vessel segment that has the same orientation (all the cross section profiles for this segment have the same orientation), and σ defines the

All Rights Reserved - Library of University of Jordan - Center of Thesis Deposit

www.manaraa.com

spread of the intensity profile. The negative sign in Equation (1) indicate that the gray levels of the vessels are darker than the background. Therefore, the shape of cross section of the blood vessels will have an opposite direction of the Gaussian curve.

To be able to detect vessels on all possible orientations, the kernel must be rotated to all possible vessel orientations and the maximum response from the filter bank is registered. Some researchers (Chaudhuri et al., 1989), and (Banumathi et al., 2003) found that rotating by 15^o over 180^o is adequate to detect vessels with an acceptable degree of accuracy (which would result in a filter bank of 12 kernels). To obtain the GMF via different rotations a neighborhood N is defined in Equation (2):

$$N = \{(u,v), |u| \leq T, |v| \leq L/2\} \qquad (2)$$

Where T is the position where the Gaussian curve trails will cut, because Gaussian curves have infinitely long double sided trails and the trails are truncated at $T = 3\sigma$ by (Chaudhuri et al., 1989). Let p_i be the point that belongs to the neighborhood N which is represented by (u, v), and this point is represented by Equation (3):

$$p_i = [u \; v] = [x \; y] \begin{bmatrix} \cos\theta & -\sin\theta \\ \sin\theta & \cos\theta \end{bmatrix}^T \qquad (3)$$

The corresponding weights in the kernel i (for θ = 15˚, i = 1,…., 12) are given by Equation (4):

$$k_i(x,y) = -\exp(-u^2/2\sigma^2) \qquad \forall p_i \in N \qquad (4).$$

The filter is normalized to have zero mean as in Equation (5):

$$k'_i(x,y) = k_i(x,y) - m_i \qquad (5)$$

All Rights Reserved - Library of University of Jordan - Center of Thesis Deposit

www.manaraa.com

Where $m_i = \frac{1}{a} \sum_{p_i \in N} k_i(x, y)$, and a denotes the number of points in N.

The kernel size of the GMF which is used in the optimization program can be calculated from (2) and is given by equation (6):

$$Kernel_size = \sqrt{(L+1)^2 + (2*T+1)^2} \qquad (6)$$

Chaudhuri et al., (1989) performed empirical measurements for the values of L and σ and found that the best parameter values that gave the maximum response were $L = 9$, $\sigma = 2$ and $T = 6$. They did not, however, present their experiments of finding L, σ and T. In this thesis, genetic algorithms are used to optimize the set {*L, σ, T*} in one experiment, and {*L, σ, T*, *NOK*} in another, where *NOK* is the number of kernels, note that the degree of rotation is computed from ($\theta = 180 / NOK$).

1.2 Detection of Blood Vessels using GMF

Applying a GMF to segment the blood vessel in retinal images required three stages (Chaudhuri et al., 1989): a preprocessing stage is needed to prepare an enhanced image for segmentation method. After that, the blood vessel are segmented by applying the GMF on the enhanced image. The last stage, which is considered as a post processing stage, is performed by thresholding the GMF output image. Details about these stages as performed by (Chaudhuri et al., 1989) are illustrated in the following sections.

All Rights Reserved - Library of University of Jordan - Center of Thesis Deposit

www.manaraa.com

1.2.1 Preprocessing Stage

Vessels detection is based on the green component of the retina images since the blood vessels have a high contrast on it. Then, this green component is smoothed by 5 × 5 average filter to reduce the affect of the noise. After that, an approximation to the image as a stationary process is performed by subtraction the local mean from the image and the pixel intensities are divided by the square root of local variances.

1.2.2 Vessel Segmentation

The twelve kernels which derived from the Gaussian approximation of the cross section of the blood vessels by (Chaudhuri et al., 1989) are convolved with the smoothed image via all twelve directions then the corresponding responses are compared and for each pixel only the maximum response is to be retained.

1.2.3 Post Processing Stage

An automatic thresholding technique is used by (Chaudhuri et al., 1989) to differentiate blood vessels from retinal background which is proposed by (Otsu, 1979). A pixel is labeled as a vessel if the convolution output at this pixel exceeds certain threshold. This means that the threshold is selected to give the maximum response of GMF.

2. Amplitude Modified Second Order GMF

Amplitude modified second order GMF is also used to detect the vessels in retinal images and it has the same idea of the GMF in the detection. But instead of using

All Rights Reserved - Library of University of Jordan - Center of Thesis Deposit

www.manaraa.com

Equation (1), it use the second derivative of this equation to construct 12 kernels that convolve with the cross section of retinal blood vessels in all possible twelve directions.

Gang et al., (2002) used a second order derivative of the GMF to add an additional parameter that helped to control the width of the blood vessels diameter, which yields an improving in the response of the GMF and increasing the success rate of detection.

The second order differential GMF (Gang et al., 2002) is described by Equation (7):

$$f(x) = \frac{1}{\sqrt{2\pi}\sigma^5}(x^2 - \sigma^2)\exp(-x^2/2\sigma^2) \qquad (7)$$

Where σ is a specific parameter of Gaussian filter function that controls the width of the filter. But from Equation (7) it is difficult to determine the width of the vessel. Therefore, an amplitude factor in the second order Gaussian function is eliminated to become as in Equation (8):

$$f(x) = (x^2 - \sigma^2)\exp(-x^2/2\sigma^2) \qquad (8)$$

Also, it is still not possible to determine the vessel width, so the amplitude factor is further modified to moderate value, which is the power of the σ in the amplitude dominator and become as follow:

$$f(x) = \frac{1}{\sqrt{2\pi}\sigma^3}(x^2 - \sigma^2)\exp(-x^2/2\sigma^2) \qquad (9)$$

Now, it is possible to measure the vessel width with a modified Gaussian filter.

Simulation for the amplitude modified second order GMF with different values of the parameter *t* which exists in Equation (10) are done by (Gang et al., 2002).

All Rights Reserved - Library of University of Jordan - Center of Thesis Deposit

www.manaraa.com

$$f(x) = \frac{1}{\sqrt{2\pi}\sigma^{t}}(x^2 - \sigma^2)\exp(-x^2/2\sigma^2) \qquad (10)$$

Mathematical analysis to the values of *t* which resulted from simulation show that the vessel's width can be measured in linear relationship with the "spreading factor" of the GMF when the magnitude coefficient of the filter is suitably assigned. Gang et al., (2002) found $t = 3.5$ is the optimal for vessel detection and measurement. Then, after finding the values of σ for each profile from Equation (10) using $t = 3.5$, a relationship between parameter σ and the actual diameter of the vessel is determined by (Gang et al., 2002) to be as in Equation (11) :

$$d = 2.03\sigma + 0.99 \qquad (11)$$

Where *d* is the diameter of the vessel.

After that, the filter is extended to be two dimensional of matching vessel segment instead of matching a single profile of the vessel cross section (Gang et al., 2002). Then, the kernel of the filter can be expressed as in Equation (12):

$$f(x,y) = \frac{1}{\sqrt{2\pi}\sigma^{3.5}}(x^2 - \sigma^2)\exp(-x^2/2\sigma^2) \quad \text{when} \quad \begin{matrix} y \le L, \\ |x - c| \le FW/2 \end{matrix} \qquad (12)$$

Where *L* is the length of the filter window, c is the *x* position of the center line of the filter window along *y* axis and *FW* is the width of the filter window. The orientation of the filter is assumed to be aligned along the *y* axis. It's the same as parameters of the matched filter {*L, σ, T*} but with different names. But, (Gang et al., 2002) used more

All Rights Reserved - Library of University of Jordan - Center of Thesis Deposit

www.manaraa.com

than one value of σ along the vessel, where the value of σ is adaptively adjusted according to the vessel width in detection.

In this thesis, we did experiments to optimize the set of $\{L, T\}$ using $t = 3.5$ and different scale of σ. Also we did another experiment to optimize the set $\{L, \sigma, T, t\}$ to increase the performance of second order GMF.

3. Genetic Algorithms

Genetic Algorithms form an effective solution for optimization problems (Goldberg, 1989) and (Mitchell, 1997), because it can be considered as probabilistic search algorithms. Therefore, it is used to improve the performance of the matched filter by finding better parameters for L, σ, and T. Initially; we will discuss the main concept for genetic algorithm. Then, the optimization of the matched filter and its second order derivative using genetic algorithm will be illustrated in subsequent sections.

Genetic algorithms operate on a set of individuals (represented by chromosomes) called population, where each individual is an encoding of the problem's input data. Each individual's fitness is calculated using an objective function. In genetic algorithms terminology, each iteration of the search is called a generation. From each generation, the fittest individuals are selected then those are pooled out to form a base for a new population (offspring) with better characteristics. Genetic algorithms are characterized by attributes such as objective function,

All Rights Reserved - Library of University of Jordan - Center of Thesis Deposit

www.manaraa.com

population diversity, encoding of the input data, selection, crossover, mutation, and population size. Below is a description of the genetic algorithms attributes:

3.1. Objective Function

It is used to assign each individual in the population a fitness value; an individual with a higher fitness represents a better solution to the problem than an individual with a lower fitness value.

3.2. Population diversity

It is one of the most important factors that determine the performance of the genetic algorithm because it enables the algorithm to search a larger region of the space. Diversity refers to the average distance between individuals in the population, where the population has a high diversity if the average distance is large; otherwise it has low diversity.

3.3. Population Size

It is the number of individuals in a population. The larger the population size, the better the chance that an optimal solution will be found.

3.4. Encoding

Genetic algorithms operate on an encoding of the problem's input data (which represents independent variables for the objective function). There are various methods to encode the problem, but the most common one is the binary encoding,

All Rights Reserved - Library of University of Jordan - Center of Thesis Deposit

www.manaraa.com

which consists from fixed bit string (strings of ones and zeros) to represent certain input data within the problem domain. The following example illustrates a binary encoding for a certain chromosome which consists of three input data to the problem.

Example 1: *Example of chromosome with binary encoding*

Input data 2

Chromosome 1: **1100100101010100111100110**

Input data 1 **Input data3**

Other encoding techniques are available such as Real-Valued, Character, Permutation, and Tree encoding. There is little work has been done on these encoding techniques due to little information available a bout genetic algorithms operators on them. However, the most appropriate encoding is strongly dependent on the problem domain and the environment where the genetic algorithms will operate.

3.5. Elitism

It is a way to ensure that the highly fitting chromosomes are not lost and copied to the new population. Elitism has been found to be very important to the performance of genetic algorithms.

3.6. Selection

Pairs of chromosomes are selected from the population to be parents for crossover operation based on their fitness values. Fittest chromosomes are pooled out to produce fittest offspring.

All Rights Reserved - Library of University of Jordan - Center of Thesis Deposit

www.manaraa.com

If the selection is strongly dependent on highly fitting chromosomes, then this can reduce the diversity in the population and can result in premature convergence. Premature convergence occurs when a local optimal solution is found however there is not enough diversity in the population to allow other better optimums to be found. In the following, we will mention various methods that used for selection process:

- ***Fitness-Proportionate Selection:*** is the most widely used method because a lot of work was done using it in early genetic algorithm studies. In this method, the selection is done randomly, where the fittest chromosome have a higher probability of being selected, which also is called "Roulette Wheel". When the population size is too small, this method becomes not suitable because may occasionally all chromosomes which selected have low fitness value.
- ***Sigma Scaling:*** after comparing all fitness values, an appropriate selection is done. By this method a premature convergence will be avoided.
- ***Rank Selection:*** each chromosome allocate a relative ranking based on its fitness value. The strength of this method that it can't be affect by highly fit chromosome since all selection is performed upon relative fitness not on absolute fitness.

3.7. Crossover

It is a procedure in which a highly fitting chromosome is given an opportunity to reproduce by exchanging pieces of its genetic information with other highly fitting chromosomes.

All Rights Reserved - Library of University of Jordan - Center of Thesis Deposit

www.manaraa.com

There is more than one way to perform a crossover:

- ***Single-Point Crossover:*** it is the most commonly form of crossover in the genetic algorithms. A single point is chosen randomly to split two chromosomes; from the beginning of the chromosome to the split point is copied from the first parent, and the rest is copied from the other parent. The following example illustrates how single-point crossover occurs between two chromosomes with a binary encoding.

  Example 2: *Example on a single-point crossover function*

  Parent 1: 10001110101011000011101

  Parent 2: 10101010110011101101010

  Crossover Point: 11

  After Crossover (Offspring): 10001110101011101101010

  Single-point crossover is not efficient due to the limitation in the number of ways the chromosomes can be split and joined. That will produce "Position Bias" problem in which the position of input data in the chromosomes will affect their ability to be combined with other input data. Therefore, it is difficult to produce certain combinations of input data due to their position and it may take several generations to generate certain combination.

- ***Two-Point Crossover:*** two crossover points are selected randomly, where from the beginning of chromosomes to the first crossover point is copied from the first parent. The part from the first to the second crossover point is copied from the other parent and the rest is copied from the first parent again. This

All Rights Reserved - Library of University of Jordan - Center of Thesis Deposit

www.manaraa.com

method used to overcome "Position Bias" problem of the single point crossover since it allows for more possible combinations of the chromosomes during crossover operation, but can't produce all possible combinations and can be more likely to cause disruption between related input data. Example 3 illustrates how two-point crossover occur between two binary chromosomes:

Example 3: *Example on a two-point crossover function*

Parent 1: 10001110101011000011101

Parent 2: 10101010110011101101010

Two Crossover Points: 8 and 15

After Crossover (Offspring): 10001110110011100011101

- ***Uniform Crossover:*** a random binary vector is created to let a crossover occur at any point in the chromosomes. Where if the value in the vector is one, the corresponding input data is copied from the first parent; otherwise the input data is copied from the second parent. This allows for the greatest number of possible outcomes from the crossover but can also be disruptive to related input data in the chromosomes. In the following example, uniform crossover is illustrated.

Example 4: *Example on the uniform crossover function*

Parent 1: 10001110101011000011101

Parent 2: 10101010110011101101010

Binary Vector: 11010111101011010100111

After Crossover (Offspring): 10101110111011101010101

All Rights Reserved - Library of University of Jordan - Center of Thesis Deposit

www.manaraa.com

3.8. Mutation

It is often applied after crossover by randomly altering some genes to individual parents. Mutation is necessary to provide population diversity and to enable the genetic algorithm to search a broader space. In the following example the mutation in case of binary encoding occurs by randomly choosing the 12^{th} bit to switch it (changing from 0 to 1 and vice versa). But, in Real-Valued encoding small numbers is added or subtracted to the selected values.

Example 5: *Example on the mutation function with binary encoding*

Parent 1: 100011101010110000011101

After Mutation (Offspring): 100011101011110000011101

Genetic algorithm iterates a fixed number of times. Since the function's upper bound (the maximum fitness value possible for an individual) is often not found, we must limit the number of generations in order to guarantee the termination of the search process. This may result in a suboptimal solution. In the next section we explain how our genetic algorithms find the best parameter for the matched filter.

Algorithm 1 shows the basic genetic algorithm steps which are common for all problems domain.

All Rights Reserved - Library of University of Jordan - Center of Thesis Deposit

www.manaraa.com

Algorithm 1 *depicts the basic steps for the genetic algorithm*

1. [Begin] Create random initial population.

2. [Fitness] Evaluate the fitness function for each chromosome in the population.

3. [New Population] Create new population by repeating the following genetic algorithm operators until the new population is complete:

- **[Selection]** Select pair of chromosomes according to their fitness to be parents.
- **[Crossover]** Recombine two parents to form new offspring.
- **[Mutation]** Make a random change to a single parent.

4. [Replace] Use the new generated population for further run of the algorithm.

5. [Test] If one of the stopping criteria is satisfied, stop, and return the best solution in the current population to the genetic algorithm.

6. [Loop] Go to step 2.

4. Optimization of the Matched Filter by using Genetic Algorithms

In Genetic Algorithm Matched Filtered (GAMF) experiments, we could obtain the best parameters L, σ, and T that result in selecting the fittest individual (the best matched filter parameters). In the following, we will mention: what is the technique used to encode these parameters, what is the fitness function and how we can evaluate it, what is the selection function that used to select the fittest individuals, how the crossover and mutation occur in the chosen encoding, and what are the fractions that

All Rights Reserved - Library of University of Jordan - Center of Thesis Deposit

www.manaraa.com

used in GAMF optimization to determine population size, crossover fraction, elite count, and mutation fraction.

Encoding

A good encoding of the input data is *Real-Valued* encoding since *L, σ,* and *T* are represented as real numbers. Thus, each chromosome consisted of three independent variables {*L, σ, T*} will be the input data used to calculate the fitness function. In other words, each individual corresponds to a GMF with an instance of {*L, σ, T*} values.

Example 6: *Example of chromosome with Real_Valued encoding which used in our GAMF.*

Parameter 2 (*σ*)

Chromosome 1: [12.5432 0.5678 4.4560]

Parameter 1 (*L*) Parameter 3 (*T*)

But, in the experiments that are performed to find the best degree of rotation, the input chromosome to the genetic algorithm becomes four instead of three, where *NOK* is the fourth input data in addition to the original three parameters *L, σ,* and *T* to become {*L, σ, T, NOK*}.

The Fitness Function

In certain experiments, we use the area under the ROC as the fitness function of the genetic algorithm, which in turn will select the fittest individual represented by

All Rights Reserved - Library of University of Jordan - Center of Thesis Deposit

www.manaraa.com

the highest area under the ROC coded by its L, σ, and T. If the area under ROC is one this means perfect detection. The area under ROC is obtained as follows:

1) let the input image be f, the input individual which consists of three independent parameters to the fitness function are$\{ L, \sigma, T\}$. Applying the GMF of $\{L, \sigma, T\}$ to f yields the matched filtered output image $f_{L\sigma T}$ which is a continuous image. By thresholding $f_{L\sigma T}$ via different threshold values from 0 to 1 in a step of 0.05 (assuming the use of normalized intensity and the number of thresholds is 20) we obtain several binary images, each image corresponds to a certain threshold.
2) Then, we calculate the true_ratio and the false_ratio for each binary image by comparing it with a corresponding hand labeled retina image denoted as h. The hand labeled image is obtained from the retinal image by an experienced observer to be used for the computer comparison purpose as described in (Staal et al., 2004). The comparison yields true pixels (pixels detected as vessels yet they appear as vessels in the hand label) and false pixels (pixels detected as vessels yet they appear as non vessels in the hand label). The true_ratio is obtained by dividing the true pixels by the number of vessel pixels in h , and the false_ratio is obtained by dividing the false pixels by the number of non vessel pixels in h.
3) The ROC is used to plot the variation of the false_ratio versus the true_ratio. Then, the area under the ROC is calculated and returned to the genetic algorithm as a fitness value.

All Rights Reserved - Library of University of Jordan - Center of Thesis Deposit

www.manaraa.com

One might argue, however, that the area under the ROC is not a proper fitness function because what is important after all is the MA value, therefore, other experiments are performed using the MA as a fitness function of the genetic algorithm which in turn will select the fittest individual that maximizing the accuracy. The MA is calculated as follow:

1) The image $f_{L\sigma T}$ is thresholded at different levels of threshold between 0 and 1 where the level is a normalized intensity value that lies in the range [0,1] (Otsu, 1979).
2) At each threshold the accuracy value is calculated. Where the accuracy for one image is calculated by taking the sum for the total number of the pixels correctly classified as a vessels and non vessels at a certain threshold. Then dividing the sum of pixels in the field of view (FOV), which is the circular area in the retina image.
3) Then, the MA between all accuracy values is selected at a certain threshold. This threshold is considered the best threshold.

Selection Function

We choose a *Rank Selection* method for Optimization of the GMF because this method not easily affect by highly fit chromosomes since all selection based on relative fitness.

All Rights Reserved - Library of University of Jordan - Center of Thesis Deposit

www.manaraa.com

Crossover Function

Because we want the largest number of possible outcomes from the crossover, *Uniform Crossover* is used as a crossover function. Example 7 illustrates how the uniform crossover occurs in case of Real-valued encoding as in GAMF.

Example 7: *Example on a uniform crossover function which is perform in our GAMF.*

Parent 1: [11.5712 0.5678 4.8932]

Parent 2: [13.7891 1.2051 7.1801]

Binary Vector: [1100110011100101]

After Crossover (Offspring1): [11.7812 1.2678 7.1902]

After Crossover (Offspring2): [13.5791 0.5051 4.8831]

Mutation

The mutation occurs on the Real-Valued by randomly adding or subtracting small values to the selected positions. Example 8 shows how the mutation occurs in GAMF.

Example 8: *Example on a mutation function which is perform in our GAMF.*

Parent 1: [13.7712 0.5058 7.1902]

Selected operations: subtract from the 2nd position one and add to the 7th position one

After Mutation (Offspring): [12.7712 1.5058 7.1902]

All Rights Reserved - Library of University of Jordan - Center of Thesis Deposit

www.manaraa.com

Other Genetic Algorithms Parameters:

The genetic operators have fixed fractions that are problem dependent. The fractions used in GMF parameters optimization are as follow:

- ***Population size:*** (30) we set the population size with a moderate number because an intensive computation is needed for determining an individual's fitness. In fact, to find the fitness values of the whole population of chromosomes, we find the kernels of 30 filters. After that each filter is applied to the retinal image and the ROC area or the MA is calculated. The block diagram in Figure 3 illustrates the steps which are needed to calculate the fitness function for one individual of the population under 15˚ degree of rotation.

All Rights Reserved - Library of University of Jordan - Center of Thesis Deposit

www.manaraa.com

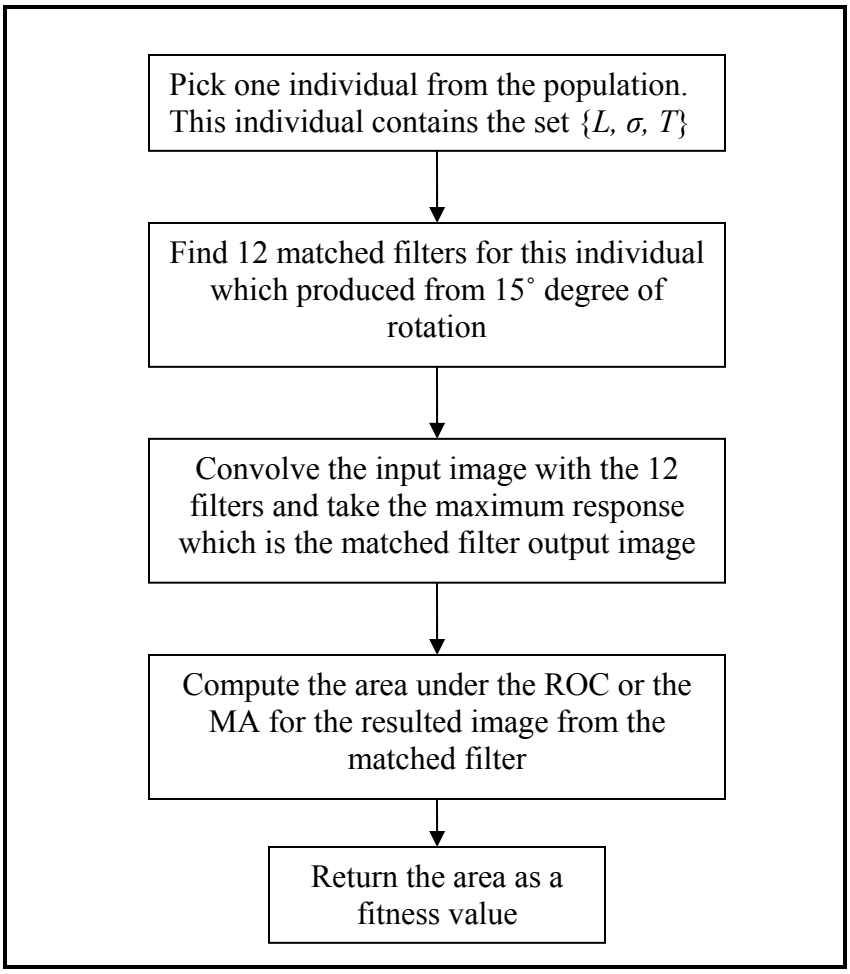

Figure 3 *Block diagram to calculate the fitness function for one individual of the population*

- ***Elite count:*** one individual with the highest area under the ROC is chosen to survive to the next generation.
- ***Crossover Fraction:*** (0.7), which specifies the fraction that forms crossover children from population other than elite children.
- ***Mutation fraction:*** the remaining individuals from the population other than elite and crossover children are mutation children.

All Rights Reserved - Library of University of Jordan - Center of Thesis Deposit

www.manaraa.com

Thus, in one generation there is one individual immigrated from the previous generation which has the highest fitness value, the numbers of crossover children are 30 × 0.7 = 21, and the remaining individuals from the population are the mutation children calculated to be 8. The block diagram that illustrates how the genetic algorithm constructs the populations in each generation is shown in Figure 4.

Stopping Criteria

The GAMF optimization is run until no improvement on the fitness values under certain number of generation. This is refers to the stall generation terminology, which is defined as follow: the genetic algorithm stops if there is no improvement in the objective function for a predetermined number of consecutive generations. The genetic algorithm is also stop if the function's upper bound is found (maximum fitness value possible for an individual, which is here 1), but this is impossible in the GMF optimization due to the false response of the GMF to the optic disk and other lesions in the retinal images. Thus, we must determine the number of generations in order to guarantee the termination of the search process.

All Rights Reserved - Library of University of Jordan - Center of Thesis Deposit

www.manaraa.com

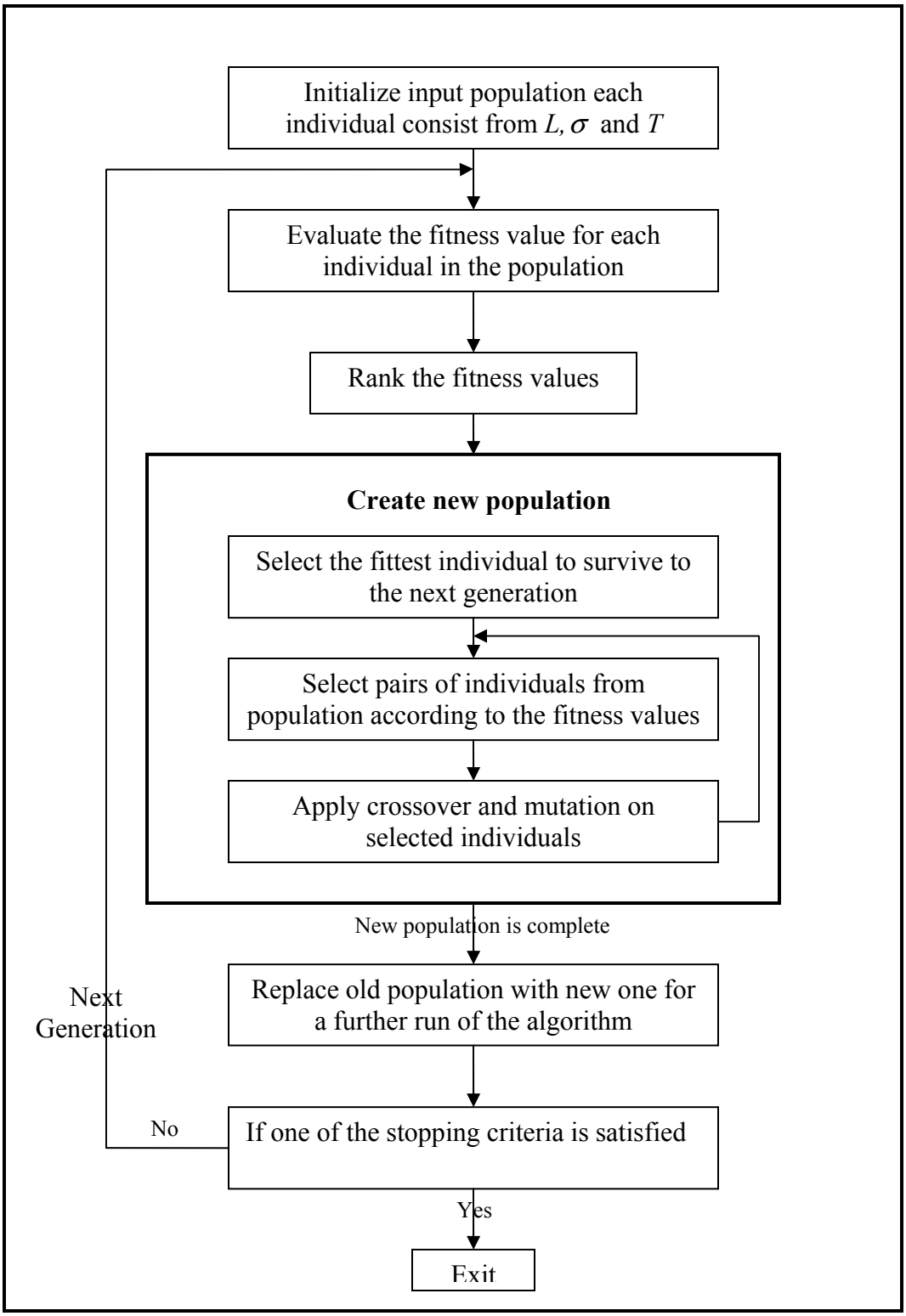

Figure 4 *Block diagram for genetic algorithm to find the best matched filter parameters*

All Rights Reserved - Library of University of Jordan - Center of Thesis Deposit

www.manaraa.com

Algorithm 2 *depicts the steps of GAMF procedure, in general*

1. **Begin**
2. **Initialize** (Range_L = [0 10], Range_σ = [0 15], Range_T = [-5 10], Crossover_Fraction = 0.7, Population_zise = 30)
3. **Generate** initial population randomly from the predetermined initial range of *L,* σ, and *T* where each individual consist from *L,* σ, and *T.*
4. **Evaluate** the fitness function for each individual in the population
5. **Rank** the fitness values
6. **Create** new population by repeating these steps:
   a. Select the individual that have the highest fitness value to survive to the next generation.

   do

   b. Select two parent individuals from the population according to their fitness.
   c. According to the crossover fraction, recombines the selected parents to produce new offspring.
   d. With mutation fraction, alter some values in the produced offspring.

   until new population is complete
7. **Replace** old population with a new population and use it for a further run of the algorithm.
8. **If** (one of the stopping criteria is met) **then**

   Evaluate the fitness function for each individual in the final population

   stop and **return** the best individual from the final population
9. **else**

   go to step 4
10. **End**

All Rights Reserved - Library of University of Jordan - Center of Thesis Deposit

www.manaraa.com

Algorithm 3 *depicts the steps to construct 12 kernels for GAMF*

1. **Begin**
2. **Initialize** (rotation_degree, L, σ, T)
3. Kernel_no ← 180 / rotation_degree
4. Kernel_size ← $sqrt((L+1)^2 + (2 * T + 1)^2)$
5. **do** i ← i + 1
6. **for** any point (x,y) in the kernel
7. u ← x * cos (rotation_degree) – y * sin (rotation_degree)
8. v ← x * sin (rotation_degree) + y * cos (rotation_degree)
9. **if** *((abs(u) <= T) & (abs(v) <= (L/2)))* **then**
10. K(x,y) ← $-exp(-u^2 /2*\sigma^2)$
11. rotation_degree ← rotation_degree + degree_increment
12. **until** i = kernel_no
13. **do** i ← i +1
14. **for** any point (x,y) in the kernel
15. **if** *((abs(u) <= T) & (abs(v) <= (L/2)))* **then**
16. K_i (x,y) ← K_i (x,y) – average (K_i)
17. **until** i = kernel_no
18. **Return** K
19. **End**

All Rights Reserved - Library of University of Jordan - Center of Thesis Deposit

www.manaraa.com

Algorithm 4 *depicts the image-filter procedure*

1. **Begin**
2. **Initialize** (I:input_image, K:kernels_vector, N:number_of_kernels, i)
3. **do** i ← i +1
4. I' (i) ← imfilter(I, K(i)) // convolve the image by kernel i
5. **until** i = N
6. I' ← max_at_each_pixel(I'(1), I'(2), ….., I(N))
7. **Return** I'
8. **End**

All Rights Reserved - Library of University of Jordan - Center of Thesis Deposit

www.manaraa.com

Algorithm 5 *depicts the steps required to evaluate the fitness function for one individual from the population.*

1. **Begin**
2. **Initialize** (I:input_image, H:hand_label_image, M:mask_image, rotation_degree, L, σ, T)
3. K ← Find_Kernel (rotation_degree, L, σ, T)
   // K contain 12 kernels
4. Result_image ← Image_Filter (K, I, M)
   // Result_image produced from convolution of the input image with the 12 kernels and compare all responses to get the maximum response.
5. ROCArea ← GA_ROCArea (Result_image, H)
   OR
   MA ← Find_MA (Result_image, H)
6. **Return** *ROCArea* OR *MA* as a fitness value
7. **End**

All Rights Reserved - Library of University of Jordan - Center of Thesis Deposit

www.manaraa.com

Algorithm 6 *depicts the steps needed to evaluate an area under the ROC*

1. **Begin**
2. **Initialize** (Result_image, H:hand_label_image, NoOfLevels, LevelDiv:1/NoOfLevels)
3. **Do** i ← i + LevelDiv
4. Thresholded_image ← threshold (Result_image)
5. No_of_true_pixel ← compare_image (thresholded_image, H)
6. No_of_false_pixel ← compare_image (thresholded_image, H)
7. True_Ratio_Vector ← No_of_true_pixel / no_of_vessels_pixel_in_H
8. False_Ratio_Vector ← No_of_false_pixel / no_of_non_vessels_pixel_in_H
9. **Until** i = NoOfLevels
10. area ← computeArea(False_Ratio_Vector, True_Ratio_Vector)

Return area

All Rights Reserved - Library of University of Jordan - Center of Thesis Deposit

www.manaraa.com

Algorithm 7 *depicts the steps required to calculate the MA to different thresholded images*

1. **Begin**
2. **Initialize** (I: input_image, j:threshold_level)
3. **do** j ← j + 0.05
4. Threshold_image ← threshold(I, j)
5. Accuracy_vector ← Find_accuracy(Thresholded_image)
6. **until** j = 1
7. best_threshold ← max(Accuracy_vector)
8. I' ← threshold(I, best_threshold)
9. **Return** I'
10. **End**

All Rights Reserved - Library of University of Jordan - Center of Thesis Deposit

www.manaraa.com

Algorithm 8 *depicts the steps required to calculate the accuracy for one image*

1. **Begin**
2. **Initialize** (thresholded_image, H:hand_label_image)
3. True_vessels ← compare_image(thresholded_image, H)
4. True_not_vessels ← compare_image(thresholded_image, H)
5. [M, N] ← size(thresholded_image)
6. FOV ← (M * N) – correctionFactor
7. accuracy ← (True_vessels + True_not_vessel) / FOV
8. **Return** accuracy
9. **End**

4.1 Implementation of the Optimized Matched Filter

The genetic algorithms are implemented in this thesis to optimize the parameters used by (Chaudhuri et al., 1989), which consist from three parameters: L is the length of the vessels segment that has the same orientation, σ is the spreading factor of the intensity profile, and T is the value where the Gaussian curve trails cut. The genetic algorithms take the range of these parameters to initialize the input population, and then they run until one of the stopping criteria is satisfied. As a result, the fittest individual which represent by the highest area under the ROC or by the MA will returned from the final population and coded by it's L, σ, and T in one experiments and L, σ, T, and NOK in another experiment. Then, these filter parameters are considered as the optimum filter for all images.

All Rights Reserved - Library of University of Jordan - Center of Thesis Deposit

www.manaraa.com

Since the original image may contain small noise and results in false detection that will increase the false ratio, a preprocessing stage is required before a genetic algorithm start searching for the best GMF parameters. This stage is performed by taking the green band of the RGB retinal image since it gives a sharp contrast to blood vessels, and then smoothing it by a 3 × 3 average filter to reduce such noise. After that, a genetic algorithm is run on a smoothed image to find the best GMF parameters which are used to derive the 12 kernels to apply them on the smoothed image. These corresponding responses from 12 kernels are compared and the maximum value at each pixel is retained.

Since each kernel from 12 kernels is convolved with the smoothed image, it is important to illustrate how the convolution occurs. The convolution process is performed by moving the kernel from point to point in image, where at each point, the response of the kernel at that point is calculated using a linear spatial filtering (Gonzalez and Woods, 2002). For a linear spatial filtering, the response is given by a sum of products of the kernel coefficients and the corresponding image pixels in the area spanned by the kernel. In general, for a linear filtering of an image *f* of size M × N with a kernel of size m × n is given by the expression:

$$g(x,y) = \sum_{s=-a}^{a}\sum_{t=-b}^{b} k(s,t) f(x+s, y+t) \qquad (13)$$

Where $a = (m-1)/2$ and $b = (n-1)/2$. To generate a complete filtered image, this equation must be applied for x = 0, 1, 2, ……., M-1 and y = 0, 1, 2, ….., N-1.

All Rights Reserved - Library of University of Jordan - Center of Thesis Deposit

www.manaraa.com

In a final stage, which is also called a post processing stage, two operations on the matched filtered output image are performed; smoothing and thresholding. The resulted image from the GMF is also smoothed by a 3 × 3 average filter to reduce such noise that produce from partially matching a non-vessels objects to the shape of the GMF. Then, the smoothed matched filtered output image is thresholded at the optimum threshold, which maximizing the accuracy as described in the previous section.

All Rights Reserved - Library of University of Jordan - Center of Thesis Deposit

www.manaraa.com

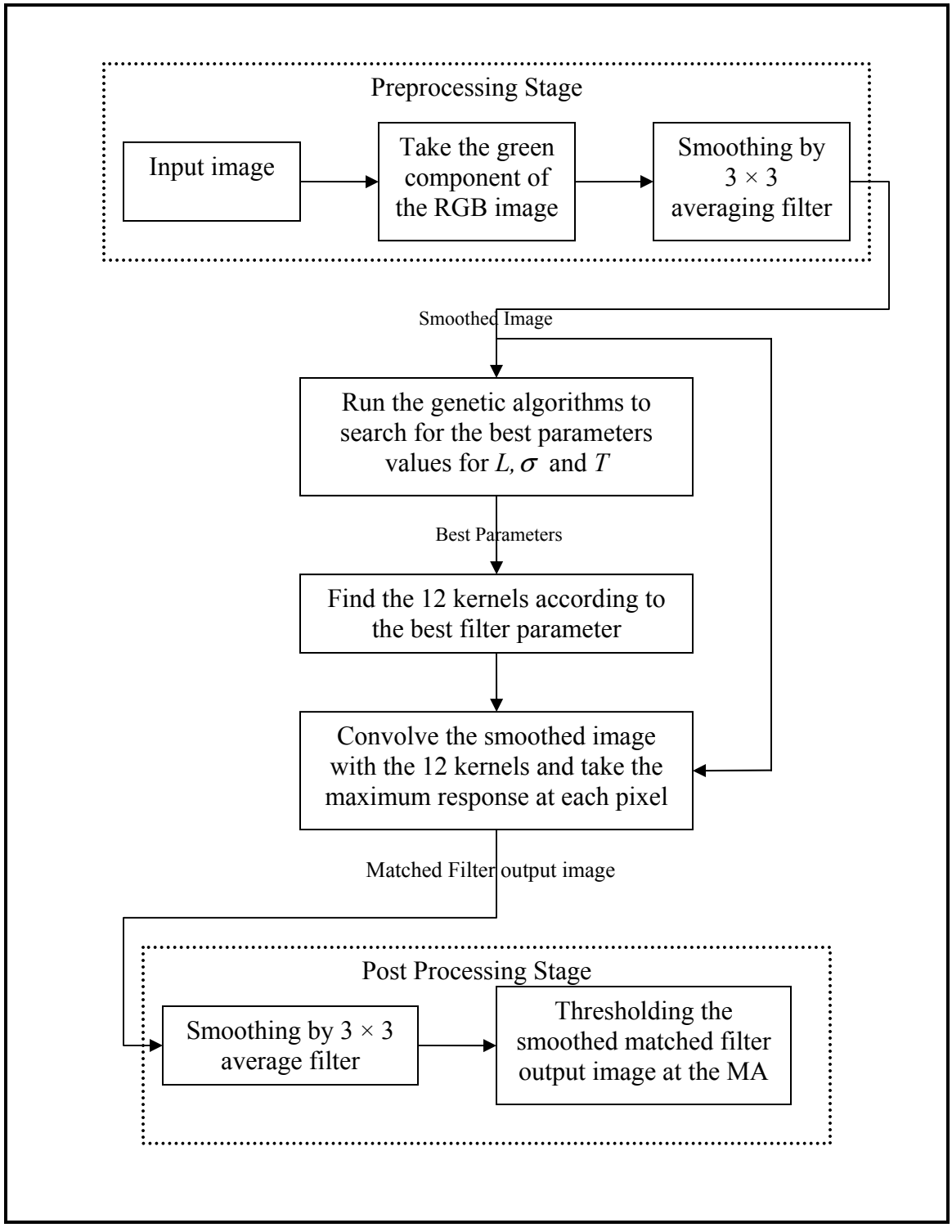

Figure 5 *Block Diagram for the GAMF optimization*

All Rights Reserved - Library of University of Jordan - Center of Thesis Deposit

www.manaraa.com

Algorithm 9 *depicts the steps required after finding the best parameter by genetic algorithm*

1. **Begin**
2. **Initialize** (I:input_image, L_{best}, σ_{best}, T_{best})
3. I_{Green} ← take_green_component(I)
4. $I_{smoothed}$ ← smooth_filter_3x3(I_{Green})
5. K ← Find_Kernel(rotation_degree, L_{best}, σ_{best}, T_{best})
6. Result_image ← image_filter($I_{smoothed}$, K)
7. I' ← threshold_at_best_threshold_level(Result_image)
8. **Return** I'
9. **End**

5. Optimization of the Second Order GMF using Genetic Algorithms

In the genetic algorithms second order GMF experiment; we also could obtain the best parameters L, σ, T, and t that result in selecting the best second order GMF parameters. Here, we will use the same genetic algorithms functions and operators that described for the GAMF experiments in the previous section. But here instead of using three input data to the fitness function, we will use four as follows $\{L, \sigma, T, t\}$, where t is an additional parameter that exist in the second order derivative of the GMF. In other words, each individuals corresponds to a second order GMF with an instance of $\{L, \sigma, T, t\}$ values is a real valued chromosome.

All Rights Reserved - Library of University of Jordan - Center of Thesis Deposit

www.manaraa.com

The fitness function for the genetic algorithm of the second order GMF is the area under the ROC, which in turn will select the fittest individual represented by the highest area under the ROC coded by its *L, σ, T,* and *t*.

5.1. Implementation of the Optimized Second Order GMF

In this thesis, also a genetic algorithms are implemented to optimize the parameters used by (Gang el al., 2002), which consist from {*L, σ, T*} parameters and *t* parameter which is added to control the width of the blood vessel diameter. Genetic algorithms take the range of these parameters to initialize the input population, and then they run until one of the stopping criteria is satisfied. As a result, the fittest individual which represent by the highest area under the ROC will returned from the final population and coded by its *L, σ, T* and *t*. Then, these filter parameters are considered as the optimum filter for all images.

Second order GMF has the same three stages of implementation of the optimized GMF in detection, but the only difference is the usage of the second order GMF equation with the new parameters found by genetic algorithm to construct the 12 kernels, Firslty, the green band of the retinal image is smoothed by 3 × 3 average filter. Then, a genetic algorithm is run to search for the best second order GMF parameters to build 12 kernels to apply them on the smoothed image. The corresponding responses from 12 kernels are compared and the maximum value at each pixel is returned. Finally, the resulting image is also smoothed by a 3 × 3 averaging filter and then is thresolded at the optimum threshold.

All Rights Reserved - Library of University of Jordan - Center of Thesis Deposit

www.manaraa.com

DISCUSSION AND ANALYSIS OF RESULTS

All Rights Reserved - Library of University of Jordan - Center of Thesis Deposit

www.manaraa.com

Discussion and Analysis of Results

An evaluation for our optimized GMF and its second order derivative is presented in this section. Depending on the used materials, the performed experiments, result analysis, performance measurements, and a comparison of the result for our optimized system with the other existing systems working in the same field are discussed.

1. Materials

The optimized GMF with the new filter parameters is tested on two databases: DRIVE (Digital Retinal Images for Vessels Extraction) database (Staal et al., 2004) and Hoover database (Hoover et al., 2000). The DRIVE database contains 40 digital retinal images, shared equally by training and test set, along with their corresponding masks and hand labels (7 of those images have some pathological changes; four of them belongs to the test set). All hand labels were obtained by an experienced pathology (Staal et al., 2004). The DRIVE images are colored RGB images were captured in a digital form using a canon CR5 nonmydriadic 3CCD camera at 45˚ field of view, where these images were obtained from a diabetic retinopathy screening program in the Netherlands each one of size 565 × 584 pixels.

The Hoover database contains 20 digital retinal images along with their corresponding hand labels (10 of those images contain some pathology). These images are also colored RGB digitize slides captured by a Topcon TRV-50 fundus camera at 35˚ field of view, where each slides were digitized to 700 × 605 pixels, 8 bits per color band.

All Rights Reserved - Library of University of Jordan - Center of Thesis Deposit

www.manaraa.com

2. Hardware and Software

The GAMF optimization is implemented using MATLAB version 7.0, and all the experiments are tested on a 1.7 GHz, 512 MB of RAM labtop running under Windows XP, Home edition.

3. Experimental Results

In genetic algorithms experiments, we must determine the number of the generations in order to guarantee the termination of the search process. This is because the GAMF does not reach to the fitness function's upper bound (which is one) due to the false response of the matched filter to the optic disc. Thus, the generations is determined to be 500, and if the search process is needed to be more than 500, the final population which produced from a favor run can be entered to be an initial population to a new run of genetic algorithm.

Different number of experiments are performed on genetic algorithms with it is a predetermined operators to search for the best parameters of the GMF and its second order derivative. Only the first image of the DRIVE database is used as input to the genetic algorithms to find these best parameters. The initial ranges of those parameters must be determined for creation of the initial population, because the performance of the genetic algorithms is dependent on a good estimation of the input data to the fitness function. The range for L is from 0 to 15, for σ is from 0 to 10, and for T is from 0 to 10. In experiments of finding the best degree of rotation, the range of *NOK* is from 6 to 72 (*i.e.* the degree of rotation is randomly chosen in the initial population between 60˚ and

All Rights Reserved - Library of University of Jordan - Center of Thesis Deposit

www.manaraa.com

2.5˚). Also, in the genetic algorithms for optimizing the second order GMF, the initial ranges of L, σ, and T are still as it is, but the value of the parameters t is picked from the range 0 to 10. Of course, these ranges are used to create just the initial population, and then the subsequent populations are created from the initial one using genetic algorithm operators (evaluation of fitness, selection, crossover, and mutation), and may result in creating input data out of ranges.

The optimized GMF and its second order derivative with those best parameters are applied to the 20 retinal images in the test set of the DRIVE database and Hoover database. The area under the ROC and Maximum Average Accuracy (MAA) are calculated for the resulting images as a performance measures. The MAA is the average accuracy for all images used in the measurements. The accuracy and the area under the ROC for one image are calculated as described in the calculation of the fitness functions in a previous section.

In all experiments, the green band is used since it gives a sharp contrast to blood vessels as proposed previously (Chaudhuri et al., 1989), (Gang et al., 2002), and (Al-Rawi et al., 2006). This also confirmed in our experiments. Verification that smoothing gives a higher area under the curve and how it can be affect on the MAA is also shown in this section. Finally, the optimized GMF and its second order derivative are compared to the other existing described detection methods for automated vessels detection.

All Rights Reserved - Library of University of Jordan - Center of Thesis Deposit

www.manaraa.com

4. Result of the GAMF Optimization

New parameters which are found by genetic algorithms using different experiments are shown in Table 1. The optimized matched filter with new proposed parameters is applied on the DRIVE database by taking the green band of the 20 retinal images in the test set to smooth them by 3 × 3 average filter. Then, the produced new filters parameters are used to construct different number of kernels to apply them on each image in the test set of the DRIVE database. After that, the resulting images are also smoothed by 3 × 3 averaging filter to threshold each image by different threshold levels to evaluate the area under the ROC and the MA.

Table 1 The new proposed filter parameters for the GMF that found by Genetic Algorithm

Filter Name	L	σ	T
Filter 1	13.6947	0.4942	5.2275
Filter 2	13.6811	1.1575	4.2361
Filter 3	13.7268	1.0485	10.5247
Filter 4	12.7252	1.2105	4.5736
Filter 5	12.5601	1.0880	4.6490
Filter 6	13.4086	0.5745	6.2866
Filter 7	8.3613	0.6119	5.7720
Filter 8	6.6902	0.5702	5.8148
Filter 9	6.6959	0.6374	5.9020
OGMF, Al-Rawi et al., (2006)	10.8	1.9	8
GMF, Chaudhuri et al., (1989)	9	2	6

The area under the ROC are computed after the true_ratio and the false_ratio are calculated at each threshold level by comparing the thresholded image with the hand_labeled image as described in algorithm 6 in a previous section. The true_ratio and

All Rights Reserved - Library of University of Jordan - Center of Thesis Deposit

www.manaraa.com

the false_ratio are shown as an example in Table 2 for the first image in the DRIVE database that thresholded at 20 threshold between 0 and 1 with increment 0.05, then the variation between these false_ratio and true_ratio are drawn in the ROC to calculate the area under this curve (as we compute the fitness function in genetic algorithm experiments) which is shown in Figure 6. But in our evaluation, instead of using 20 different threshold levels to compute the ROC, we use 1000 thresholds between 0 and 1 with increment 0.001. Figure 7 shows the area under ROC for the first image in the DRIVE database using 1000 thresholds to Filter 1. Figure 8 shows the average ROC areas for 20 images in the test set of the DRIVE database using the same filter.

Table 2 True and false ratio for the first image using Filter 1

Threshold Levels	True Ratio	False Ratio
0.00	1.0000	1.0000
0.05	0.9940	0.2849
0.10	0.9512	0.0854
0.15	0.8691	0.0396
0.20	0.7775	0.0218
0.25	0.6649	0.0118
0.30	0.5460	0.0066
0.35	0.4418	0.0039
0.40	0.3586	0.0026
0.45	0.2836	0.0018
0.50	0.2161	0.0013
0.55	0.1628	0.0010
0.60	0.1243	0.0009
0.65	0.0965	0.0008
0.70	0.0783	0.0007
0.75	0.0639	0.0006
0.80	0.0509	0.0005
0.85	0.0384	0.0005
0.90	0.0290	0.0004
0.95	0.0220	0.0004

All Rights Reserved - Library of University of Jordan - Center of Thesis Deposit

المنارة للاستشارات
www.manaraa.com

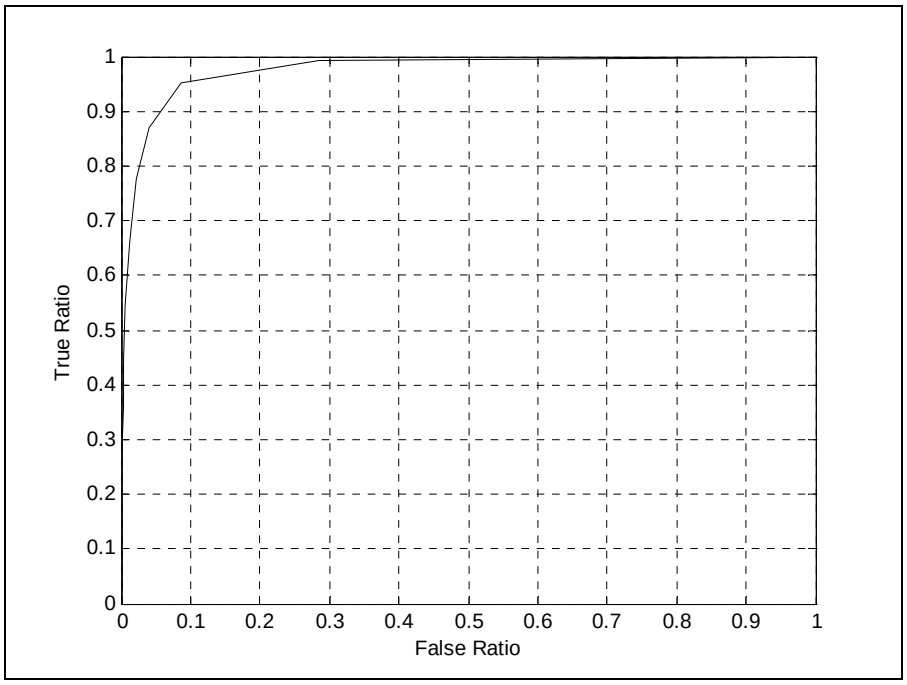

Figure 6 *The ROC area for the first image in the DRIVE database using Filter 2 under20 thresholds*

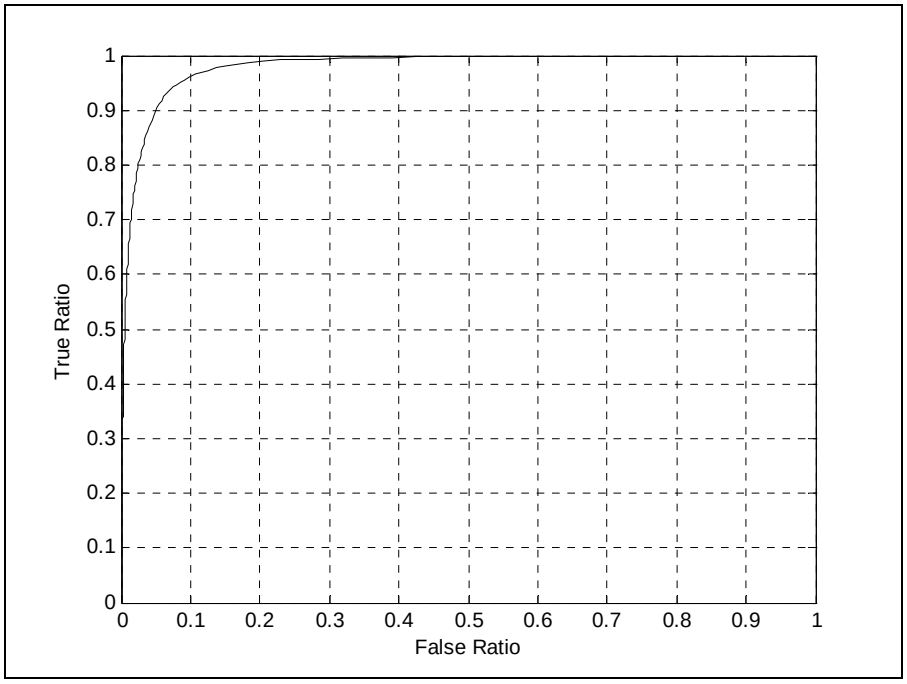

Figure 7 *The ROC area for the first image in the DRIVE database using Filter 2 under 1000 thresholds*

All Rights Reserved - Library of University of Jordan - Center of Thesis Deposit

www.manaraa.com

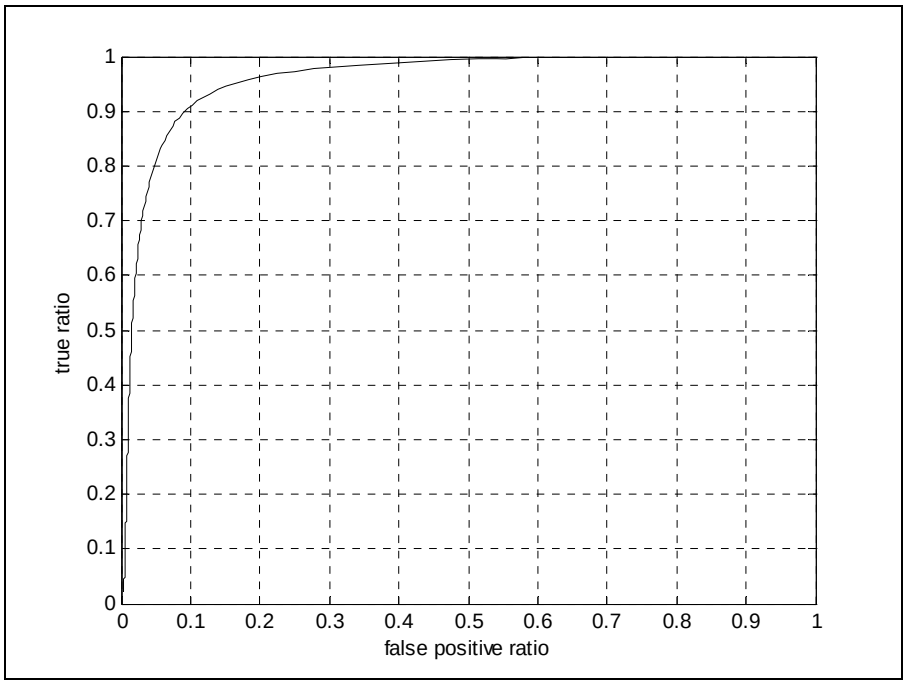

Figure 8 *Average ROC area for 20 images in the test set of the DRIVE database using Filter 2*

Results of the comparisons to (Chaudhuri et al., 1989), referred as Gaussian Matched Filter (GMF) and (Al-Rawi et al., 2006) referred as Optimized Gaussian Matched Filter (OGMF) are shown in Table 3. It is obvious that the new filter parameters found in this work gives the highest area under the ROC and MAA. Therefore they are superior matched filter parameters. These results are comparable with other detection techniques that require many steps and complex algorithms.

All Rights Reserved - Library of University of Jordan - Center of Thesis Deposit

www.manaraa.com

Table 3 Comparison of GAMF filters with the GMF and OGMF filters on a test set of the DRIVE database.

Filter Name	NOK	Kernel size	Average ROC area	MAA	Time needed to vessel detection of one image in sec
Filter 1	12	17 × 17	0.9609	0.9427	1.906
Filter 2	58	19 × 19	0.9604	0.9401	7.125
Filter 3	12	17 × 17	0.9602	0.9403	1.750
Filter 4	12	1 9 × 19	0.9596	0.9405	1.750
Filter 5	12	17 × 17	0.9593	0.9411	1.750
Filter 6	12	17 × 17	0.9591	0.9430	2.156
Filter 7	38	13 × 13	0.9578	0.9425	3.656
Filter 8	32	11 × 11	0.9572	0.9421	3.110
Filter 9	38	11 ×11	0.9596	0.9425	4.250
OGMF	12	17 × 17	0.9456	0.9369	2.140
GMF	12	19 × 19	0.8082	0.8850	1.703

Average area under the ROC and the MAA that result from applying Filter 1, 3, and 4 to 40 images in the DRIVE database are shown in Table 4.

Table 4 Area under the ROC and the MAA for the 40 image in the DRIVE database

Filter Name	Average ROC area	MAA
Filter 1	0.9592	0.9417
Filter 3	0.9586	0.9394
Filter 4	0.9580	0.9396

In a same manner, the optimized GMF is also applied on a Hoover database. Table 5 shows the average area under the ROC and the MAA for the 20 retinal images in the Hoover database for a five filters from Table1. Figure 9 shows matched filtered

All Rights Reserved - Library of University of Jordan - Center of Thesis Deposit

www.manaraa.com

output image and the corresponding thresholded one at the best threshold for the seventh image in the Hoover database and also shows the green band for the original image and the corresponding hand labeled-image.

Table 5 Area under the ROC and the MAA for the Hoover database

Filter Name	Average ROC area	MAA
Filter 6	0.9349	0.9386
Filter 1	0.9345	0.9376
Filter 4	0.9340	0.9367
Filter 5	0.9339	0.9369
Filter 3	0.9334	0.9360

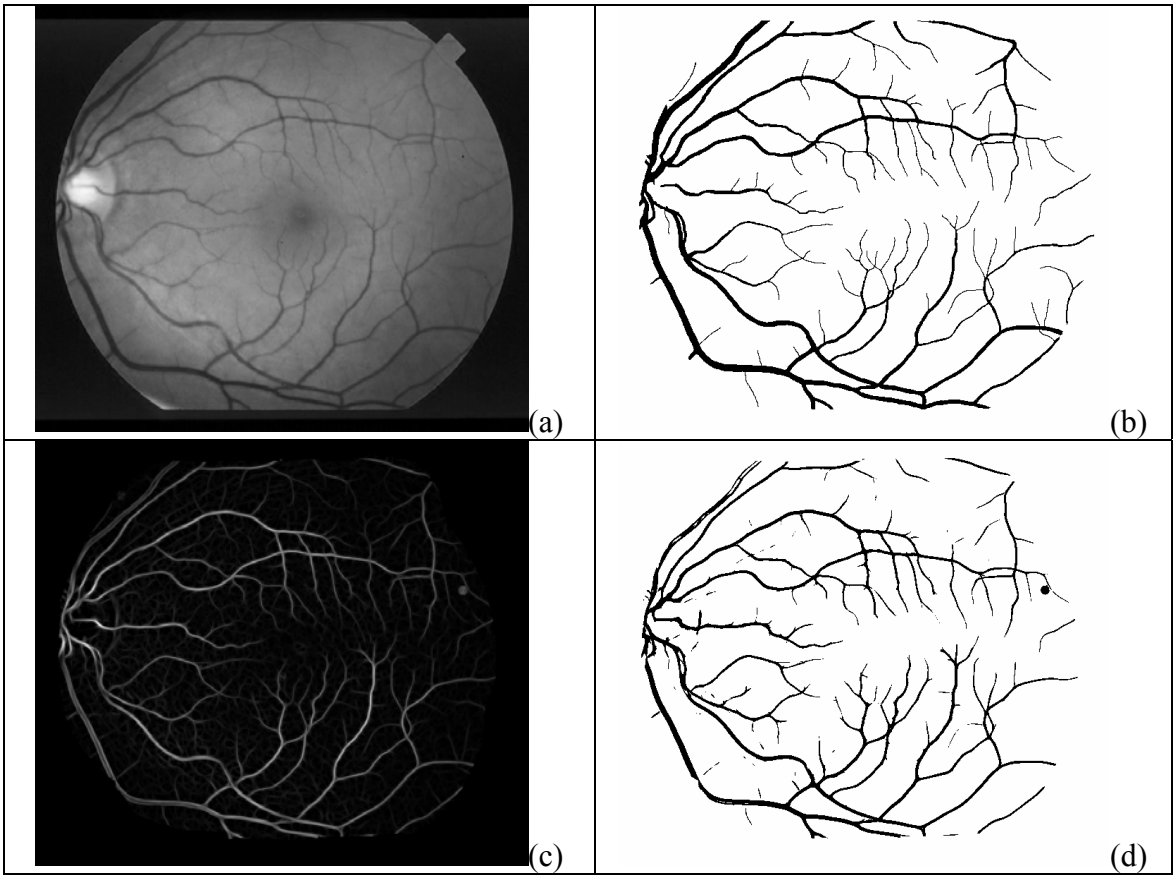

Figure 9 (a) *The green band on the original image from the 7th image in Hoover database* (b) *The hand labeled image for a.* (c) *The matched output image using Filter 1* (d) *The thresholded image at the best threshold.*

All Rights Reserved - Library of University of Jordan - Center of Thesis Deposit

www.manaraa.com

As an example for some of kernels that produced from Filter 1 and Filter 4 at different rotations are shown in Figure 10 and Figure 11 respectively. In fact, these kernels in the convolution process have real values but for displaying purpose, the weighting coefficients in the kernels are multiplied by a scale factor of 10 and rounded to their nearest integer. To illustrate how these kernels have a Gaussian shaped curve, a 3-D graph for kernels of the Filter 1 is drawn in Figure 12.

0	0	0	0	0	0	0	0	0	0	0	0	0	0	0	0	0
0	0	0	0	0	0	0	0	0	0	0	0	0	0	0	0	0
0	0	0	0	0	0	0	0	0	0	0	0	0	0	0	0	0
0	0	1	1	1	1	1	1	1	1	1	1	1	1	1	0	0
0	0	1	1	1	1	1	1	1	1	1	1	1	1	1	0	0
0	0	1	1	1	1	1	1	1	1	1	1	1	1	1	0	0
0	0	1	1	1	1	1	1	1	1	1	1	1	1	1	0	0
0	0	0	0	0	0	0	0	0	0	0	0	0	0	0	0	0
0	0	-9	-9	-9	-9	-9	-9	-9	-9	-9	-9	-9	-9	-9	0	0
0	0	0	0	0	0	0	0	0	0	0	0	0	0	0	0	0
0	0	1	1	1	1	1	1	1	1	1	1	1	1	1	0	0
0	0	1	1	1	1	1	1	1	1	1	1	1	1	1	0	0
0	0	1	1	1	1	1	1	1	1	1	1	1	1	1	0	0
0	0	1	1	1	1	1	1	1	1	1	1	1	1	1	0	0
0	0	0	0	0	0	0	0	0	0	0	0	0	0	0	0	0
0	0	0	0	0	0	0	0	0	0	0	0	0	0	0	0	0
0	0	0	0	0	0	0	0	0	0	0	0	0	0	0	0	0

(a)

0	0	0	0	0	0	0	0	0	1	0	0	0	0	0	0	0
0	0	0	0	0	0	0	1	1	1	0	0	0	0	0	0	0
0	0	0	0	0	-6	1	1	1	1	1	0	0	0	0	0	0
0	0	0	1	0	-8	-2	1	1	1	1	1	0	0	0	0	0
0	0	1	1	1	-4	-7	1	1	1	1	1	0	0	0	0	0
0	1	1	1	1	0	-8	-3	1	1	1	1	1	0	0	0	0
0	1	1	1	1	1	-2	-8	0	1	1	1	1	0	0	0	0
0	0	1	1	1	1	1	-6	-5	1	1	1	1	1	0	0	0
0	0	1	1	1	1	1	-1	-9	-1	1	1	1	1	1	0	0
0	0	0	1	1	1	1	1	-5	-6	1	1	1	1	1	0	0
0	0	0	0	1	1	1	1	0	-8	-2	1	1	1	1	1	0
0	0	0	0	1	1	1	1	1	-3	-8	0	1	1	1	1	0
0	0	0	0	0	1	1	1	1	1	-7	-4	1	1	1	0	0
0	0	0	0	0	1	1	1	1	1	-2	-8	0	1	0	0	0
0	0	0	0	0	0	1	1	1	1	1	-6	0	0	0	0	0
0	0	0	0	0	0	0	1	1	1	0	0	0	0	0	0	0
0	0	0	0	0	0	0	1	0	0	0	0	0	0	0	0	0

(b)

Figure 10 *Two kernels produced from filter1 at (a) zero degree (b) 60 degree*

All Rights Reserved - Library of University of Jordan - Center of Thesis Deposit

www.manaraa.com

0	0	0	0	0	0	0	0	0	0	0	0	0	0	0	0	0	0	0
0	0	0	0	0	0	0	0	0	0	0	0	0	0	0	0	0	0	0
0	0	0	0	0	0	0	0	3	0	0	0	0	0	0	0	0	0	0
0	0	0	0	0	0	0	3	3	3	0	0	0	0	0	0	0	0	0
0	0	0	0	0	0	-2	1	3	3	3	0	0	0	0	0	0	0	0
0	0	0	0	0	-7	-5	-2	1	3	3	3	0	0	0	0	0	0	0
0	0	0	0	-2	-5	-7	-5	-2	1	3	3	3	0	0	0	0	0	0
0	0	0	3	1	-2	-5	-7	-5	-2	1	3	3	3	0	0	0	0	0
0	0	3	3	3	1	-2	-5	-7	-5	-2	1	3	3	3	0	0	0	0
0	0	0	3	3	3	1	-2	-5	-7	-5	-2	1	3	3	3	0	0	0
0	0	0	0	3	3	3	1	-2	-5	-7	-5	-2	1	3	3	3	0	0
0	0	0	0	0	3	3	3	1	-2	-5	-7	-5	-2	1	3	0	0	0
0	0	0	0	0	0	3	3	3	1	-2	-5	-7	-5	-2	0	0	0	0
0	0	0	0	0	0	0	3	3	3	1	-2	-5	-7	0	0	0	0	0
0	0	0	0	0	0	0	0	3	3	3	1	-2	0	0	0	0	0	0
0	0	0	0	0	0	0	0	0	3	3	3	0	0	0	0	0	0	0
0	0	0	0	0	0	0	0	0	0	3	0	0	0	0	0	0	0	0
0	0	0	0	0	0	0	0	0	0	0	0	0	0	0	0	0	0	0
0	0	0	0	0	0	0	0	0	0	0	0	0	0	0	0	0	0	0

(a)

0	0	0	0	0	0	0	0	0	0	0	0	0	0	0	0	0	0	0
0	0	0	0	0	0	0	0	0	0	0	0	0	0	0	0	0	0	0
0	0	0	0	0	0	0	0	0	0	0	0	0	0	0	0	0	0	0
0	0	0	0	0	3	3	1	-4	-7	-4	1	3	3	0	0	0	0	0
0	0	0	0	0	3	3	1	-4	-7	-4	1	3	3	0	0	0	0	0
0	0	0	0	0	3	3	1	-4	-7	-4	1	3	3	0	0	0	0	0
0	0	0	0	0	3	3	1	-4	-7	-4	1	3	3	0	0	0	0	0
0	0	0	0	0	3	3	1	-4	-7	-4	1	3	3	0	0	0	0	0
0	0	0	0	0	3	3	1	-4	-7	-4	1	3	3	0	0	0	0	0
0	0	0	0	0	3	3	1	-4	-7	-4	1	3	3	0	0	0	0	0
0	0	0	0	0	3	3	1	-4	-7	-4	1	3	3	0	0	0	0	0
0	0	0	0	0	3	3	1	-4	-7	-4	1	3	3	0	0	0	0	0
0	0	0	0	0	3	3	1	-4	-7	-4	1	3	3	0	0	0	0	0
0	0	0	0	0	3	3	1	-4	-7	-4	1	3	3	0	0	0	0	0
0	0	0	0	0	3	3	1	-4	-7	-4	1	3	3	0	0	0	0	0
0	0	0	0	0	3	3	1	-4	-7	-4	1	3	3	0	0	0	0	0
0	0	0	0	0	0	0	0	0	0	0	0	0	0	0	0	0	0	0
0	0	0	0	0	0	0	0	0	0	0	0	0	0	0	0	0	0	0
0	0	0	0	0	0	0	0	0	0	0	0	0	0	0	0	0	0	0

(b)

Figure 11 *2 kernels fromFilter4 at (a) 45 degree (b) 90 degree*

All Rights Reserved - Library of University of Jordan - Center of Thesis Deposit

www.manaraa.com

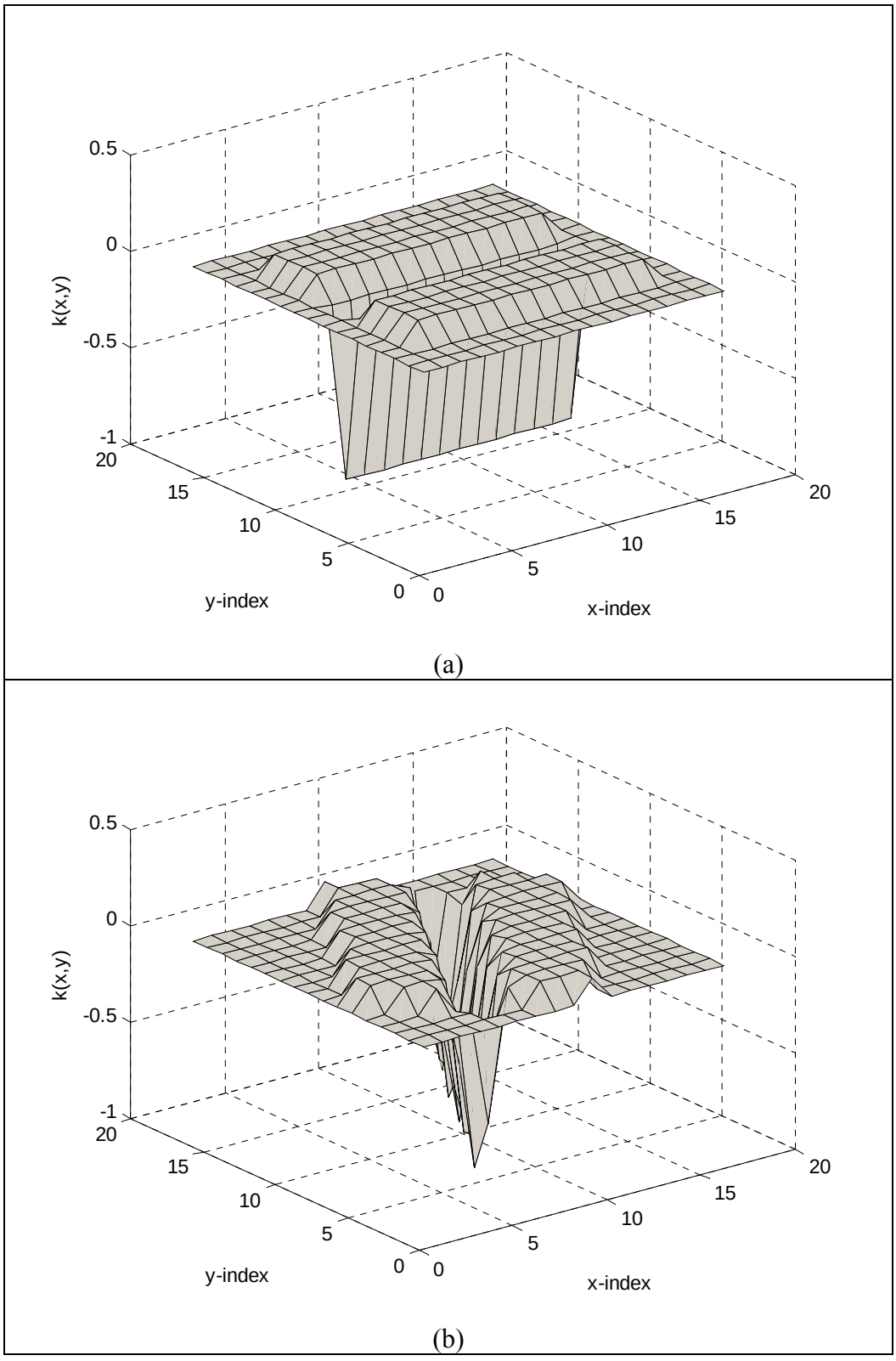

Figure 12 *A 3-D graph for the kernel produced from filter 1 at (a) zero degree (b) 60 degree of rotation which shown in figure 10*

All Rights Reserved - Library of University of Jordan - Center of Thesis Deposit

www.manaraa.com

The GMF is usually rotated by 15˚ to produce 12 kernels in different directions (Banumathi et al., 2003) and (Chaudhuri et al., 1989). We have carried out different number of experiments to verify this further. Initially: Experiments under different degrees of rotation are performed to show whether there it's better to use other degrees to rotate the GMF rather than using 15 as a degree of rotation for a certain filter parameters. These experiments are illustrated in Table 6 and Table 7 using Filter 3 and Filter 6 with the following parameters (L, σ, T) = (13.7268, 1.0485, 4.2337), and (L, σ, T) = (13.4086, 0.5745, 6.2866) respectively. Table 8 shows the comparison of the MA upon rotating Filter 6 by different angles. The last two rows in these tables show the average and standard deviation of the areas under the ROC for the 20 retinal images of the test set.

It must be noted that if *NOK* is 12 in Table 3, this means that *NOK* value is held fixed to genetic optimization and only (L, σ, T) are optimized. In addition, θ which is the degree of rotating the filter is calculated using ($\theta = 180 / NOK$) and in all forthcoming, mentioning only (L, σ, T) means that the filter is rotated via 15˚ (*NOK=12*) unless stated otherwise.

All Rights Reserved - Library of University of Jordan - Center of Thesis Deposit

www.manaraa.com

Table 6 The area under the ROC for the 20 image in the test set of the DRIVE database using Filter 6 via different degree of rotations.

Img no	θ = 60°	θ = 30 °	θ = 15°	θ = 7.5 °	θ = 5 °	θ = 2.5°
1	0.9716	0.9778	0.9780	0.9781	0.9782	0.9783
2	0.9686	0.9749	0.9751	0.9751	0.9753	0.9753
3	0.9540	0.9628	0.9633	0.9632	0.9637	0.9637
4	0.9481	0.9543	0.9546	0.9546	0.9549	0.9549
5	0.9473	0.9525	0.9526	0.9524	0.9528	0.9528
6	0.9410	0.9495	0.9498	0.9497	0.9501	0.9502
7	0.9430	0.9505	0.9509	0.9509	0.9512	0.9512
8	0.9431	0.9506	0.9511	0.9510	0.9518	0.9517
9	0.9441	0.9514	0.9516	0.9515	0.9519	0.9519
10	0.9519	0.9586	0.9589	0.9588	0.9592	0.9592
11	0.9379	0.9456	0.9460	0.9461	0.9467	0.9467
12	0.9503	0.9570	0.9574	0.9577	0.9579	0.9579
13	0.9463	0.9545	0.9547	0.9549	0.9550	0.9552
14	0.9639	0.9709	0.9709	0.9709	0.9713	0.9713
15	0.9591	0.9646	0.9650	0.9650	0.9654	0.9654
16	0.9510	0.9583	0.9584	0.9583	0.9587	0.9587
17	0.9485	0.9556	0.9555	0.9552	0.9561	0.9560
18	0.9521	0.9575	0.9579	0.9578	0.9582	0.9582
19	0.9628	0.9677	0.9678	0.9677	0.9683	0.9683
20	0.9578	0.9631	0.9634	0.9635	0.9638	0.9639
mean	**0.9521**	**0.9589**	**0.9591**	**0.9591**	**0.9595**	**0.9595**
Std	**0.0093**	**0.0088**	**0.0087**	**0.0087**	**0.0087**	**0.0087**

All Rights Reserved - Library of University of Jordan - Center of Thesis Deposit

www.manaraa.com

Table 7 The area under the ROC for the 20 image in the test set of the DRIVE database using Filter 3 via different degree of rotations.

Img no	θ = 60°	θ = 30 °	θ = 15°	θ = 7.5 °	θ = 5 °	θ = 2.5°
1	0.973	0.9801	0.9803	0.9803	0.9654	0.9669
2	0.9686	0.9756	0.9758	0.9761	0.9585	0.9592
3	0.9498	0.9615	0.9620	0.9627	0.9439	0.9452
4	0.9475	0.9552	0.9556	0.9556	0.9368	0.9371
5	0.9455	0.9525	0.9528	0.9532	0.9395	0.9404
6	0.9404	0.9493	0.9497	0.95	0.9212	0.9237
7	0.9435	0.9525	0.9531	0.9534	0.9325	0.9323
8	0.9432	0.9526	0.9529	0.9535	0.927	0.9279
9	0.944	0.9528	0.9529	0.9532	0.9314	0.9334
10	0.9509	0.9596	0.9600	0.9603	0.9452	0.9458
11	0.9382	0.9481	0.9483	0.9488	0.9243	0.9243
12	0.9481	0.9574	0.9575	0.9578	0.9382	0.9396
13	0.9443	0.9544	0.9543	0.9544	0.9309	0.9324
14	0.9625	0.9716	0.9717	0.972	0.9554	0.9564
15	0.9586	0.9657	0.9661	0.9664	0.9507	0.95
16	0.9513	0.9605	0.9604	0.9607	0.9407	0.943
17	0.948	0.9563	0.9563	0.9568	0.9264	0.9288
18	0.9524	0.959	0.9592	0.9595	0.9393	0.9415
19	0.9645	0.9707	0.9708	0.9712	0.9585	0.9592
20	0.9583	0.965	0.9652	0.9653	0.9499	0.9525
mean	**0.9516**	**0.9600**	**0.9602**	**0.9606**	**0.9408**	**0.9420**
Std	**0.0096**	**0.0089**	**0.0089**	**0.0088**	**0.0125**	**0.0124**

All Rights Reserved - Library of University of Jordan - Center of Thesis Deposit

المنارة للاستشارات
www.manaraa.com

Table 8 The MA for the 20 image in the test set of the DRIVE database using Filter 6 via different degree of rotations.

img no	θ = 60°	θ = 30 °	θ = 15°	θ = 7.5 °	θ = 5 °	θ = 2.5°
1	0.9491	0.9547	0.9548	0.9545	0.9548	0.9548
2	0.9422	0.9481	0.9483	0.9482	0.9483	0.9483
3	0.9342	0.9403	0.9406	0.9402	0.9403	0.9401
4	0.9351	0.9393	0.9394	0.9396	0.9395	0.9395
5	0.9351	0.9399	0.9404	0.9402	0.9404	0.9403
6	0.9306	0.9352	0.9353	0.9351	0.9355	0.9354
7	0.9289	0.9339	0.9344	0.9342	0.9346	0.9346
8	0.9303	0.9337	0.9341	0.9339	0.9343	0.9341
9	0.9369	0.9411	0.9408	0.9404	0.9403	0.9401
10	0.9404	0.9443	0.9447	0.9448	0.9452	0.9451
11	0.9312	0.9360	0.9359	0.9357	0.9360	0.9360
12	0.9357	0.9406	0.9412	0.9410	0.9411	0.9409
13	0.9290	0.9355	0.9360	0.9360	0.9363	0.9363
14	0.9447	0.9502	0.9501	0.9499	0.9501	0.9501
15	0.9459	0.9495	0.9497	0.9497	0.9500	0.9499
16	0.9352	0.9418	0.9420	0.9418	0.9421	0.9420
17	0.9397	0.9437	0.9437	0.9435	0.9442	0.9441
18	0.9420	0.9456	0.9457	0.9457	0.9460	0.9460
19	0.9516	0.9575	0.9573	0.9571	0.9574	0.9574
20	0.9424	0.9455	0.9461	0.9461	0.9464	0.9463
mean	**0.9380**	**0.9428**	**0.9430**	**0.9429**	**0.9431**	**0.9431**
std	**0.0067**	**0.0067**	**0.0066**	**0.0066**	**0.0066**	**0.0067**

The results in Table 6 show that when the degree of rotation is decreased, the area under the ROC is increased by a small ratio. However, this conclusion is not valid for Table 7, which shows reduction in the area under the ROC at 5° and 2.5° of rotation, and the corresponding conclusions are shown in Figure 13 and 14 that plot the average area under the ROC for the 20 DRIVE images respectively under different rotations. Therefore, the natural selection experiments of the genetic algorithms are performed to

All Rights Reserved - Library of University of Jordan - Center of Thesis Deposit

www.manaraa.com

find the best degree of rotation. The input chromosome to the genetic algorithm becomes four instead of three. The *NOK* is the fourth input data in addition to the original three parameters $L, \sigma,$ and T to become (L, σ, T, NOK). The *NOK* is the number of kernels where the degree of rotation is computed from it. Filters 2, 7, 8, and 9 which exist in Table1 are the resulting filters from these experiments.

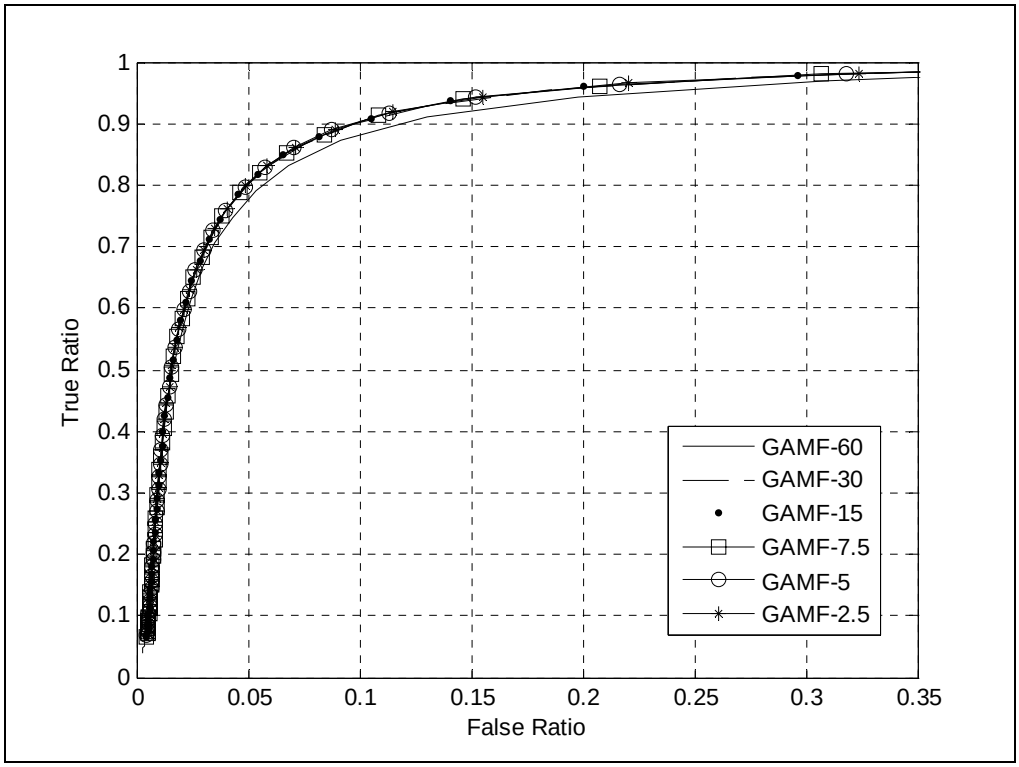

Figure 13 *The average area under the ROC for the 20 retinal images of the DRIVE database under different rotations using Filter 6.*

All Rights Reserved - Library of University of Jordan - Center of Thesis Deposit

www.manaraa.com

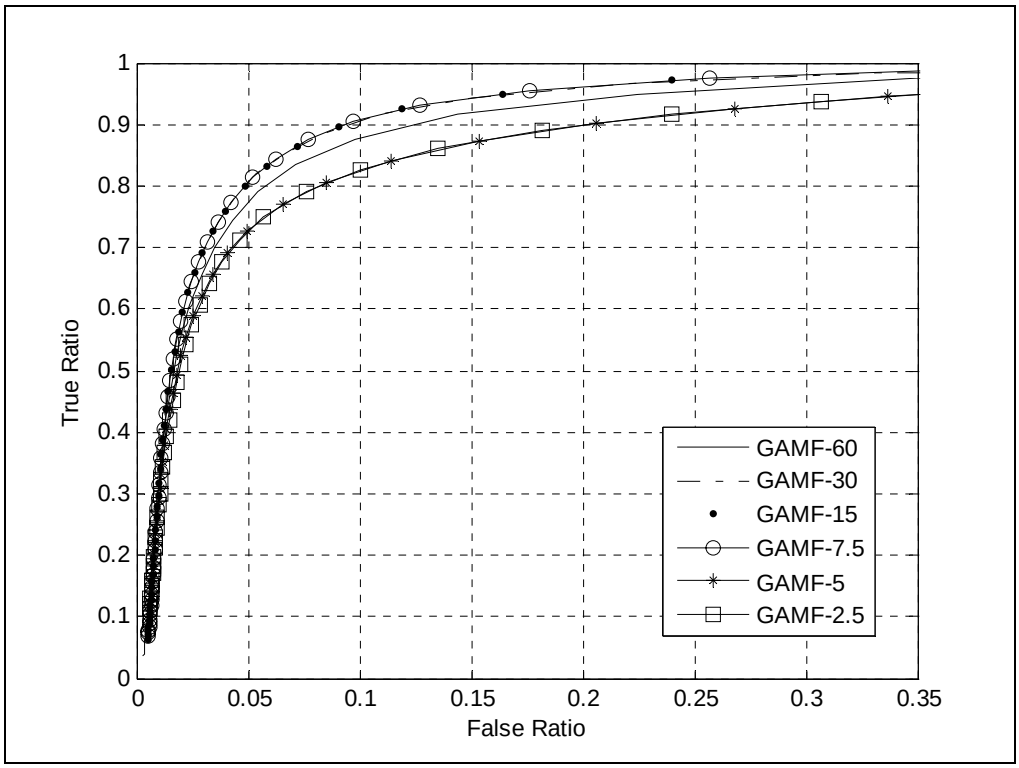

Figure 14 *The average area under the ROC for the 20 retinal images of the DRIVE database under different rotations using Filter 3.*

A clear difference can be seen between matched filter output images and the corresponding thresholded ones obtained by the optimized GMF using Filter 6 under 60˚, 30˚, 15˚, 7.5˚, 5˚, and 2.5˚ of rotations in Figure 15. This figure also shows the green band of the original image and the hand labeled image for the first image in the DRIVE database for comparison purposes. Also, using Filter 7, the matched filter output image and the corresponding thresholded one at the best threshold, are shown in Figure 15 too.

All Rights Reserved - Library of University of Jordan - Center of Thesis Deposit

www.manaraa.com

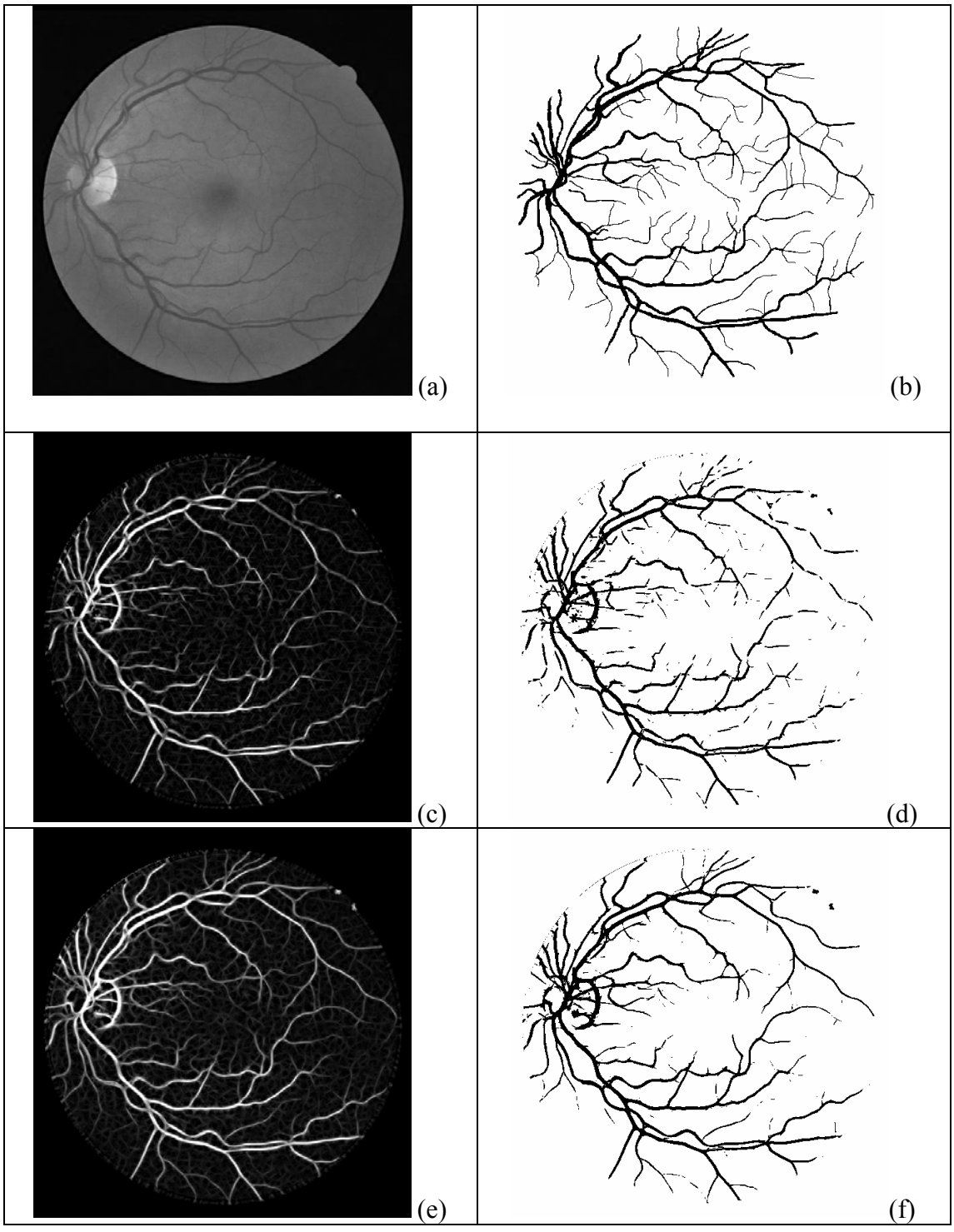

All Rights Reserved - Library of University of Jordan - Center of Thesis Deposit

www.manaraa.com

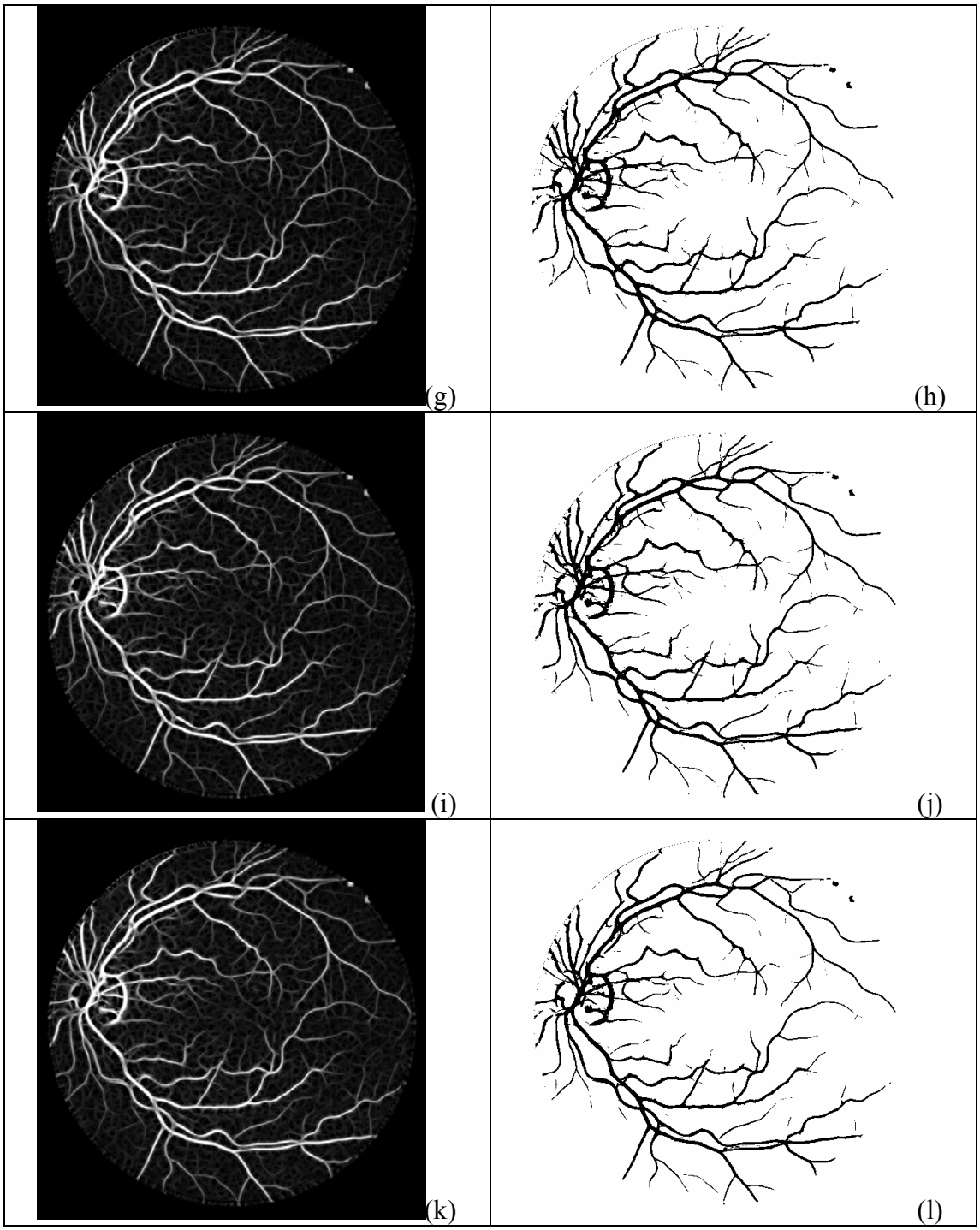

All Rights Reserved - Library of University of Jordan - Center of Thesis Deposit

www.manaraa.com

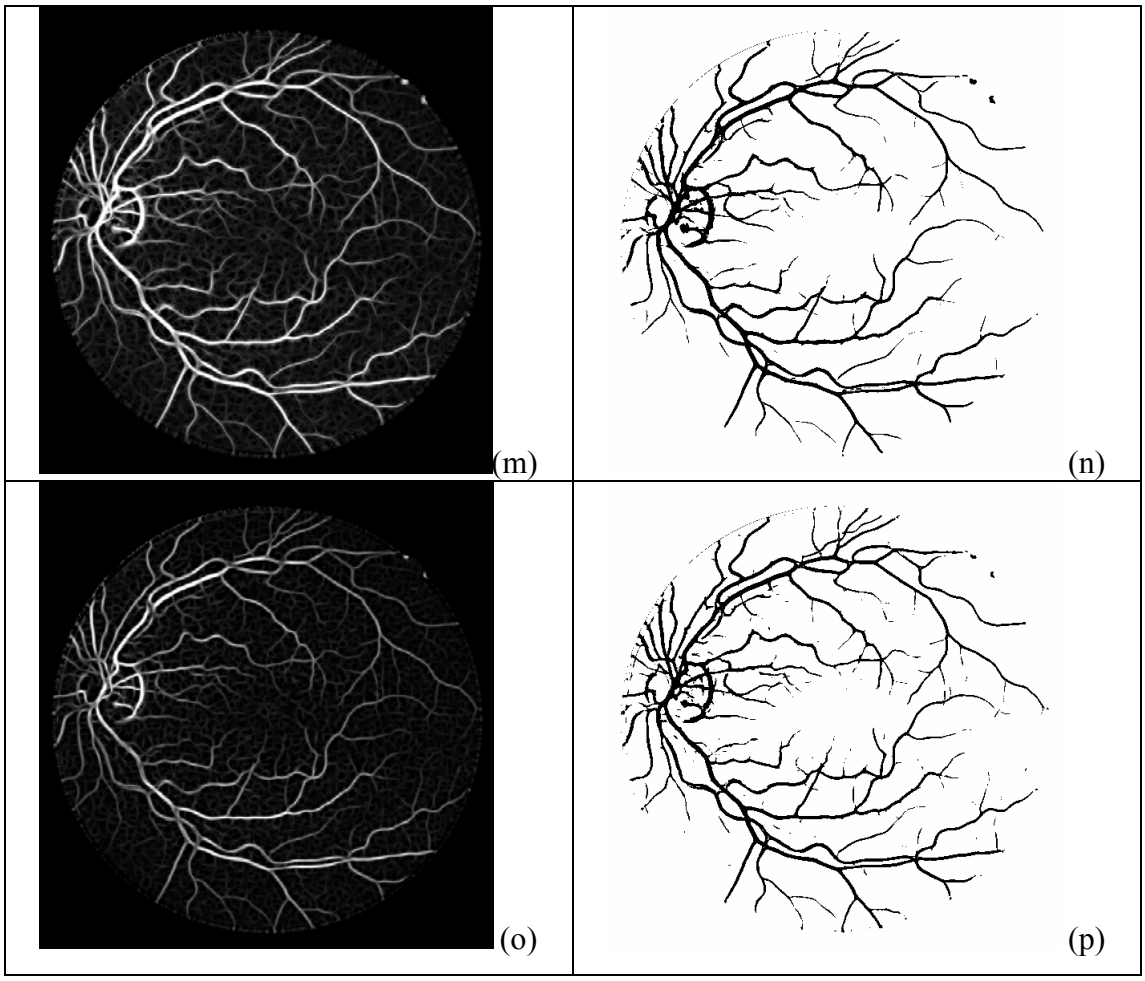

Figure 15 *(a) The green band of the original image (b) Hand labeled image. (c), (e), (g), (i), (k), and (m) Results of applying the optimized GMF with Filter 6 under these amount θ = 60˚, 30˚, 15˚, 7.5˚, 5˚, and 2.5˚ respectively and the corresponding thresholded images at the best threshold are shown in (d), (f), (h), (j), (l), and (n). (o) Result of applying the optimized GMF with Filter 7. (p) The corresponding thresholded image of (o).*

It is worth to mention that the fitness function which used to find Filter 7, 8, and 9 is the MA to obtain the best value for the *NOK* which produce the best degree of rotation that maximizing the accuracy. From this, we conclude that the filter parameters which results from the genetic algorithms that use a MA as fitness function give a lower area under the ROC. This is because while the genetic algorithm is running, it searches for the parameters that maximizing the accuracy without taking the area under the ROC into

All Rights Reserved - Library of University of Jordan - Center of Thesis Deposit

www.manaraa.com

consideration. In contrast, the genetic algorithms that have the area under the ROC as a fitness function give the highest performance in both measures.

Figure 15 (o) and (p) shows the matched filtered output image and the corresponding thresholded one at the optimum threshold using Filter 7 which produce from experiment that use a MA as a fitness function. Because our goal when finding these filters parameters is maximizing the accuracy, small vessels start to appear in the thresholded image in parallel with small amount of noises that yield to lowering the average area under the ROC as we can see in Figure 15.

In the experiment that we try to find the best degree of rotation that uses the area under the ROC as a fitness function, we got Filter 2 which has a high area under the ROC (0.9604). This filter results in constructing 58 kernels, which needs more time than other filters to apply it on one image (7.125 secs). But, Filter 1 which has the highest area under the ROC (0.9609) and constructs 12 kernels, takes shorter time (1.906 secs). This is also true for other filters, therefore, we conclude that using 15 as a degree of rotation is adequate to achieve good results.

The verification that the green band of a digital retinal image is more appropriate than other bands is shown in the below experiments. In one experiment, we implemented filter 6 with parameters (L, σ, T) = (13.4086, 0.5745, 6.2866) to each band of the retinal image. From the results shown in Table 9 we can see that the performance of the green band gives the highest area under the ROC not forgetting

All Rights Reserved - Library of University of Jordan - Center of Thesis Deposit

www.manaraa.com

that the green band has been used in genetic optimization. To be sure that this is not a learning process (a phenomena known as overfitting) on the green band, we ran an additional two different genetic optimizations on each of the red and the blue bands. In each run a different band of the first image in the DRIVE database is used as an input to the genetic optimization. Then, for comparison purpose, the resulting filter parameters from each band are applied to the corresponding bands in the 20 retinal images of the test set of the DRIVE database. As shown in Table 10, the green band has a highest area under the ROC. The Blue and the red bands are not suitable for detection of the blood vessel from the retinal images, because the blue band does not have enough details, and the red band has much noise. Therefore, the areas under the ROC for the red and blue bands are lower than the area under the ROC for the green band.

Table 9 Average area under the ROC for the 20 retinal images of the DRIVE under different bands using Filter 6

Band	Average ROC Area
Green	0.9591
Blue	0.9227
Red	0.9071

Table 10 Average area under the ROC for filters that results from genetic algorithm experiments on a Red and Blue band and comparing it to the green band using Filter 2 on a test set of the DRIVE database

Genetic Algorithm (GA) on	Filters Found by GA			Average ROC Area
	L	σ	T	
Green Band	13.6947	0.4942	5.2275	0.9609
Blue Band	20.5874	0.7678	4.6285	0.9265
Red Band	15.0804	1.0707	3.4808	0.9130

All Rights Reserved - Library of University of Jordan - Center of Thesis Deposit

المنارة للاستشارات
www.manaraa.com

Because the original image may contain some noise and could lead to false detection pre-processing and/or post-processing steps might be required to improve the results. Thus, smoothing the green band of the retinal image prior and after the application of matched filter image by using a 3×3 average filter gives a higher area under the ROC curve, Table 11 shows that. Unfortunately, smoothing as described above gives a lower MAA due to blurring small details in the retinal images that yields sometimes to loose some of small vessels.

Table 11 Differences in the average area under the ROC and MAAs that result from smoothing the green band for the test set of the DRIVE database.

Filter Name	Average ROC area without smoothing	Average ROC area with smoothing	MAA without smoothing	MAA with smoothing
Filter 6	0.9559	0.9591	0.9430	0.9377
Filter 1	0.9545	0.9609	0.9427	0.9382
Filter 4	0.9518	0.9596	0.9405	0.9380
Filter 3	0.9513	0.9602	0.9403	0.9379
Filter 5	0.9513	0.9593	0.9411	0.9383

It is very important in real world implementations to know how to automatically find the highest accuracy of the threshold image since no hand label exits. To find the best threshold that can be used to segment the matched filter output image, a good thresholding procedure is needed. A simple method is performed by calculating the accuracy at each threshold, and the threshold which gives the maximum accuracy is determined and is considered the best threshold. For all images,

All Rights Reserved - Library of University of Jordan - Center of Thesis Deposit

www.manaraa.com

the average of the best thresholds that gives the MA is calculated. This best average threshold value can then be used to automatically segment any continuous image produced by the matched filter. Using the matched filter that has the parameters (L, σ, T) = (13.4086, 0.5745, 6.2866), the best average threshold values are calculated for the 20 image of the test set of the DRIVE database, Table 12 gives the MA and the best average thresholds found.

Table 12 Determining the average threshold of the matched filter with Filter 6 for the test set of the DRIVE database.

Image number	Maximum Accuracy	Threshold at Maximum Accuracy	Accuracy at Average Threshold	Error Rate between the MA and Accuracy calculated at the Average Threshold
1	0.9548	0.3000	0.9549	0.0001
2	0.9483	0.3500	0.9480	0.0003
3	0.9406	0.2500	0.9373	0.0033
4	0.9394	0.3500	0.9394	0.0000
5	0.9404	0.2500	0.9370	0.0034
6	0.9353	0.2500	0.9323	0.0030
7	0.9344	0.3500	0.9336	0.0008
8	0.9341	0.3000	0.9341	0.0000
9	0.9408	0.2500	0.9386	0.0022
10	0.9447	0.3000	0.9444	0.0003
11	0.9359	0.4000	0.9309	0.0050
12	0.9412	0.3000	0.9412	0.0000
13	0.9360	0.3000	0.9355	0.0005
14	0.9501	0.3500	0.9490	0.0011
15	0.9497	0.4500	0.9435	0.0062
16	0.9420	0.3000	0.9417	0.0003
17	0.9437	0.3000	0.9439	0.0002
18	0.9457	0.3500	0.9458	0.0001
19	0.9573	0.3000	0.9575	0.0002
20	0.9461	0.3000	0.9455	0.0006
Mean	**0.9430**	**0.3150**	**0.9417**	**0.0013**
Standard Deviation	**0.0066**	**0.0516**	**0.0072**	**0.0018**

All Rights Reserved - Library of University of Jordan - Center of Thesis Deposit

www.manaraa.com

Table 13 shows the mean and the standard deviation of the MA, best thresholds, accuracy at the best average threshold, and the error rate between the MA and accuracy calculated at the best average threshold for different filter parameters as given in Table 1 of the 20 images of the test set of the DRIVE database.

Table 13 The difference in MAA between thresholding at the best threshold and thresholding at the average threshld.

Filter Number	Maximum Accuracy	Average Threshold at Maximum Accuracy	Accuracy at Average Threshold	Error Rate between the MA and Accuracy calculated at the Average Threshold
Mean(Filter1)	0.9401	0.3675	0.9389	0.0013
STD (Filter1)	0.0067	0.0613	0.0072	0.0005
Mean(Filter2)	0.9427	0.2575	0.9416	0.0012
STD (Filter2)	0.0068	0.0438	0.0074	0.0005
Mean(Filter3)	0.9403	0.3400	0.9391	0.0011
STD (Filter3)	0.0068	0.0576	0.0072	0.0004
mean(Filter4)	0.9405	0.3650	0.9392	0.0013
STD (Filter4)	0.0068	0.0587	0.0072	0.0004
mean(Filter5)	0.9411	0.3500	0.9398	0.0012
STD (Filter5)	0.0068	0.0487	0.0072	0.0005
mean(Filter6)	0.9430	0.3150	0.9417	0.0013
STD (Filter6)	0.0066	0.0516	0.0072	0.0006
mean(Filter7)	0.9425	0.2175	0.9416	0.0009
STD (Filter7)	0.0075	0.0373	0.0077	0.0002
mean(Filter8)	0.9421	0.1650	0.9413	0.0008
STD (Filter8)	0.0078	0.0235	0.0080	0.0001
mean(Filter9)	0.9425	0.1700	0.9417	0.0009
STD (Filter9)	0.0076	0.0299	0.0079	0.0003

As can be seen in Table 13, Filter 1 is chosen as the best filter since it gives the highest average ROC area and MAA among other matched filters, though some might choose Filter 6.

All Rights Reserved - Library of University of Jordan - Center of Thesis Deposit

www.manaraa.com

The Difference between thresholding the matched output images at the best threshold and at the best average threshold are illustrated in Figure 16 for the first five images in the DRIVE database. As we note, there is no difference between these images, therefore we can use the best average threshold to automatically threshold any image produced by the matched filter.

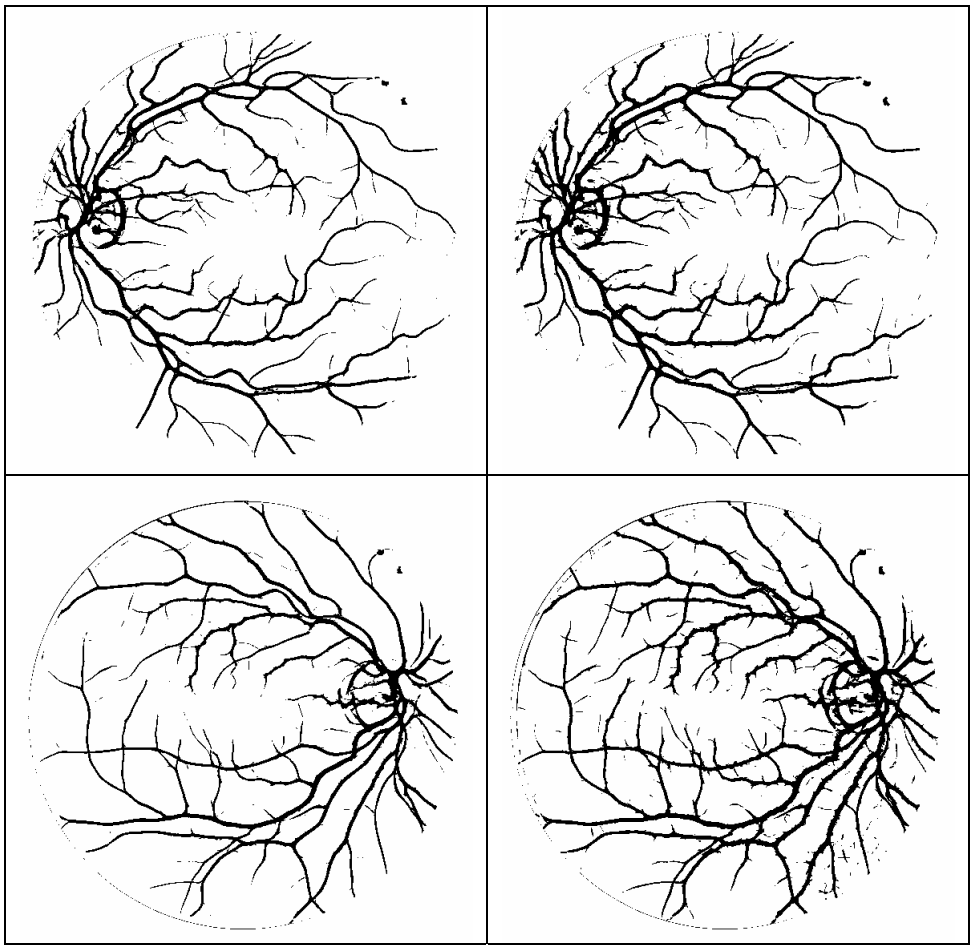

All Rights Reserved - Library of University of Jordan - Center of Thesis Deposit

www.manaraa.com

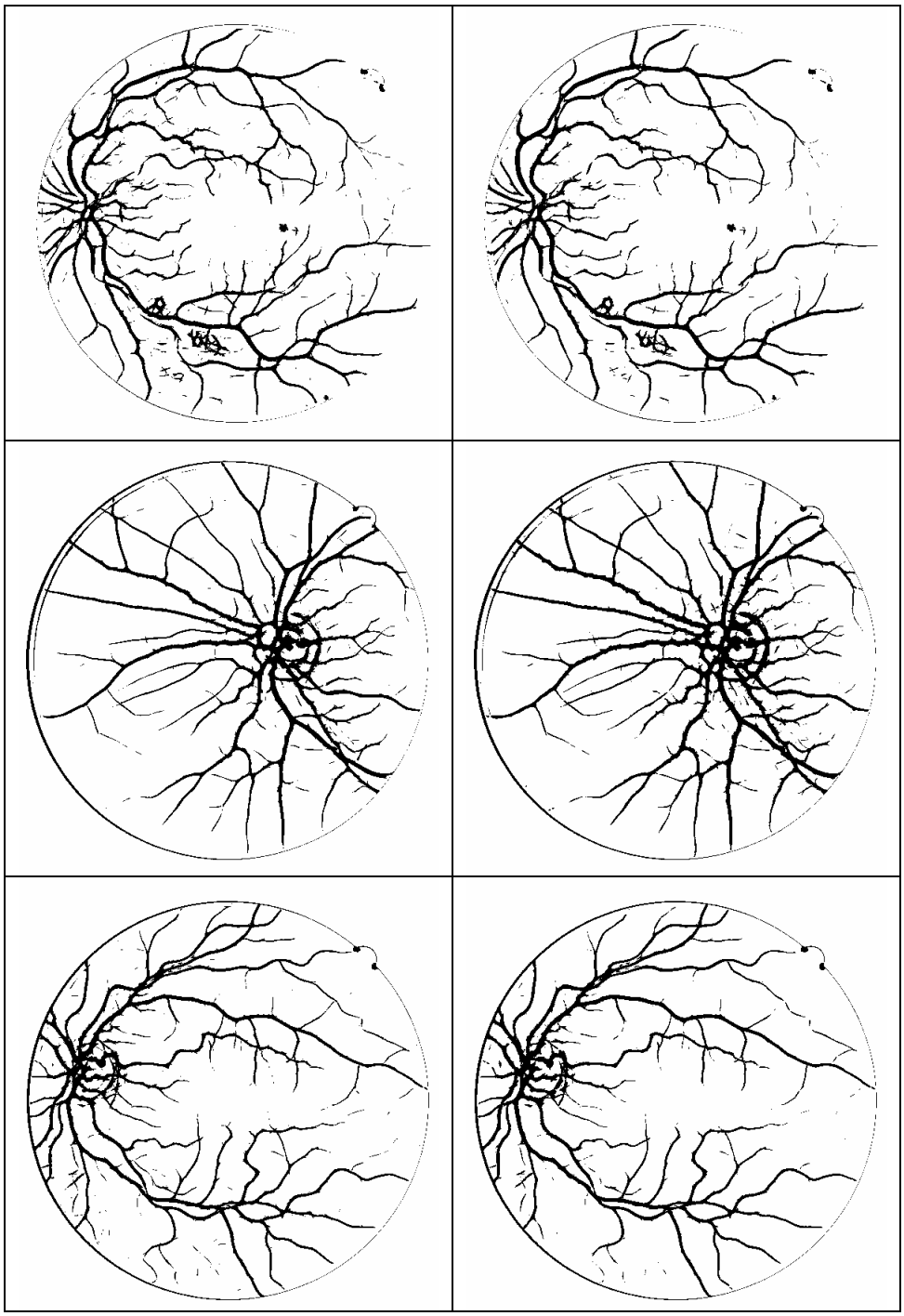

Figure 16 *The Difference between thresholding the matched output images at the optimum threshold* (in the first column) *and at the average threshold (0.2575) of the Filter 1* (in the second column) for the first five images in the DRIVE database.

All Rights Reserved - Library of University of Jordan - Center of Thesis Deposit

www.manaraa.com

All the previous results and experiments are performed on the bitmap images (that have an extension .BMP). This kind of images gives a higher average area under the ROC and MAA than using JPEG images. The results of using JPEG images for computing an average area under the ROC and MAA for all filters in Table 1 are exist in Appendix A. Also the results of applying the filter 6 on components other than the green band gives a higher average area then using BMP images.

5. Results of the Second Order GMF Optimization

Optimizing the second order GMF consists of two phases of experiments; Firstly, experiments on a genetic algorithms to find better set of $\{L, \sigma, T, t\}$ parameters are conducted on the first image of the DRIVE database. Results of these experiments are shown in Table 14. We achieve the highest ROC with Filter 10 and the ROC diagram for this filter on 20 retinal images in the test set of the DRIVE database is shown in Figure 17. The matched filter output image and the corresponding thresholded one at the best threshold by Filter 10 are shown in Figure18.

Table 14 The new proposed filter parameters for the second order GMF that found by Genetic Algorithm

Filter Name	L	σ	T	t	NOK	Average ROC area	MAA
Filter 10	14.9781	1.3558	7.3223	1.4395	21 × 21	0.9616	0.9405
Filter 11	15.3362	1.5619	7.6672	5.5482	21 × 21	0.9609	0.9398
Filter 12	12.6243	1.0202	5.4239	-6.3232	17 × 17	0.9604	0.9372
Filter 14	17.2832	1.6184	16.7462	-16.9825	23 × 23	0.9602	0.9367
Filter 15	17.3297	1.6530	14.3777	-8.9212	23 × 23	0.9601	0.9384
Filter 13	20.4177	1.0921	4.372	3.1493	25 × 25	0.9599	0.9384

All Rights Reserved - Library of University of Jordan - Center of Thesis Deposit

المنارة للاستشارات
www.manaraa.com

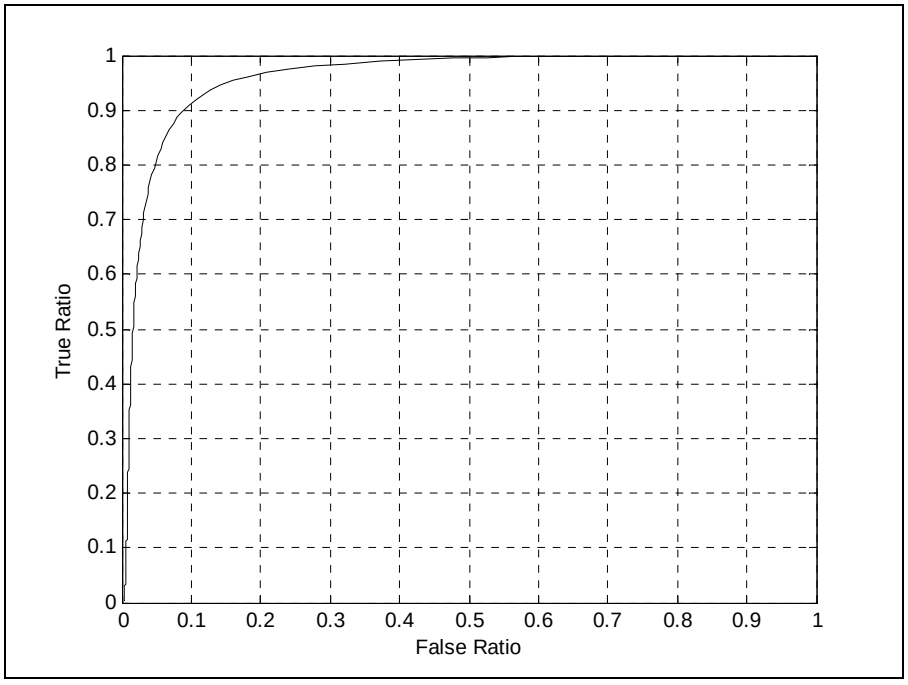

Figure 17 *Average ROC area for 20 images in the test set of the DRIVE database using Filter 10.*

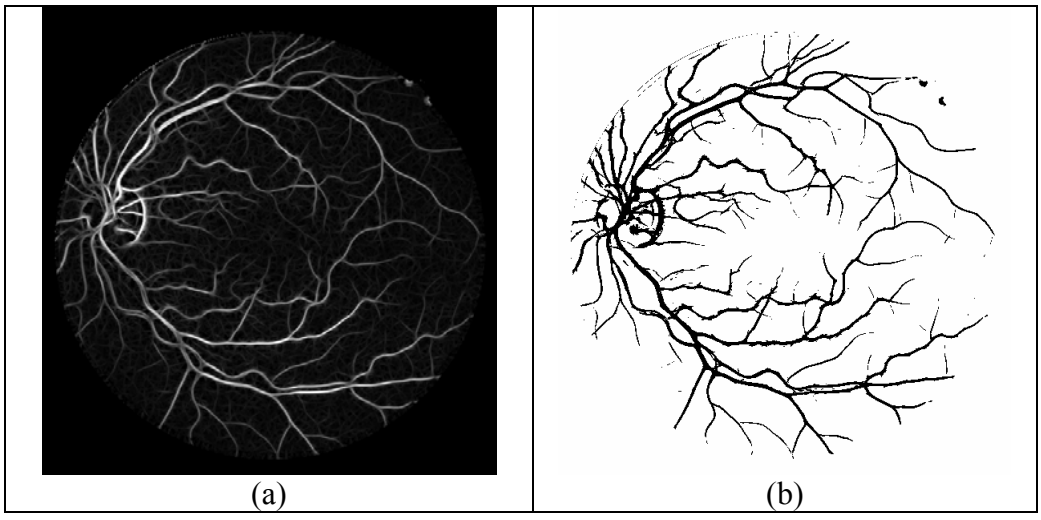

Figure 18 *(a) Result of applying the optimized second order GMF using Filter 10 (b) the corresponding thresholded image at the best threshold.*

The results shown in Table 15 are different from the results of (Gang et al., 2002). They didn't determine certain values for σ that exist in the second order GMF to wok

All Rights Reserved - Library of University of Jordan - Center of Thesis Deposit

www.manaraa.com

with it, where the values of σ was adaptively adjusted according to the vessel width in the detection, which consider a hard work. Therefore, we found a specified value for σ with a combination of *L*, *T*, and *t* as in Table 14.

Another experiments are conducted on a genetic algorithm to find better value for {*L, T*} where the value of *t* is set as proposed by (Gang et al., 2002) and we set a different scale of σ as {0.5, 1, 1.5, 2.5}. These experiments give an acceptable area under the ROC but give lower accuracy. However, (Gang et al., 2002) didn't mention in their experiments what the values were used for σ or at least what the initial values, and they achieve 94.3% of detection for the blood vessels without using standard databases. The results of our experiments on a genetic algorithm are shown in Table 15.

Table 15 New parameters for {*L, T*} while t = 3. 5 and the values of σ are {0.5, 1, 1.5, 2.5} for the second order GMF on the test set of the DRIVE database.

L1	L2	L3	L4	T1	T2	T3	T4	Average ROC area	MAA
19.7106	61.9359	21.3867	63.7904	7.0872	22.3909	4.9152	0.0221	0.9584	0.9378
10.9506	24.1763	23.5337	42.9453	28.2158	5.3594	14.6095	13.3025	0.9565	0.9300

The detection of blood vessels using the GMF with new filter parameters is good enough to give an acceptable accuracy of detection, because the second order GMF give more false response to the optic disc other than the GMF. Also results of applying the second order GMF to the JPEG images are shown in Appendix A.

All Rights Reserved - Library of University of Jordan - Center of Thesis Deposit

www.manaraa.com

6. A Comparison with Other Detection Techniques

A comparison between vessels detection methods is performed to show where the performance of the optimized matched filter and its second order derivative by genetic algorithm stands with respect to other detection algorithms. The comparison depends on the area under the ROC and the MAA, where the test set of the DRIVE database are used for evaluating the accuracy of the methods. Figure 19 shows the average areas under the ROC for the 20 DRIVE images using nine different methods. GMF is the original Gaussian Matched Filter with its original parameters (L, σ, T) = (9, 2, 6) as proposed by (Chaudhuri et al., 1989). GAMF is the optimized Gaussian matched filter by genetic algorithm with parameters (L, σ, T) = (13.6947, 0.4942, 5.2275) which is Filter 1 in Table 1. OGMF is the Optimization Gaussian Matched Filter by (Al-Rawi et al., 2006) using (L, σ, T) = (10.8, 1.9, 8).

All Rights Reserved - Library of University of Jordan - Center of Thesis Deposit

www.manaraa.com

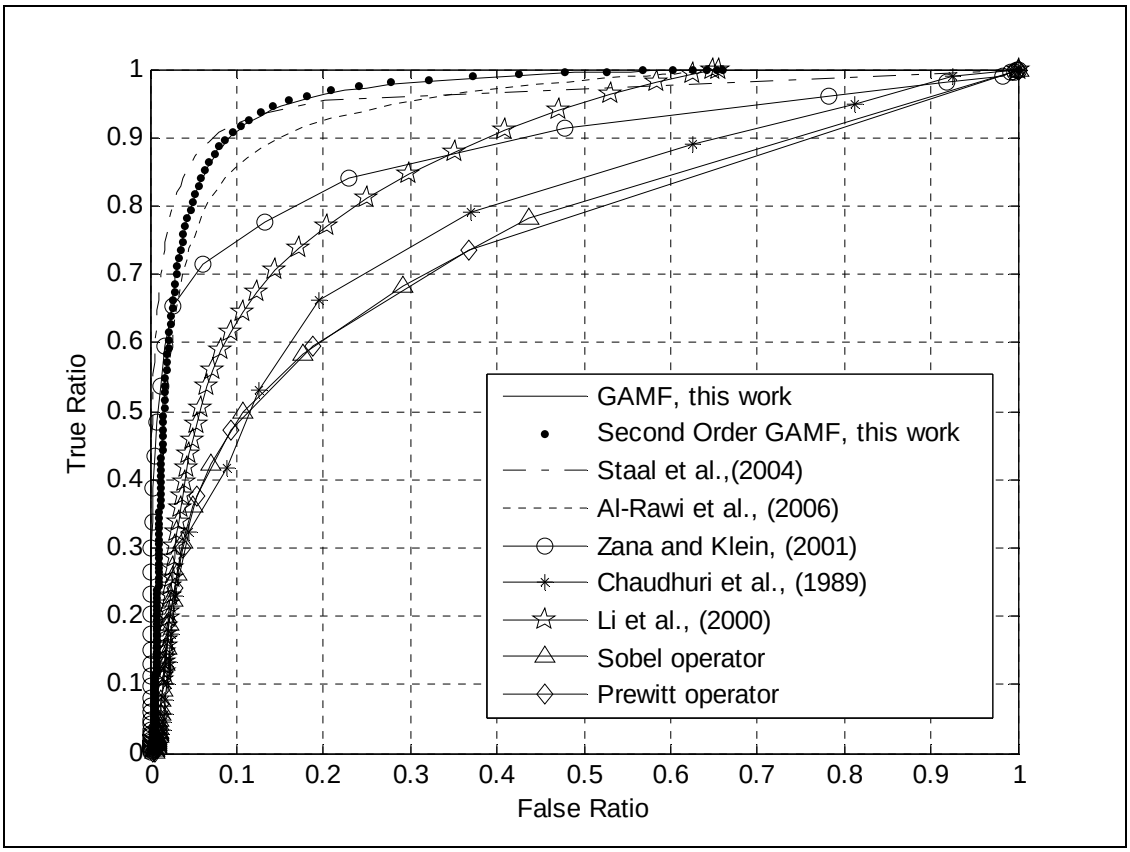

Figure 19 *Average area under the ROC for 20 images in the test set of the DRIVE database for nine different methods.*

As we notice in Figure 19, the (Staal et al., 2004) method has a higher area under the ROC when the false ratio is less than 0.11; otherwise, our algorithms (GAMF and the Second order GAMF) has a higher area. This is because the false response of a GMF and its second order derivative to the optic disk is higher than that of the Staal's, which they used a supervised method that computes many feature vectors to classify vessel from non-vessel pixels.

An overview of the comparison between the previous methods and the proposed GAMF is shown in Table 16. All the average ROC areas and the MAAs described in Table 16 are found by our programs and not adopted from other papers. Matched filtered

All Rights Reserved - Library of University of Jordan - Center of Thesis Deposit

www.manaraa.com

output images for the GMF and the OGMF methods are found by entering its parameters as an input to the GMF program. The output images from Kirsh's (Li et al., 2000), Sobel, and Prewitt operators are found by applying its filters bank to the green band of the retinal images. It is worth to mentioning that the filtered output images from (Zana and Klein, 2001) and (Staal et al., 2004) methods are downloaded from the website (http://www.isi.uu.nl/Research/Databases) and used to compute the ROC area and the MAA. These images and the corresponding thresholded ones at the optimum threshold are shown in Figure 20.

Table 16 Comparison of different methods with the improved matched filter and its second order derivative using 20 images in the test set of the DRIVE database using 50 different threshold levels.

Vessel Detection Method	Average ROC area	MAA	Time needed to vessel detection of one image in sec
GAMF (Filter 2, this work)	0.9609	0.9427	1.906 seconds on a 1.7 GHz, centrino
Second order GAMF, (Filter 10 this work)	0.9616	0.9405	2.515 seconds on a 1.7 GHz, centrino
OGMF, Al-Rawi et al., (2006)	0.9456	0.9369	2.140 seconds on a 1.7 GHz, centrino
GMF, Chaudhuri et al., (1989)	0.8082	0.8850	1.703 seconds on a 1.7 GHz,, centrino
Staal et al., (2004)	0.9587	0.9547	900 seconds on a 1-GHz PC
Zana and Klien, (2001)	0.9174	0.9439	NA
Kirshes, Li et el., (2000)	0.8692	0.8977	0.64 seconds on a 1.6 GHz, centrino
Sobel operator	0.7540	0.8947	0.26 seconds on a 1.7 GHz, centrino
Prewitt operator	0.7468	0.8956	0.28 seconds on a 1.7 GHz, centrino

These output images from different segmentation methods are used to compute the ROC areas and the MAA. Due to differentiations in the levels of and in other steps (like smoothing, ….) to the output images from segmentation methods which used by our

All Rights Reserved - Library of University of Jordan - Center of Thesis Deposit

www.manaraa.com

program and that used in author's programs, there is a small difference between the values of the average ROC areas and MAA which are existed in our research and those values which present in the author's researches.

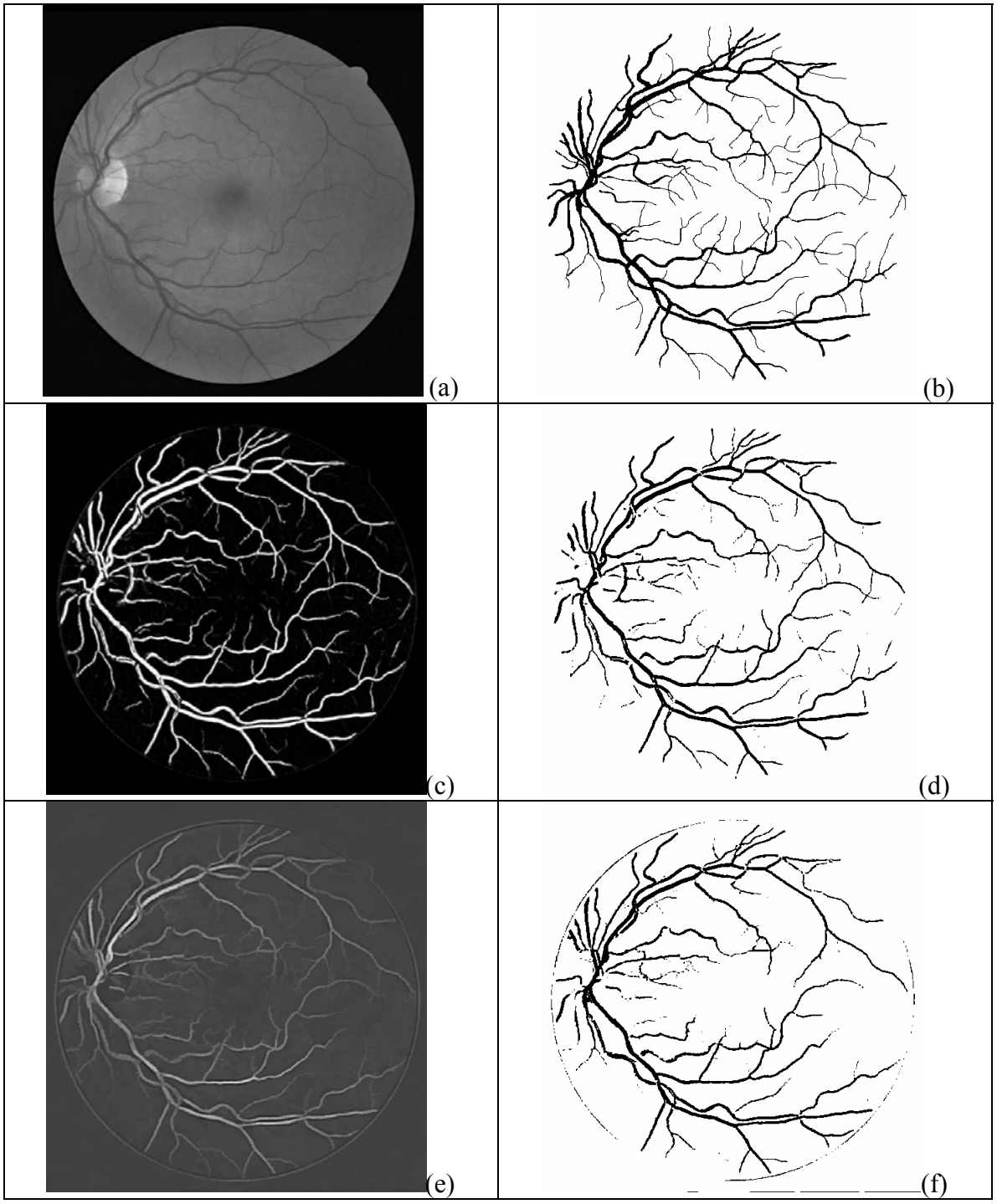

All Rights Reserved - Library of University of Jordan - Center of Thesis Deposit

www.manaraa.com

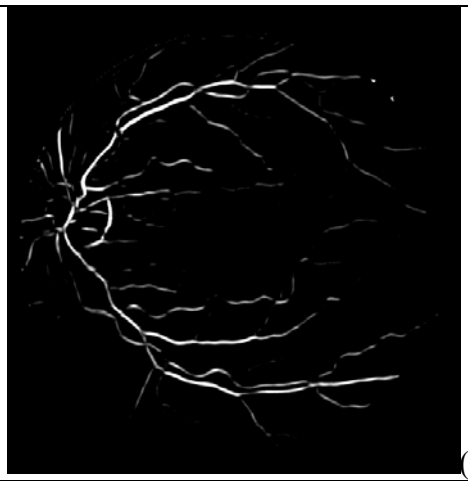
(g)

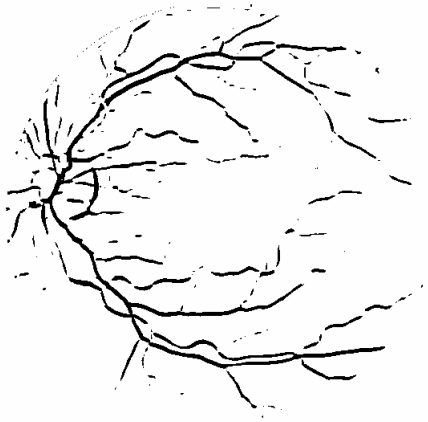
(h)

(i)

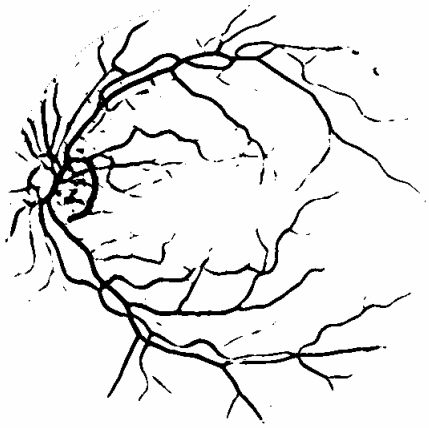
(j)

(k)

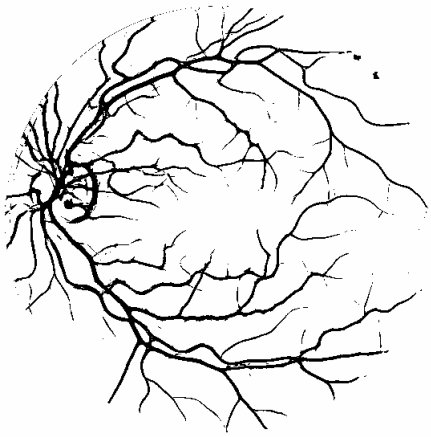
(l)

All Rights Reserved - Library of University of Jordan - Center of Thesis Deposit

www.manaraa.com

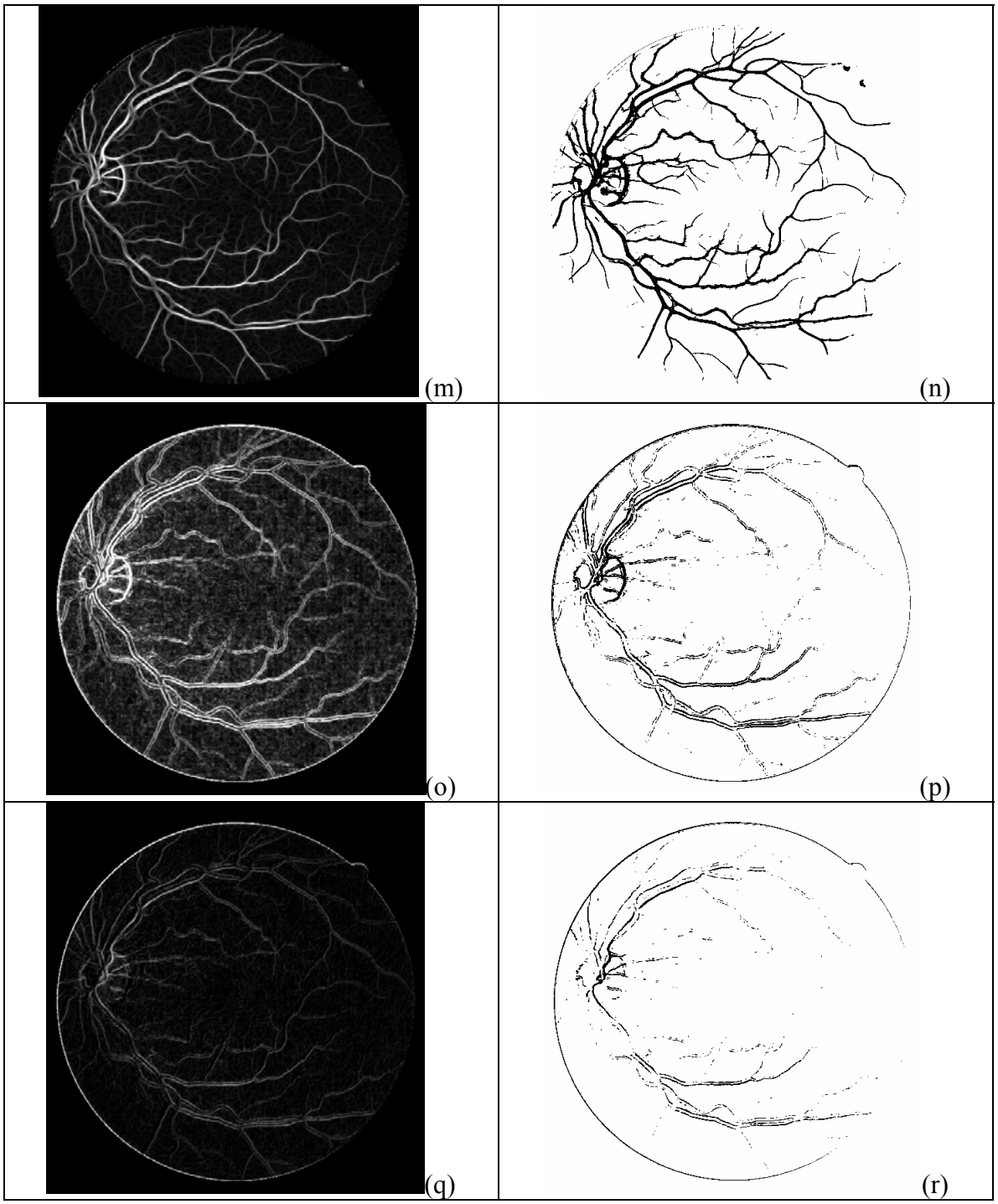

Figure 20 The output image from different segmentation methods and the corresponding thresholded *ones (a) The green band of the original image. (b) Hand labeled image. (c) and (d) Staal et al., method. (e) and (f) Zana and Klien method. (g) and (h) GMF method by Chaudhuri et al. (i) and (j) OGMF method by Al- Rawi et al. (k) and (l) GAMF. (m) and (n) second order GAMF. (o) and (p) Li et al. method. (q) and (r) Sobel method.*

All Rights Reserved - Library of University of Jordan - Center of Thesis Deposit

www.manaraa.com

The results of applying the GMF, OGMF, and GAMF to the whole DRIVE and Hoover database are shown in Appendix B, and Appendix C respectively. The original 20 images in the test set of the DRIVE database are shown in Figure 26 in Appendix B. The comparison between the hand labeled images with segmented images using the GMF, the OGMF, and the GAMF (Filter 1) methods at the best threshold for 20 images in the test set of the DRIVE database are shown in Figure 27. While Figure 28 shows a comparison between the segmented images at the best threshold with that thresholded at the best average threshold for the GAMF method using Filter 6.

The original 20 images of the Hoover database are shown in Figure 29 in Appendix C. The comparison between the hand labeled images, and the results of segmentation using the GMF, the OGMF, and the GAMF (Filter 1) methods at the best threshold for images in the Hoover database are shown in Figure 30. Figure 30 shows a comparison between the segmented images at the best threshold with that thresholded at the best average threshold for the GAMF method using Filter 6.

All Rights Reserved - Library of University of Jordan - Center of Thesis Deposit

www.manaraa.com

CONCLUSIONS AND FUTURE WORKS

All Rights Reserved - Library of University of Jordan - Center of Thesis Deposit

www.manaraa.com

Conclusions and Future Work

1. Conclusions

In this thesis, an improvement on the response and the performance of the matched filter and its second order derivative has been achieved by proposing superior filter parameters. Genetic algorithms have been used to search the fittest Gaussian matched filter parameters by comparing a detected-image with a hand labeled-image of the first image in the DRIVE database to calculate the area under the ROC or the MA which are considered as a fitness functions. Many genetic algorithms experiments have been performed resulting in many filters each correspond to the set (L, σ, T). Further evaluations shows that the filter with parameters (L, σ, T) = (13.6947, 0.4942, 5.2275) and its kernels rotated by 15˚ gives the highest area under the ROC. The time it requires to apply is short (1.906 seconds) compared to other filters. Using genetic algorithms, experiments have been carried out on the components of the retinal image other than the green band and showed that the green band gives the best results.

- Experiments under different degrees of rotations showed that rotating the matched filters by 15˚ and 30˚ is adequate to achieve good results in a minimal time.
- All filters could not detect small vessels to an accurate degree.
- All the Gaussian matched filters obtained via genetic algorithms outperform previous matched filters with empirical parameters estimation and it is comparable to the best known vessel detection technique.

All Rights Reserved - Library of University of Jordan - Center of Thesis Deposit

www.manaraa.com

- Performing smoothing with an average filter on each retina image gives higher ROC area but results in lowering MAA due to blurring small details in the retinal images which results in lose of image fine details.
- Using the area under the ROC as a fitness function is better than using the MA.

One of the astonishing results is that the value of σ, which determines the spread of the Gaussian of the matched filter, is less than one (sometimes near 0.5) in most of the performed optimization experiments. This contradicts the $\sigma = 2$ value originally appeared in the work of Chaudhuri et al., (1989) and $\sigma = 1.9$ that appeared in the work of Al-Rawi et al., (2006).

In this thesis, we could achieve new parameters that optimized the response of the matched filter, but the false response of the optic disc still present as unsolved weak point (which reduces the MAA) that needs further investigation and studies to solve it.

2. Future Work

Since till now no one automated segmentation technique could achieve accurate results as those of the manual one, room is still open for further improvements. As a future work we recommend that:

- Reducing the effect of the false response of the matched filter to the optic disc and other lesions in retinal images by training a certain classifier after applying the optimized matched filter to classify a vessel from non vessel pixels.

All Rights Reserved - Library of University of Jordan - Center of Thesis Deposit

www.manaraa.com

- Developing an automated system to analyze the retinal images and considers the optimized matched filter as an initial task for this system.
- Applying the genetic algorithm to find better filter parameters if someone like to apply a matched filter to detect blood vessels in other parts in human body.
- Modifying the matched filter to detect small vessels.

All Rights Reserved - Library of University of Jordan - Center of Thesis Deposit

www.manaraa.com

References

Abedel-Azeem, S., and Auda, G., (2002). **"An Algorithm for Enhancing Retinal Vessel Detection Filters,"** Proceedings of the Medical Image Understanding and Analysis Conference, the University of Portsmouth, UK, July 22-23.

Ahrens, B., (2005)**. "Genetic Algorithm Optimization of Superresolution Parameters,"** Proceedings of the 2005 Conference on Genetic and Evolutionary computation. Washington DC, 2, 2083-2089.

Al-Rawi, M. S., Qutaishat, M. A., and Arrar, M. R., (2006). **"An improved matched filter for blood vessel detection of digital retinal images,"** Computers in Biology and Medicine, In Press.

Banumathi, A., Karthika, R., and Kumar, A., (2003). **"Performance analysis of matched filter techniques for automated detection of blood vessels in retinal images,"** TENCON 2003. Conference on Convergent Technologies for Asia-Pacific Region 2, 543- 546.

Bevilacqua, A., Campanini, R., and Lanconelli, N., (2001). **"Optimization of a Distributed Genetic Algorithm on a Cluster of Workstations for the Detection of Microcalcifications,"** International Journal of Modern Physics C - Computing and Physics, 12(1) 55-70.

Chanwimaluang, T., and Fan, G., (2003). **"An efficient blood vessel detection algorithm for retinal images using local entropy thresholding,"** Proceeding of the IEEE Intl. Symp. on Circuits and Systems, 5, 21-24.

Chaptatape, O., Zheng L., and Krishnan, S. M., (1998). **"Retinal blood vessel detection and tracking by matched Gaussian and Kalman filter,"** Proceedings of the 20th Annul International Conference of the IEEE Engineering in Medicine and Biology Society, 20(6), 3144-3149.

Chaudhuri, S., Chatterjee, S., Katz, N., Nelson, M., and Goldbaum, M., (1989). **"Detection of blood vessels in retinal images using two dimensional matched filters,"** IEEE Transactions on Medical Imaging 8(3), 263-269.

All Rights Reserved - Library of University of Jordan - Center of Thesis Deposit

www.manaraa.com

Chutatape, O., Zheng, L., and Krishnan, S. M., (1998). **"Retinal blood vessel detection and tracking by matched Gaussian and Kalman filter,"** Proceeding 20th IEEE Annual Conference on Engineering in Medicine and Biology Society 6, 3144-3149.

Cornforth, D. J., Jelinek , H. F., Leandro J. J. G., Soares J.V.B., Cesar-Jr, R. M., Cree, M. J., Mitchell, P., and Bossomaier, T., (2004). **"Development of retinal blood vessel segmentation methodology using wavelet transforms for assessment of diabetic retinopathy,"** Proceedings of the Eighth Asia Pacific Symposium on Intelligent and Evolutionary Systems, Cairns, Australia, 50-60.

Cree, M., Cornforth, D., and Jelinek, H., (2005). "**Vessel segmentation and tracking using a two-dimensional model,"** Proceedings of the Image and Vision Computing Conference, New Zealand, University of Otago, 345-350.

Cree, M., Leandro, J., Soares, J., Cesar, R., Tang, G., Jelinek, H., and Cornforth, D., (2005). "**Comparison of Various Methods to Delineate Blood Vessels in Retinal Images,"** Proceedings of the 16th National Congress of the Australian Institute of Physics, Canbera, Australia.

Gang, L., Chutatape, O., and Krishnan, S. M., (2002). **"Detection and measurement of retinal vessels in fundus image using amplitude modified second order Gaussian filter,"** IEEE Transactions on Biomedical Engineering 49(2), 168-172.

Goatman, K., Cree, M., Olson, J., Forrester, J., and Sharp, P., (2003). **"Automated measurement of microaneurysm turnover,"** Investigative Ophthalmology and Visual Science 44(12), 5335-5341.

Goldbaum, M., Moezzi, S., Taylor, A., Chatterjee, S., Boyd, J., Hunter, E., and Jain, R., (1996). **"Automated diagnosis and image understanding with object extraction, object classification, and inferencing in retinal images,"** IEEE International Conference on Image Processing, Proceedings 3, 695-698.

Goldberg, D. E., (1989**). "Genetic algorithms in search, optimization and machine learning,"** Addison Wesley, New York.

Gonzalez, R.C., and Woods, R.E. (2002). **"Digital Image Processing,"** (2nd edition), United States: Prentice Hall, Inc.

All Rights Reserved - Library of University of Jordan - Center of Thesis Deposit

www.manaraa.com

Haralick, R. M., Lee, J. S. J., and Shapiro L. G., (1987). **"Morphological edge detection,"** IEEE J. Robotics Automat., RA-3, 142-155.

Holland, J.H., (1975). **"Adaptation in Natural and Artificial Systems,"** University of Michigan Press, Ann Arbor.

Hongqing, Z., (2004). **"Segmentation of blood vessels in retinal images using 2-D entropies of gray level-gradient co-occurrence matrix,"** Proceedings of the IEEE Intl Conf on Acoustics, Speech, and Signal Processing (ICASSP'2004).

Hoover, A., and Goldbaum, M., (2003). **"Locating the optic nerve in a retinal image using the fuzzy convergence of the blood vessels,"** IEEE Transactions on Medical Imaging 22(8), 951-958.

Hoover, A., Kouzntesova, V., and Goldbaum, M., (2000). **"Locating blood vessels in retinal images by piecewise threshold probing of a matched filter responses,"** IEEE Transactions on Medical Imaging 19(3), 203-210.

Jorge, L., Roberto, C., and Herbert, J., (2001). **"Blood vessels segmentation in retina: preliminary assessment of the mathematical morphology and of the wavelet transform techniques,"** XIV Brazilian Symposium on Computer Graphics and Image Processing.

Li, H., and Chutatape, O., (2000). **"Fundus image features extraction, "** Proceeding of the 22nd Annul EMBS International Conference, 3071–3073.

Mitchell, M., (1997). **"An introduction to genetic algorithms,"** The MIT Press, Cambridge, Massachusetts.

Niemeijer, M., Staal, J., van Ginneken, B., Loog, M., and Abramoff, M.D., (2004). **"Comparative study of retinal vessel segmentation methods on a new publicly available databases,"** Medical Imaging: Physiology, Function, Structure from Medical Images. Edited by Amini, Amir A; Manduca, Armando. Proceedings of the SPIE 5370, 648-656.

All Rights Reserved - Library of University of Jordan - Center of Thesis Deposit

www.manaraa.com

O'Gorman, L., and Nickerson, J. V., (1988). **"Matched filter design for fingerprint image enhancement,"** Proceedings of the IEEE Int. Conference, 4coust., Speech, and Signal Processing, New York, 916-919.

Otoba, K. Tanaka, and M. Hitafuji, (1998). **"Image processing and interactive selection with Java based on genetic algorithms,"** In: 3rd IFAC/CIGR Workshop on Artificial Intelligence in Agriculture Makuhari, Japan, 83-88.

Rousselle, J. J., Vincent , N., and Verbeke, N., (2003). **"Genetic algorithm to set active contour,"** Proceedings International Conference on Computer Analysis of Images and Patterns, Groningen, The Netherlands, 345-352.

Silva, N. C., and Santa Rosa, A. N. C., (2002). **"Estimative of SOM Learning Parameters Using Genetic Algoritms,"** In: 6th World Multiconference on Systemics, Cybernetics and Informatics (SCI 2002), 2002, Orlando, FL USA., 31-36.

Simunic, K., and S. Loncaric. (1998). **"A Genetic Search-Based Partial Image Matching,"** Proceedings of the 2nd IEEE International Conference on Intelligent Processing Systems (ICIPS 98), Australia: Gold Coast, 119–122.

Singer, D. E., Nathan, D. M., Fogel, H. A., and Schachar, A. P., (1992). **"Screening for diabetic retinopathy,"** Ann. Intern. Med., (116), 660-671.

Soares, J., Leandro, J., Cesar, R., Jelinek, H., and Cree, M., (2005). "**Using the 2-D morlet wavelet with supervised classification for retinal vessel segmentation,"** Conferences on the Brazilian symposium on computer graphics and image processing.

Sofka, M., and Stewart, C. V., (2005). **"Retinal Vessel Extraction Using Multiscale Matched Filters Confidence and Edge Measures,"** Technical Report # 05-20, Department of Computer Science, Rensselaer Polytechnic Institute.

Staal, J., Ginneken, B., Niemeijer, M., Viegever, A., and Abramoff, M.D., (2004). **"Ridge based vessel segmentation in color images of the retina,"** IEEE Transaction on Medical Imaging 23(4), 501-509.

All Rights Reserved - Library of University of Jordan - Center of Thesis Deposit

www.manaraa.com

Tolias, Y. A., and Panas, S. M., (1998). **"A fuzzy vessel tracking algorithm for retinal images based on fuzzy clustering,"** IEEE Transaction on Midical Imaging, 17(2), 263-273.

Wang, Y., and Lee, S.C.,(1997). **"A Fast Method for Automated Detection Of Blood Vessels in Retinal Images,"** Conference Record of the Thirty-First Asilomar Conferences on Signals, Systems and Computers, 2, 1700-1704.

Wu, D., Ming, Z., Jyh-Charn, L., and Bauman, W., (2006). "**On the adaptive detection of blood vessels in retinal images,"** IEEE Transaction on Biomedical Engineering, 53(2) 341-343.

Zana, F., and Klein, J. C., (1999). **"A multimodal registration algorithm of eye fundus images using vessels detection and Hough transform,"** IEEE Transactions on Medical Imaging 18(5), 419-428.

Zana, F., and Klein, J.C., (2001). **"Segmentation of vessel like patterns using mathematical morphology and curvature evaluation,"** IEEE Transactions on Image Processing 10(7), 1010-1019.

Zhou, L., Rzeszotarski, M., Singerman, L. J., and Chokreff, J. M., (1994**). "The detection and quantification of retinopathy using digital angiograma,"** IEEE Transaction on Medical Imaging 13, 616-626.

All Rights Reserved - Library of University of Jordan - Center of Thesis Deposit

www.manaraa.com

APPENDIX A

All Rights Reserved - Library of University of Jordan - Center of Thesis Deposit

www.manaraa.com

1. Result of the GAMF Optimization using JPEG Images

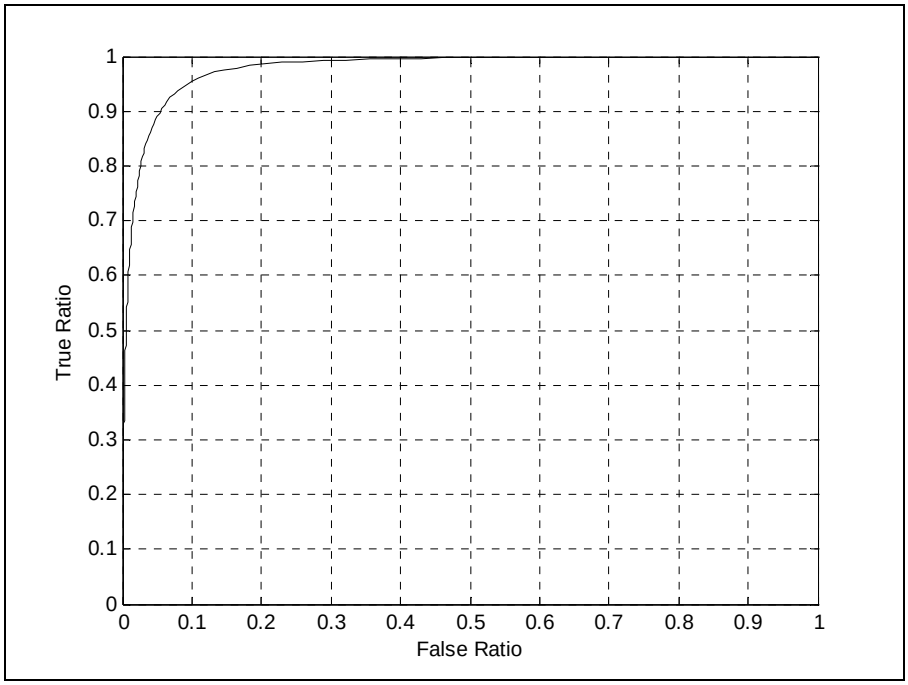

Figure 21 *The ROC area for the first image in the DRIVE database that has JPEG extension using Filter 1 under 1000 thresholds*

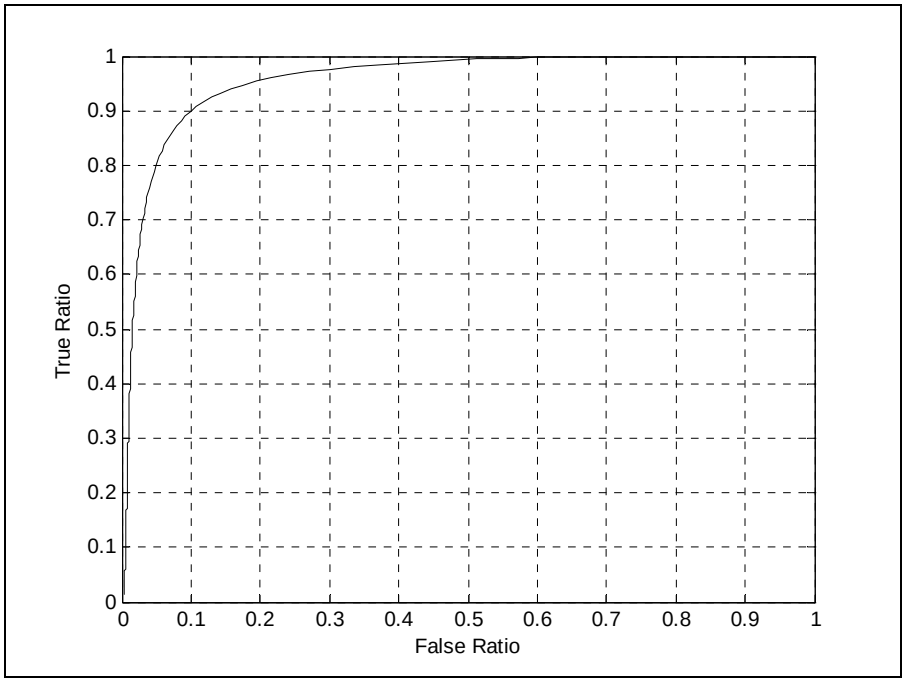

Figure 22 *Average ROC area for 20 JPEG images in the test set of the DRIVE database using Filter 1.*

All Rights Reserved - Library of University of Jordan - Center of Thesis Deposit

www.manaraa.com

Table 17 Comparison of GAMF filters with the GMF and OGMF filters on a test set of the DRIVE database which has JPEG images.

Filter Name	NOK	Kernel size	Average ROC area	MAA	Time needed to vessel detection of one image in sec
Filter 1	12	17 × 17	0.9582	0.9420	1.906
Filter 2	58	19 × 19	0.9583	0.9405	7.125
Filter 3	12	17 × 17	0.9580	0.9403	1.750
Filter 4	12	1 9 × 19	0.9573	0.9406	1.750
Filter 5	12	17 × 17	0.9570	0.9411	1.750
Filter 6	12	17 × 17	0.9560	0.9422	2.156
Filter 7	38	13 × 13	0.9549	0.9416	3.656
Filter 8	32	11 × 11	0.9542	0.9407	3.110
Filter 9	38	11 ×11	0.9540	0.9413	4.250
OGMF	12	17 × 17	0.9374	0.9392	2.140
GMF	12	19 × 19	0.7550	0.8850	1.703

Table 18 Area under the ROC and the MAA for the 40 image in the DRIVE database (JPEG images)

Filter Name	Average ROC area	MAA
Filter 2	0.9565	0.9410
Filter 3	0.9559	0.9394
Filter 4	0.9557	0.9397

All Rights Reserved - Library of University of Jordan - Center of Thesis Deposit

www.manaraa.com

Table 19 The area under the ROC for the 20 image in the test set of the DRIVE database (JPEG images) using Filter 6 via different degree of rotations.

Img no	θ = 60°	θ = 30 °	θ = 15°	θ = 7.5 °	θ = 5 °	θ = 2.5°
1	0.9690	0.9756	0.9761	0.9763	0.9764	0.9764
2	0.9668	0.9724	0.9727	0.9726	0.9728	0.9728
3	0.9503	0.9600	0.9604	0.9604	0.9609	0.9609
4	0.9448	0.9513	0.9517	0.9516	0.9520	0.9519
5	0.9440	0.9491	0.9493	0.9491	0.9497	0.9496
6	0.9384	0.9460	0.9463	0.9464	0.9468	0.9470
7	0.9402	0.9478	0.9483	0.9482	0.9484	0.9484
8	0.9394	0.9467	0.9474	0.9474	0.9483	0.9482
9	0.9388	0.9459	0.9462	0.9460	0.9464	0.9463
10	0.9476	0.9542	0.9547	0.9546	0.9549	0.9549
11	0.9358	0.9435	0.9441	0.9442	0.9447	0.9447
12	0.9461	0.9534	0.9540	0.9541	0.9544	0.9545
13	0.9421	0.9501	0.9503	0.9505	0.9506	0.9508
14	0.9616	0.9690	0.9693	0.9692	0.9695	0.9696
15	0.9577	0.9636	0.9641	0.9642	0.9645	0.9646
16	0.9464	0.9546	0.9547	0.9546	0.9550	0.9549
17	0.9435	0.9505	0.9507	0.9504	0.9512	0.9511
18	0.9483	0.9539	0.9543	0.9543	0.9546	0.9547
19	0.9596	0.9651	0.9651	0.9650	0.9656	0.9656
20	0.9543	0.9596	0.9600	0.9601	0.9605	0.9605
mean	**0.9487**	**0.9556**	**0.9560**	**0.9560**	**0.9564**	**0.9564**
Std	**0.0097**	**0.0093**	**0.0093**	**0.0093**	**0.0092**	**0.0093**

All Rights Reserved - Library of University of Jordan - Center of Thesis Deposit

www.manaraa.com

Table 20 The area under the ROC for the 20 image in the test set of the DRIVE database (JPEG images) using Filter 3 via different degree of rotations.

Img no	θ = 60°	θ = 30 °	θ = 15°	θ = 7.5 °	θ = 5 °	θ = 2.5°
1	0.9708	0.9785	0.9788	0.9789	0.9626	0.9643
2	0.9677	0.9739	0.9742	0.9744	0.9565	0.9578
3	0.9469	0.9598	0.9604	0.9612	0.9403	0.9417
4	0.9444	0.9527	0.9531	0.9534	0.9330	0.9331
5	0.9429	0.9502	0.9505	0.9511	0.9360	0.9371
6	0.9385	0.9467	0.9472	0.9476	0.9168	0.9195
7	0.9409	0.9504	0.9509	0.9511	0.9277	0.9277
8	0.9403	0.9497	0.9504	0.9512	0.9227	0.9239
9	0.9397	0.9480	0.9482	0.9488	0.9250	0.9272
10	0.9469	0.9556	0.9562	0.9566	0.9410	0.9417
11	0.9377	0.9474	0.9478	0.9484	0.9225	0.9225
12	0.9446	0.9547	0.9550	0.9556	0.9334	0.9354
13	0.9405	0.9510	0.9511	0.9513	0.9265	0.9280
14	0.9611	0.9705	0.9707	0.9711	0.9524	0.9537
15	0.9573	0.9653	0.9658	0.9662	0.9481	0.9474
16	0.9473	0.9575	0.9576	0.9579	0.9363	0.9387
17	0.9433	0.9527	0.9529	0.9535	0.9214	0.9241
18	0.9495	0.9563	0.9568	0.9571	0.9356	0.9383
19	0.9622	0.9690	0.9692	0.9697	0.9550	0.9561
20	0.9552	0.9618	0.9622	0.9624	0.9448	0.9477
mean	**0.9489**	**0.9576**	**0.9580**	**0.9584**	**0.9369**	**0.9383**
Std	**0.0100**	**0.0094**	**0.0093**	**0.0093**	**0.0131**	**0.0130**

All Rights Reserved - Library of University of Jordan - Center of Thesis Deposit

المنارة للاستشارات
www.manaraa.com

Table 21 The MA for the 20 image in the test set of the DRIVE database (JPEG images) using Filter 6 via different degree of rotations.

img no	θ = 60°	θ = 30 °	θ = 15°	θ = 7.5 °	θ = 5 °	θ = 2.5°
1	0.9482	0.9537	0.9542	0.9541	0.9541	0.9540
2	0.9427	0.9486	0.9489	0.9489	0.9488	0.9487
3	0.9342	0.9394	0.9399	0.9398	0.9401	0.9400
4	0.9352	0.9385	0.9391	0.9390	0.9392	0.9390
5	0.9343	0.9386	0.9392	0.9392	0.9395	0.9395
6	0.9298	0.9340	0.9346	0.9345	0.9349	0.9347
7	0.9283	0.9333	0.9337	0.9337	0.9339	0.9339
8	0.9288	0.9321	0.9325	0.9326	0.9330	0.9330
9	0.9347	0.9385	0.9388	0.9385	0.9387	0.9386
10	0.9391	0.9440	0.9440	0.9439	0.9438	0.9437
11	0.9317	0.9358	0.9359	0.9359	0.9362	0.9361
12	0.9349	0.9400	0.9403	0.9402	0.9407	0.9407
13	0.9272	0.9340	0.9340	0.9341	0.9344	0.9344
14	0.9452	0.9505	0.9501	0.9500	0.9504	0.9504
15	0.9464	0.9498	0.9500	0.9501	0.9504	0.9504
16	0.9344	0.9402	0.9404	0.9403	0.9408	0.9408
17	0.9378	0.9413	0.9418	0.9417	0.9421	0.9420
18	0.9416	0.9447	0.9454	0.9454	0.9453	0.9453
19	0.9493	0.9558	0.9560	0.9560	0.9564	0.9563
20	0.9426	0.9455	0.9456	0.9455	0.9453	0.9452
mean	**0.9373**	**0.9419**	**0.9422**	**0.9422**	**0.9424**	**0.9423**
std	**0.0068**	**0.0070**	**0.0069**	**0.0069**	**0.0068**	**0.0068**

All Rights Reserved - Library of University of Jordan - Center of Thesis Deposit

المنارة للاستشارات
www.manaraa.com

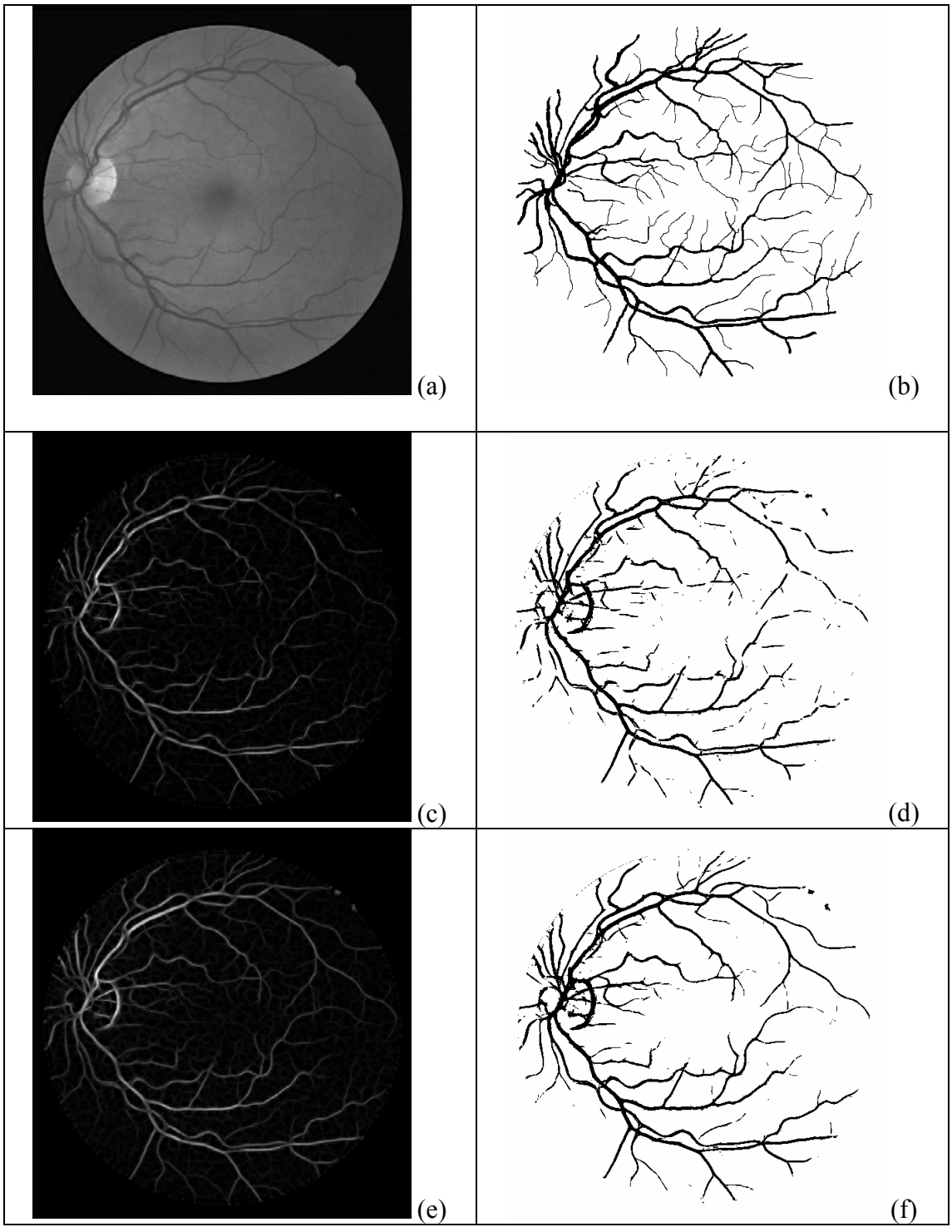

All Rights Reserved - Library of University of Jordan - Center of Thesis Deposit

www.manaraa.com

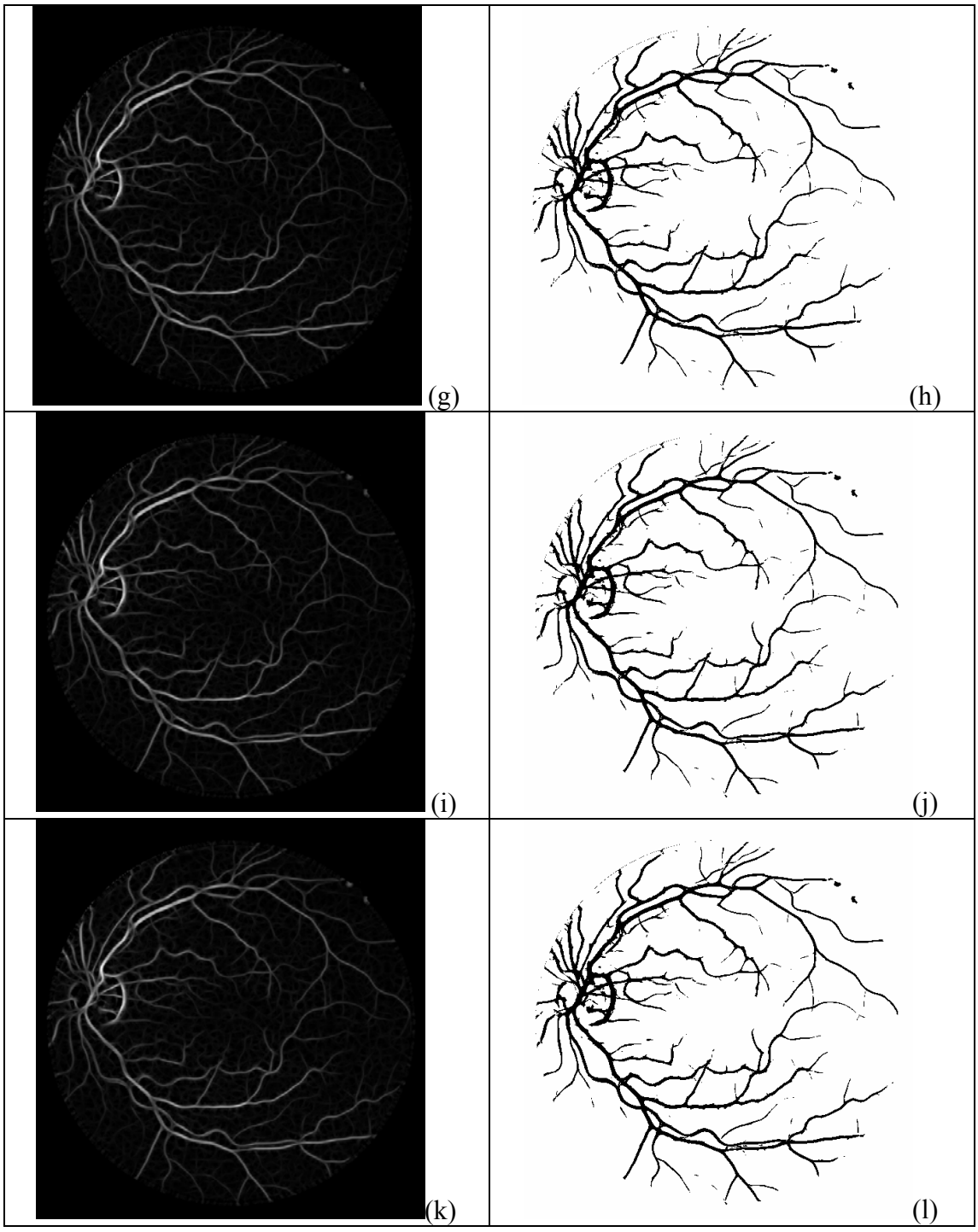

All Rights Reserved - Library of University of Jordan - Center of Thesis Deposit

www.manaraa.com

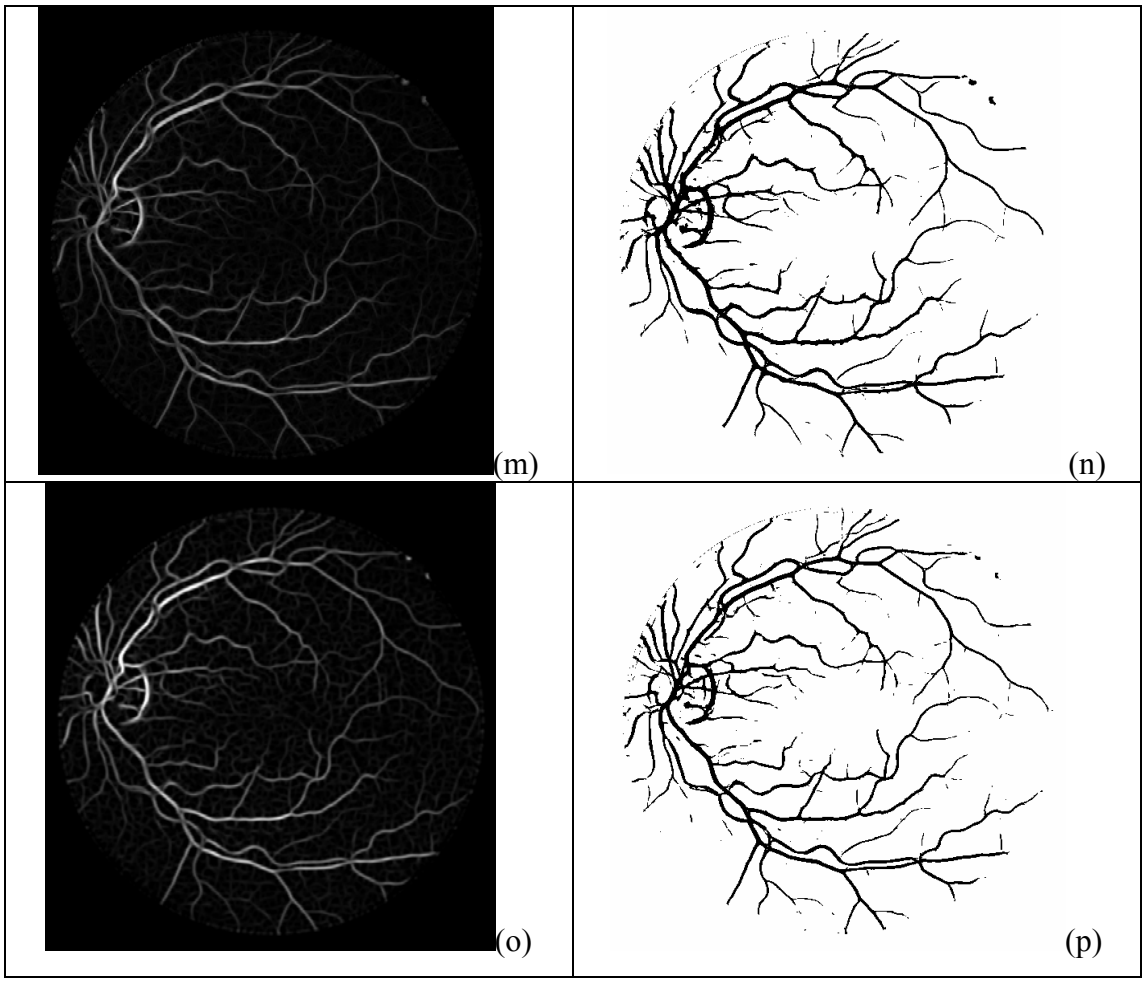

Figure 23 *(a) The green band of the original image (b) Hand labeled image. (c), (e), (g), (i), (k), and (m) Results of applying the optimized GMF with Filter 6 under these amount θ = 60˚, 30˚, 15˚, 7.5˚, 5˚, and 2.5˚ respectively and the corresponding thresholded images at the best threshold are shown in (d), (f), (h), (j), (l), and (n). (o) Result of applying the optimized GMF with Filter 7. (p) The corresponding thresholded image of (o).* All of these images are JPEG images.

All Rights Reserved - Library of University of Jordan - Center of Thesis Deposit

www.manaraa.com

Table 22 Average area under the ROC for the 20 retinal images of the DRIVE (JPEG images) under different bands using Filter 6.

Band	Average ROC Area
Green	0.9560
Red	0.9405
Blue	0.9387

Table 23 Average area under the ROC for filters that results from genetic algorithm experiments on a Red and Blue band and comparing it to the green band using Filter 1 on a test set of the DRIVE database (JPEG images).

Genetic Algorithm (GA) on	Filters Found by GA			Average ROC Area
	L	σ	T	
Green Band	13.6947	0.4942	5.2275	0.9582
Red Band	15.0804	1.0707	3.4808	0.9455
Blue Band	20.5874	0.7678	4.6285	0.9428

Table 24 Differences in the average area under the ROC and MAAs that result from smoothing the green band for the test set of the DRIVE database (JPEG images).

Filter Name	Average ROC area without smoothing	Average ROC area with smoothing	MAA without smoothing	MAA with smoothing
Filter 3	0.9580	0.9580	0.9403	0.9374
Filter 6	0.9533	0.9560	0.9422	0.9368
Filter 1	0.9526	0.9582	0.9420	0.9376
Filter 4	0.9498	0.9573	0.9406	0.9371
Filter 5	0.9494	0.9570	0.9411	0.9374

All Rights Reserved - Library of University of Jordan - Center of Thesis Deposit

المنارة للاستشارات
www.manaraa.com

Table 25 Determining the average threshold of the matched filter with Filter 6 for the test set of the DRIVE database (JPEG images).

Image number	Maximum Accuracy	Threshold at Maximum Accuracy	Accuracy at Average Threshold	Error Rate between the MA and Accuracy calculated at the Average Threshold
1	0.9542	0.3000	0.9541	0.0001
2	0.9489	0.3000	0.9488	0.0001
3	0.9399	0.2500	0.9373	0.0026
4	0.9391	0.3000	0.9391	0.0000
5	0.9392	0.2500	0.9364	0.0028
6	0.9346	0.2500	0.9318	0.0028
7	0.9337	0.3500	0.9331	0.0006
8	0.9325	0.3000	0.9327	0.0002
9	0.9388	0.2500	0.9369	0.0019
10	0.9440	0.2500	0.9431	0.0009
11	0.9359	0.3500	0.9332	0.0027
12	0.9403	0.3000	0.9405	0.0002
13	0.9340	0.3000	0.9342	0.0002
14	0.9501	0.3500	0.9498	0.0003
15	0.9500	0.4000	0.9457	0.0043
16	0.9404	0.3000	0.9405	0.0001
17	0.9418	0.3000	0.9418	0.0000
18	0.9454	0.3000	0.9454	0.0000
19	0.9560	0.3000	0.9562	0.0002
20	0.9456	0.2500	0.9448	0.0008
Mean	0.9422	0.2975	0.94127	0.0010
Standard Deviation	0.0069	0.0413	0.0072	0.0013

All Rights Reserved - Library of University of Jordan - Center of Thesis Deposit

www.manaraa.com

Table 26 The difference in MAA between thresholding at the best threshold and thresholding at the average threshld.

Filter Number	Maximum Accuracy	Average Threshold at Maximum Accuracy	Accuracy at Average Threshold	Error Rate between the MA and Accuracy calculated at the Average Threshold
Mean(Filter1)	0.9405	0.3500	0.9395	0.0009
STD (Filter1)	0.0068	0.0459	0.0071	0.0011
Mean(Filter2)	0.9420	0.2375	0.9412	0.0011
STD (Filter2)	0.0069	0.0319	0.0071	0.0011
Mean(Filter3)	0.9403	0.3125	0.9396	0.0008
STD (Filter3)	0.0069	0.0455	0.0070	0.0011
mean(Filter4)	0.9406	0.3425	0.9397	0.0009
STD (Filter4)	0.0070	0.0438	0.0071	0.0011
mean(Filter5)	0.9411	0.3175	0.9403	0.0009
STD (Filter5)	0.0069	0.0438	0.0070	0.0012
mean(Filter6)	0.9422	0.2975	0.9413	0.0010
STD (Filter6)	0.0069	0.0413	0.0072	0.0013
mean(Filter7)	0.9416	0.1950	0.9411	0.0006
STD (Filter7)	0.0075	0.0276	0.0075	0.0010
mean(Filter8)	0.9407	0.1550	0.9403	0.0004
STD (Filter8)	0.0079	0.0154	0.0079	0.0004
mean(Filter9)	0.9413	0.1575	0.9409	0.0006
STD (Filter9)	0.0078	0.0183	0.0077	0.0008

All Rights Reserved - Library of University of Jordan - Center of Thesis Deposit

www.manaraa.com

2. Results of the Second Order GMF Optimization using JPEG Images

Table 27 The new proposed filter parameters for the second order GMF that found by Genetic Algorithm using JPEG images.

Filter Name	L	σ	T	t	NOK	Average ROC area	MAA
Filter 10	14.9781	1.3558	7.3223	1.4395	21 × 21	0.9594	0.9411
Filter 11	15.3362	1.5619	7.6672	5.5482	21 × 21	0.9586	0.9388
Filter 12	12.6243	1.0202	5.4239	-6.3232	17 × 17	0.9583	0.9359
Filter 13	17.2832	1.6184	16.7462	-16.9825	23 × 23	0.9577	0.9386
Filter 14	17.3297	1.6530	14.3777	-8.9212	23 × 23	0.9576	0.9386
Filter 15	20.4177	1.0921	4.372	3.1493	25 × 25	0.9581	0.9340

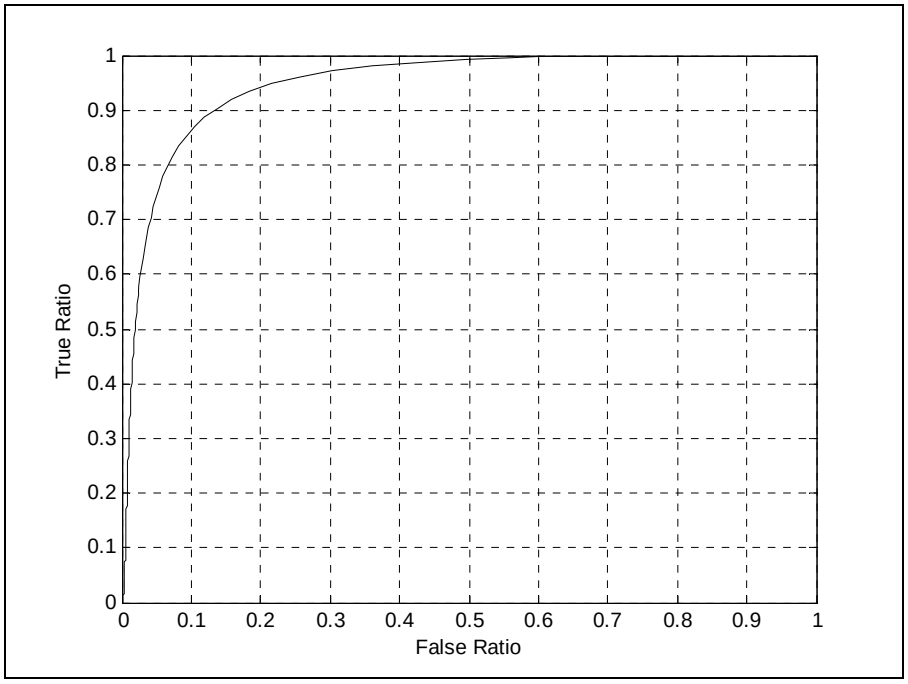

Figure 24 *Average ROC area for 20 images in the test set of the DRIVE database (JPEG images) using Filter 10.*

All Rights Reserved - Library of University of Jordan - Center of Thesis Deposit

www.manaraa.com

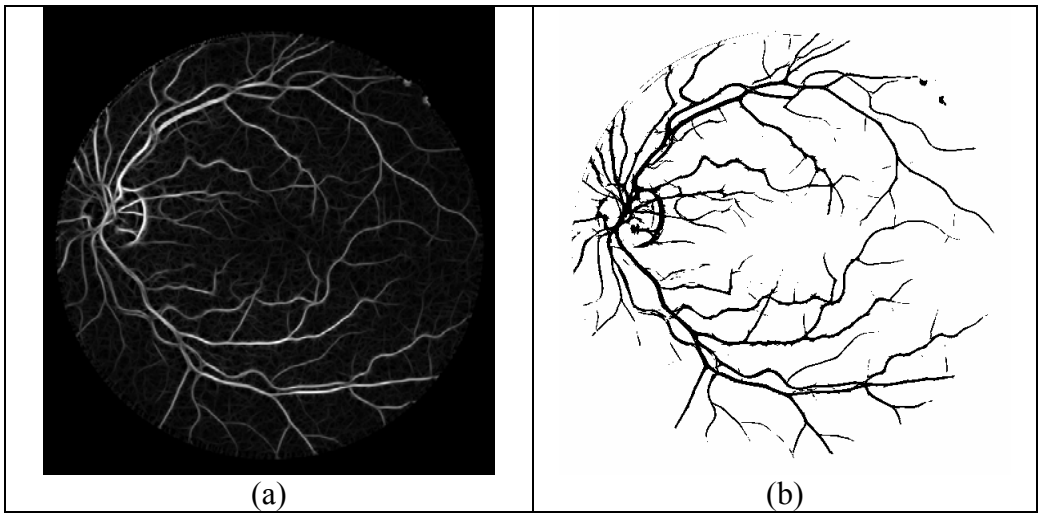

Figure 25 *(a) Result of applying the optimized second order GMF using Filter 10 (b) the corresponding thresholded image at the best threshold for the first image in the DRIVE database (JPEG image).*

Table 28 New parameters for $\{L, T\}$ while t = 3. 5 and the values of σ are {0.5, 1, 1.5, 2.5} for the second order GMF on the test set of the DRIVE database (JPEG images).

L1	L2	L3	L4	T1	T2	T3	T4	Average ROC area	MAA
19.7106	61.9359	21.3867	63.7904	7.0872	22.3909	4.9152	0.0221	0.9566	0.9358
10.9506	24.1763	23.5337	42.9453	28.2158	5.3594	14.6095	13.3025	0.9553	0.9317

All Rights Reserved - Library of University of Jordan - Center of Thesis Deposit

www.manaraa.com

APPENDIX B

All Rights Reserved - Library of University of Jordan - Center of Thesis Deposit

www.manaraa.com

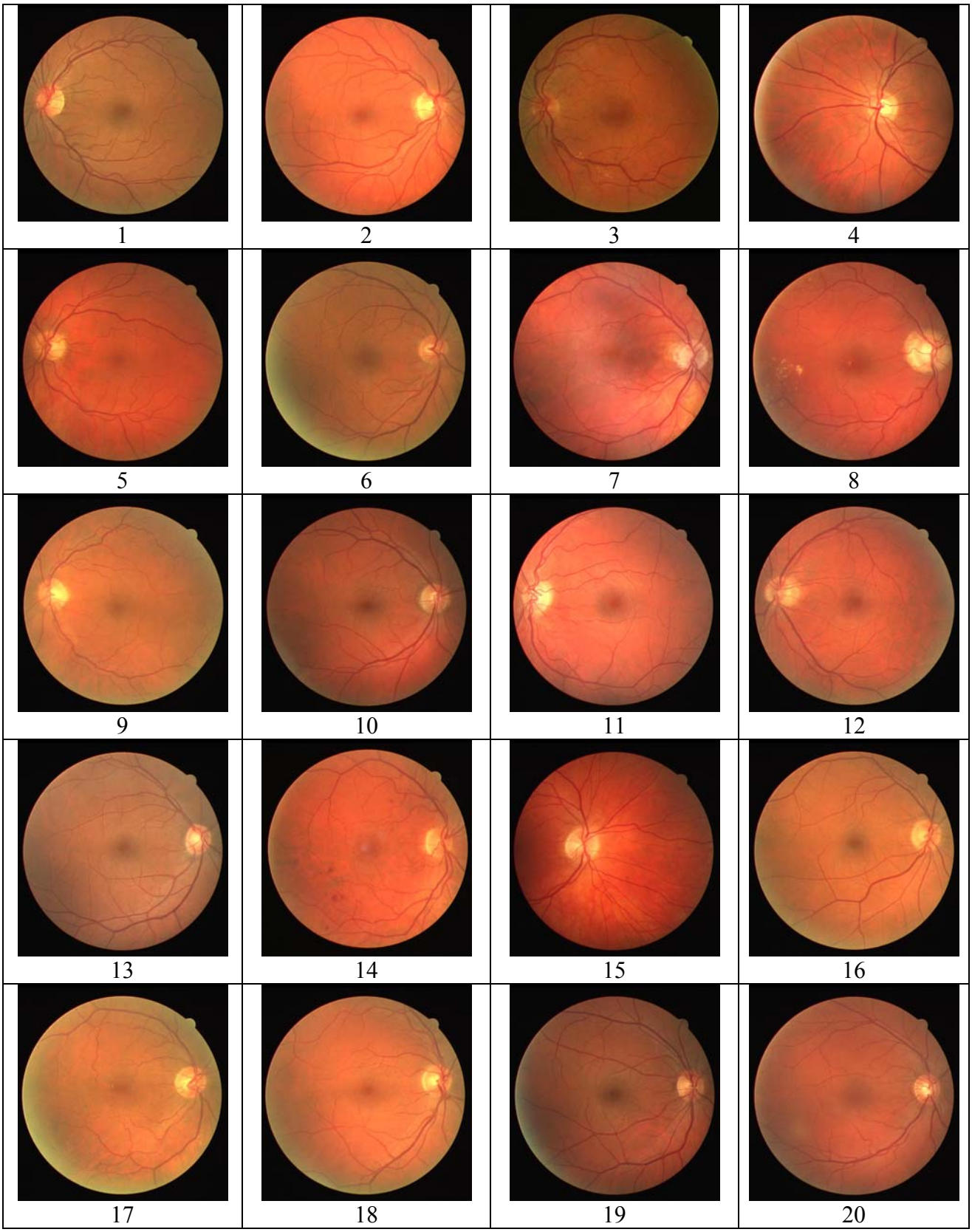

Figure 21 *The 20 original images in the test set of the DRIVE database*

All Rights Reserved - Library of University of Jordan - Center of Thesis Deposit

المنارة للاستشارات
www.manaraa.com

Hand Label	GMF	OGMF	GAMF(Filter1)
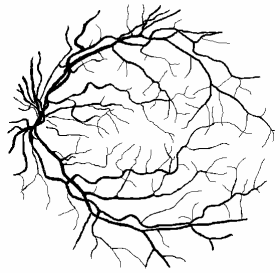 1	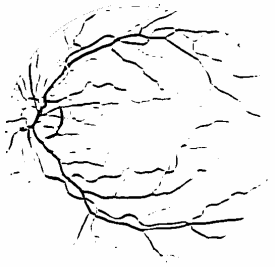	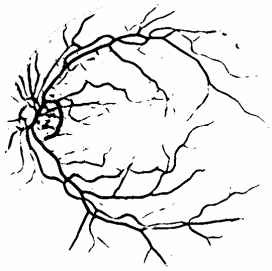	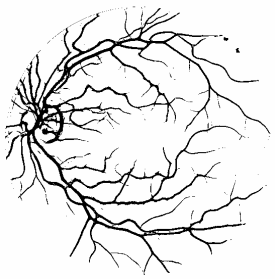
2	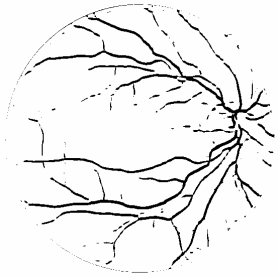	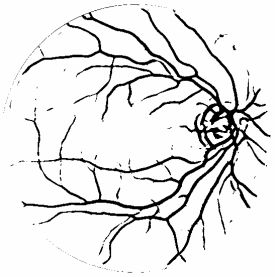	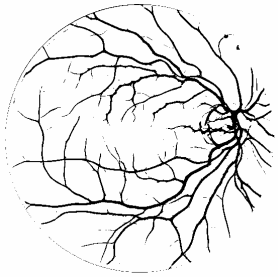
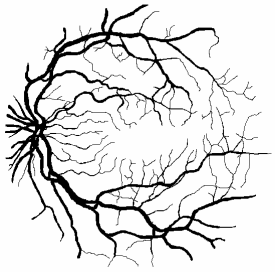 3	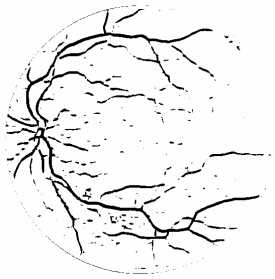		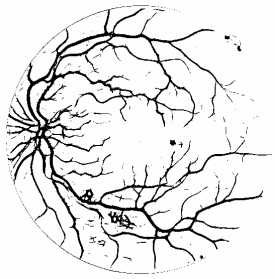
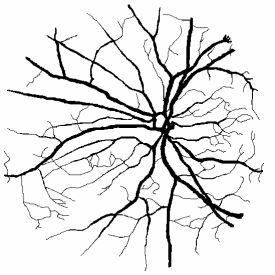 4	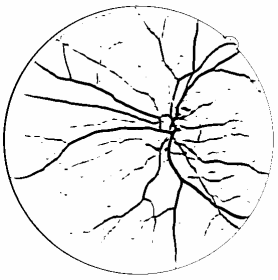	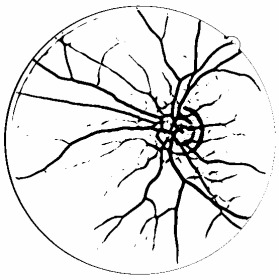	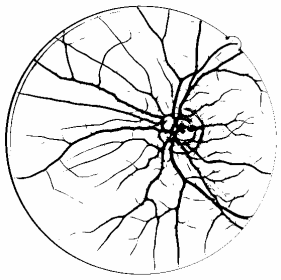
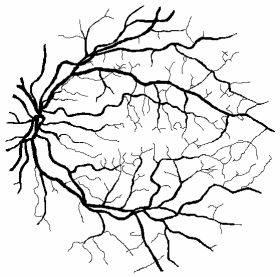 5	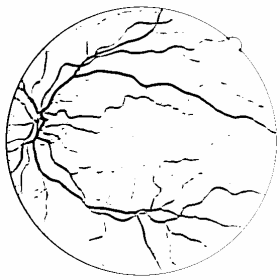	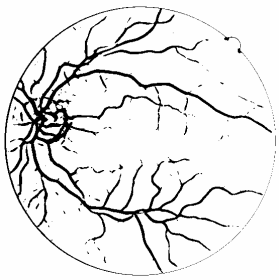	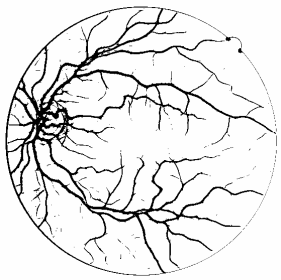

All Rights Reserved - Library of University of Jordan - Center of Thesis Deposit

المنارة للاستشارات
www.manaraa.com

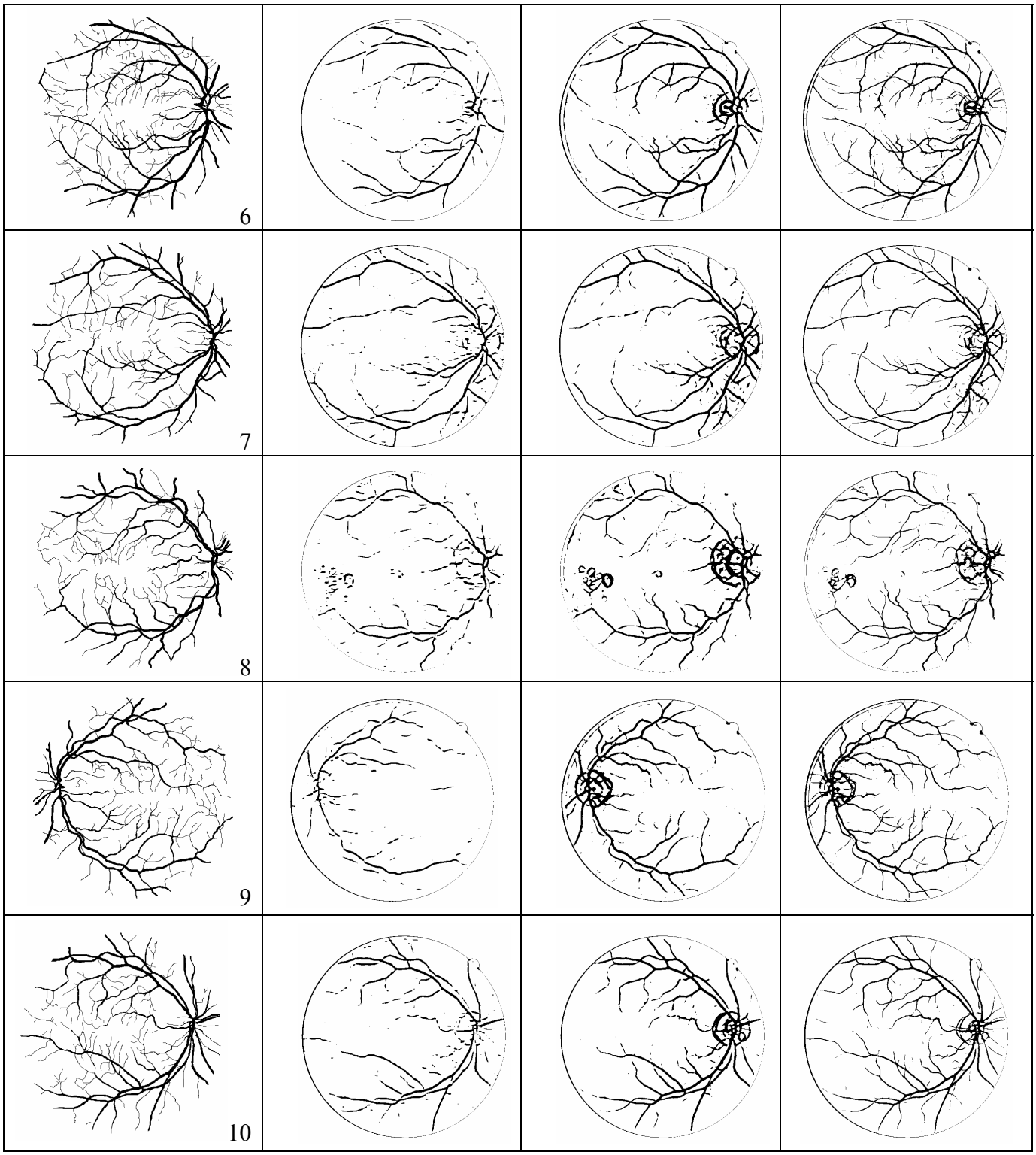

All Rights Reserved - Library of University of Jordan - Center of Thesis Deposit

www.manaraa.com

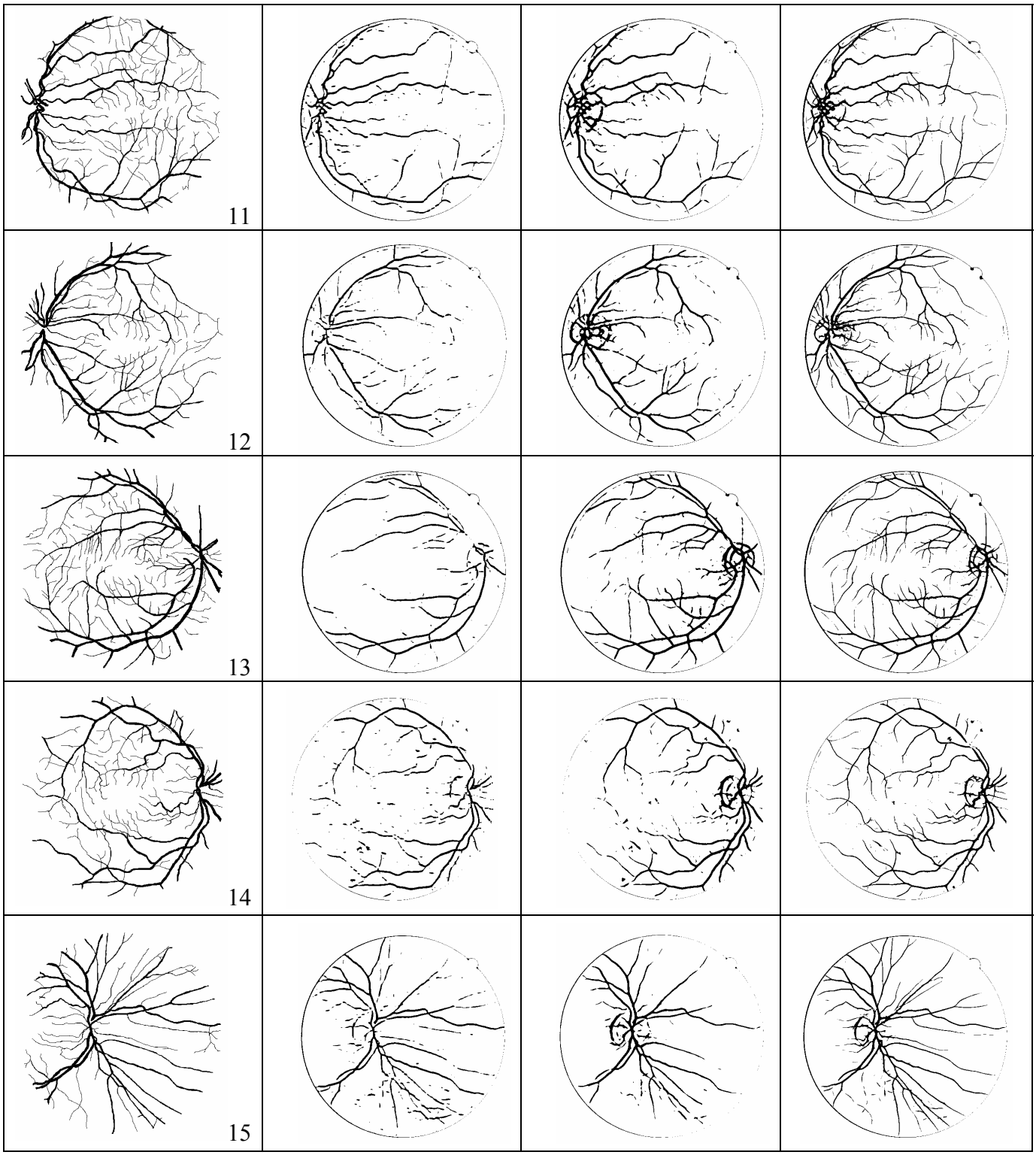

All Rights Reserved - Library of University of Jordan - Center of Thesis Deposit

www.manaraa.com

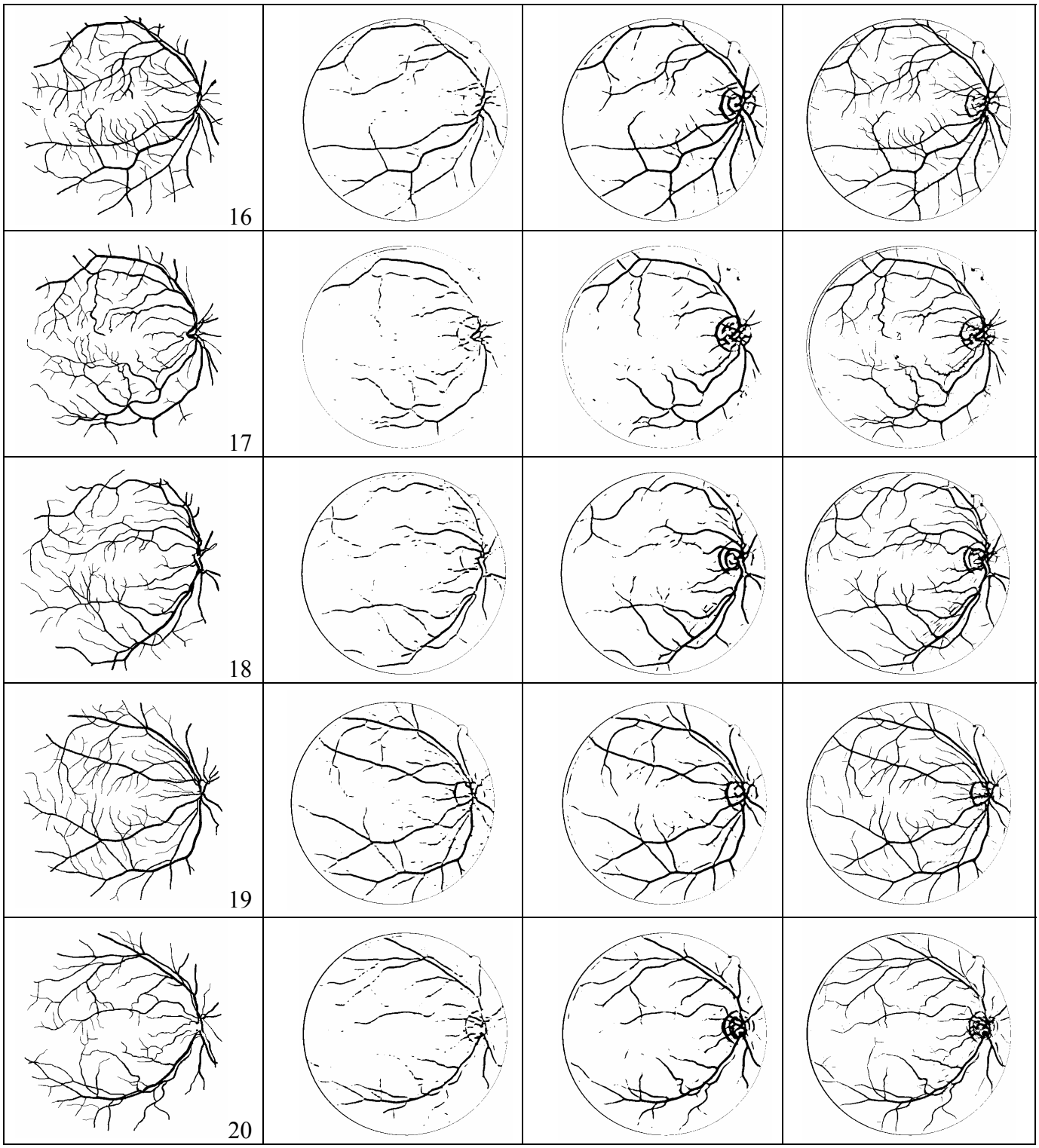

Figure 22 *The First column is the Hand labeled images and the second, third, and fourth columns are the segmented images using GMF, OGMF, and GAMF (Filter 1) respectively where each image is thresholded at the best threshold for the test set of the DRIVE database.*

All Rights Reserved - Library of University of Jordan - Center of Thesis Deposit

www.manaraa.com

GAMF(Filter 6) at the best threshold	GAMF (Filter 6) at the best average threshold (0.315)	GAMF(Filter 6) at the best threshold	GAMF (Filter 6) at the best average threshold (0.315)
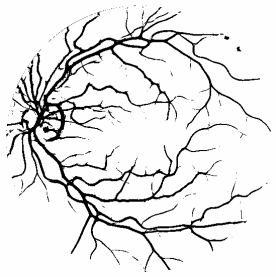 1	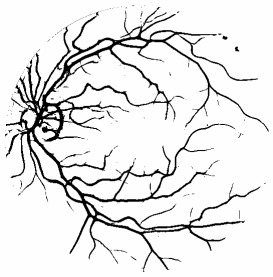 1	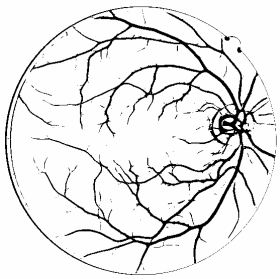 6	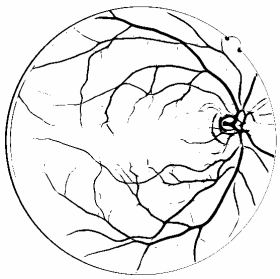 6
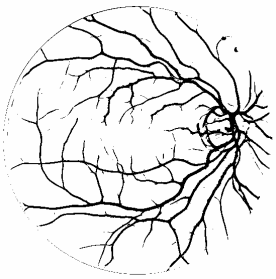 2	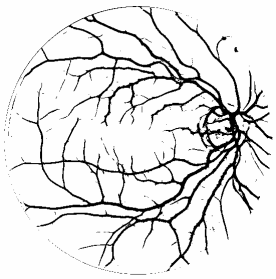 2	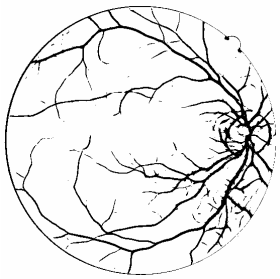 7	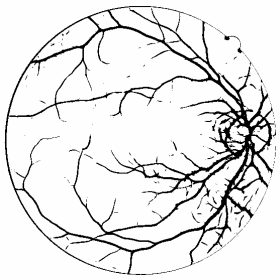 7
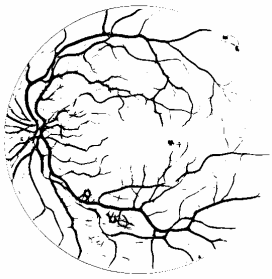 3	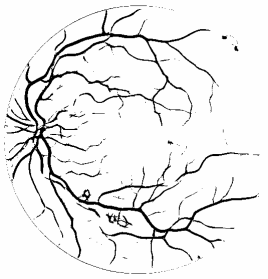 3	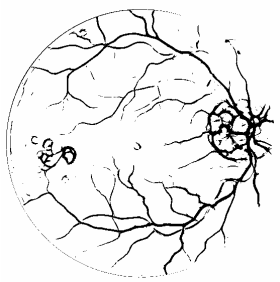 8	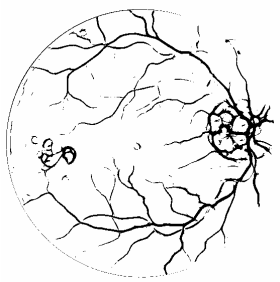 8
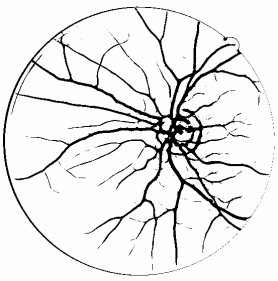 4	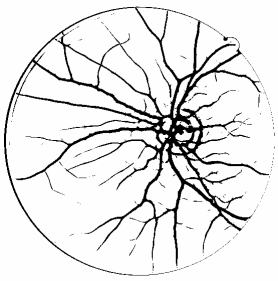 4	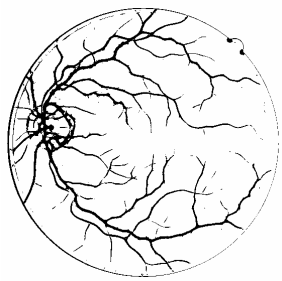 9	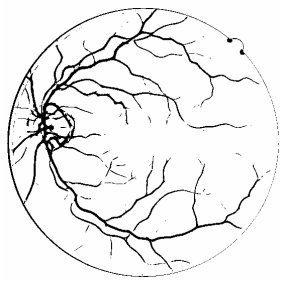 9
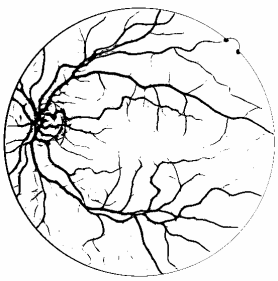 5	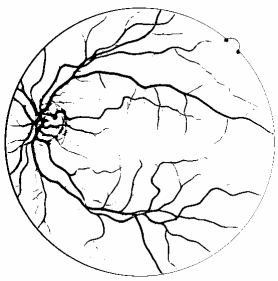 5	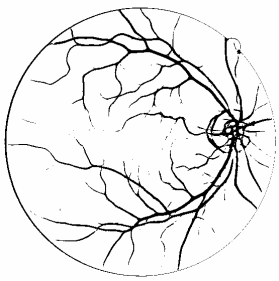 10	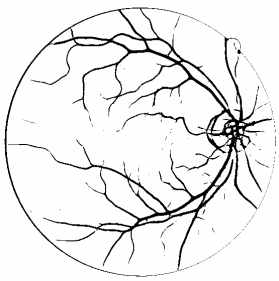 10

All Rights Reserved - Library of University of Jordan - Center of Thesis Deposit

المنارة للاستشارات
www.manaraa.com

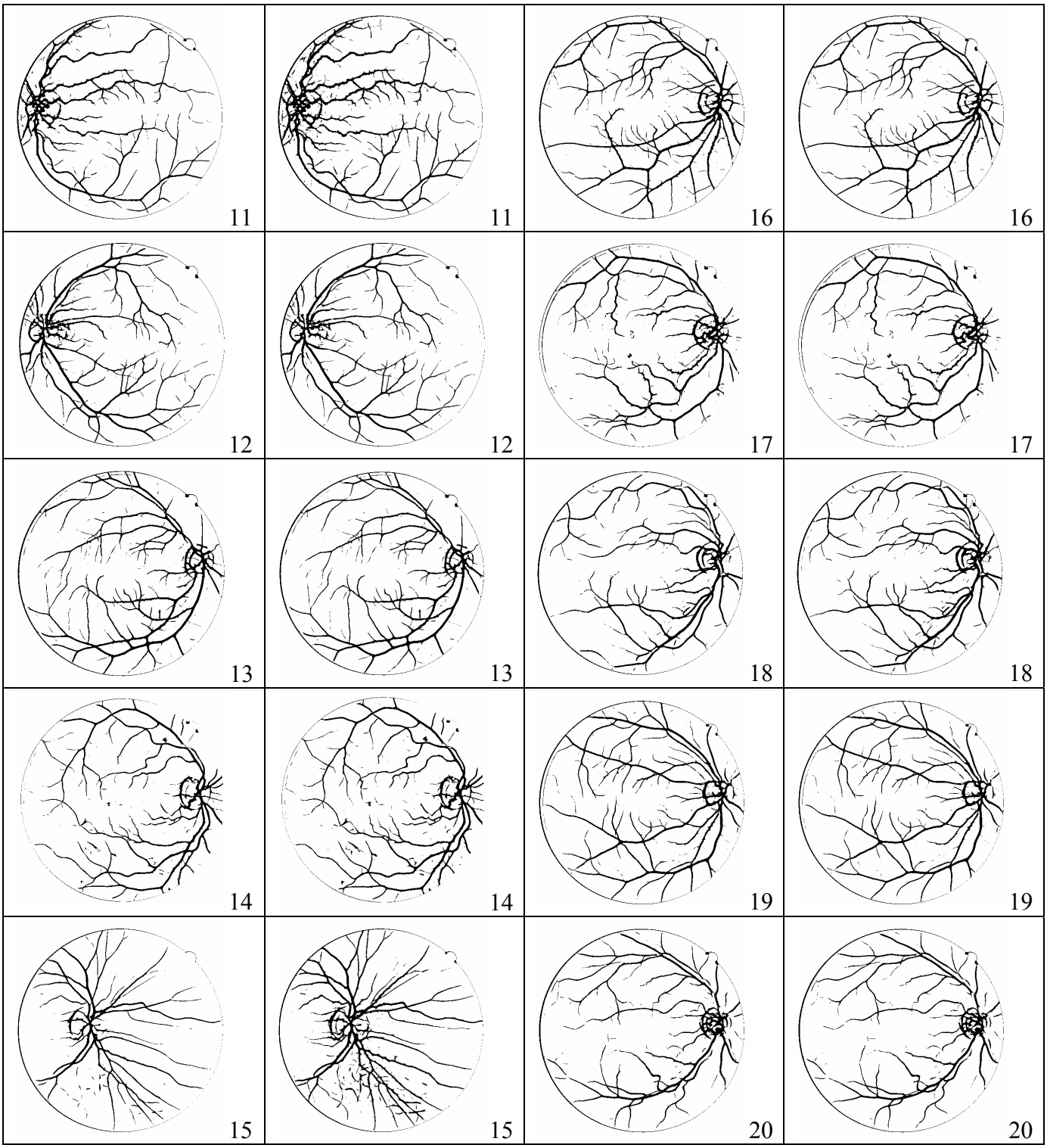

Figure 23 *The first and the third columns are the segmented images by GAMF(Filter 6) at the best thresholds, and the second and fourth columns are the segmented images using GAMF(Filter 6) at the best average threshold (0.315) for the test set of the DRIVE database.*

All Rights Reserved - Library of University of Jordan - Center of Thesis Deposit

المنارة للاستشارات
www.manaraa.com

APPENDIX C

All Rights Reserved - Library of University of Jordan - Center of Thesis Deposit

www.manaraa.com

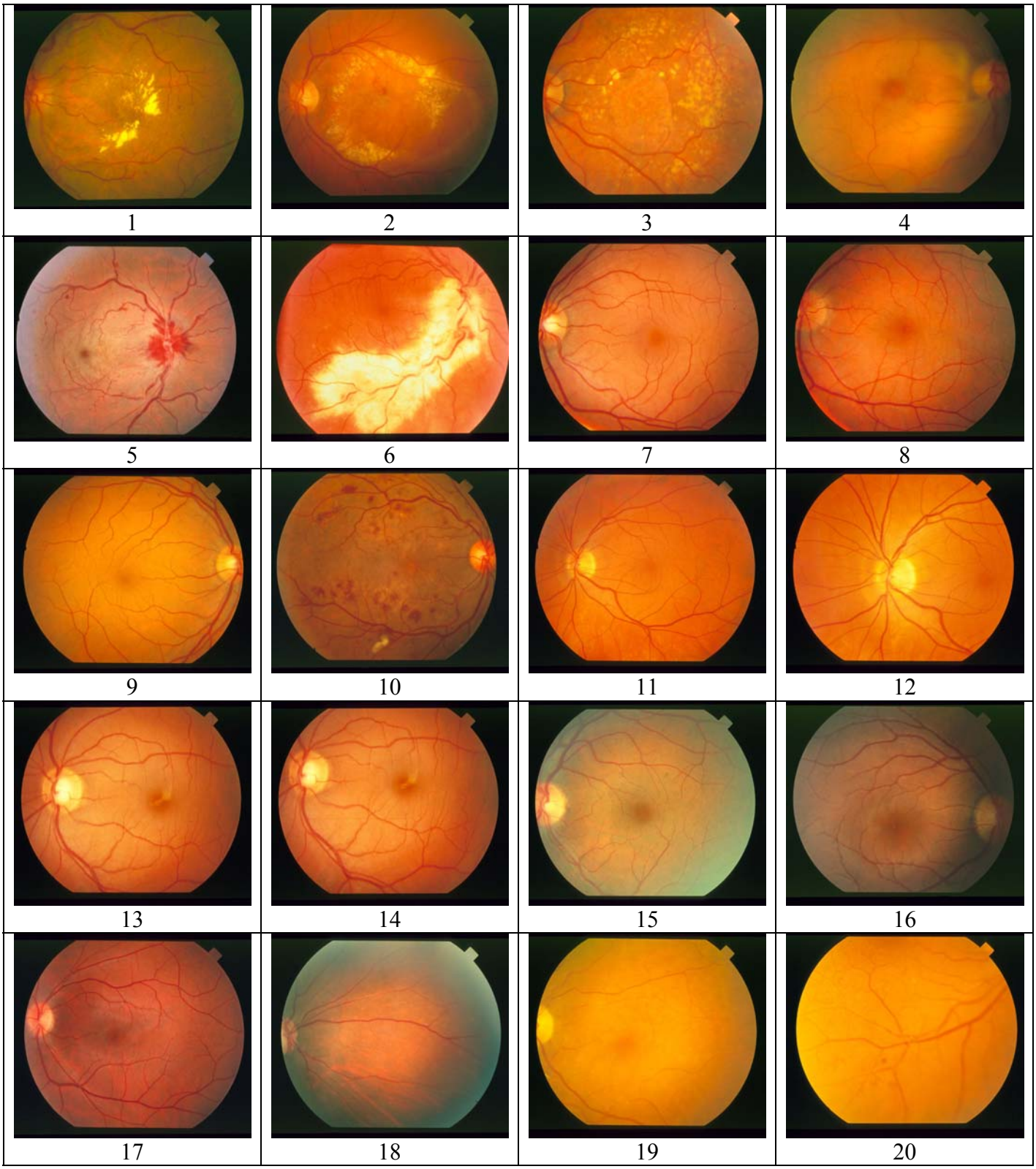

Figure 24 *The 20 original images in the Hoover database.*

All Rights Reserved - Library of University of Jordan - Center of Thesis Deposit

المنارة للاستشارات
www.manaraa.com

Hand Label	GMF	OGMF	GAMF(Filter 1)
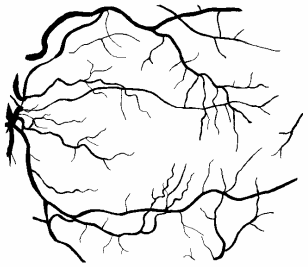 1	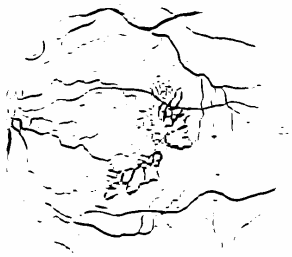	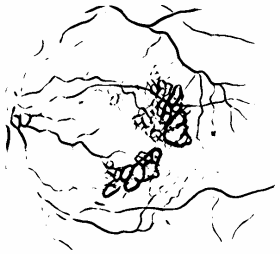	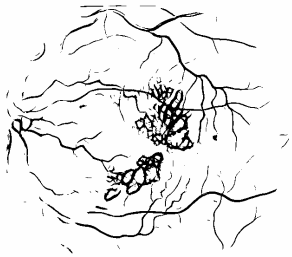
2	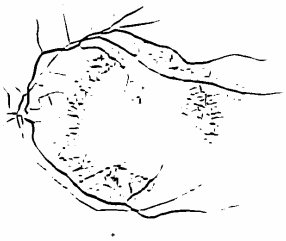		
3		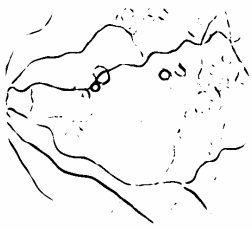	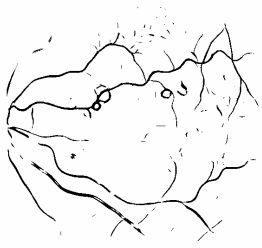
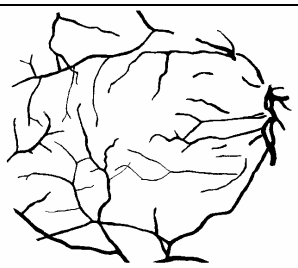 4		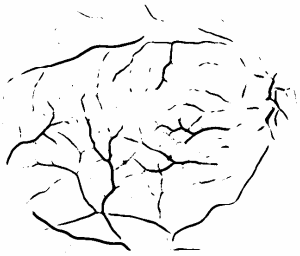	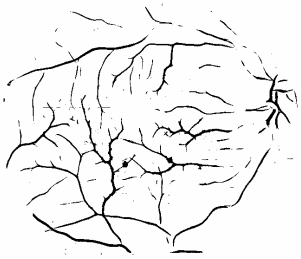
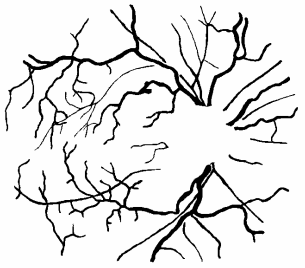 5	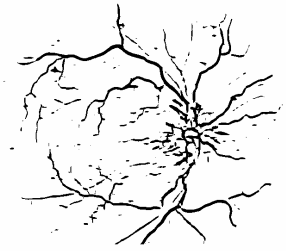		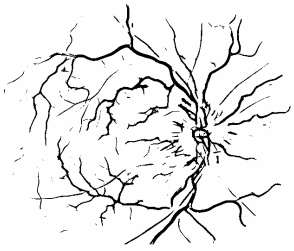

All Rights Reserved - Library of University of Jordan - Center of Thesis Deposit

المنارة للاستشارات
www.manaraa.com

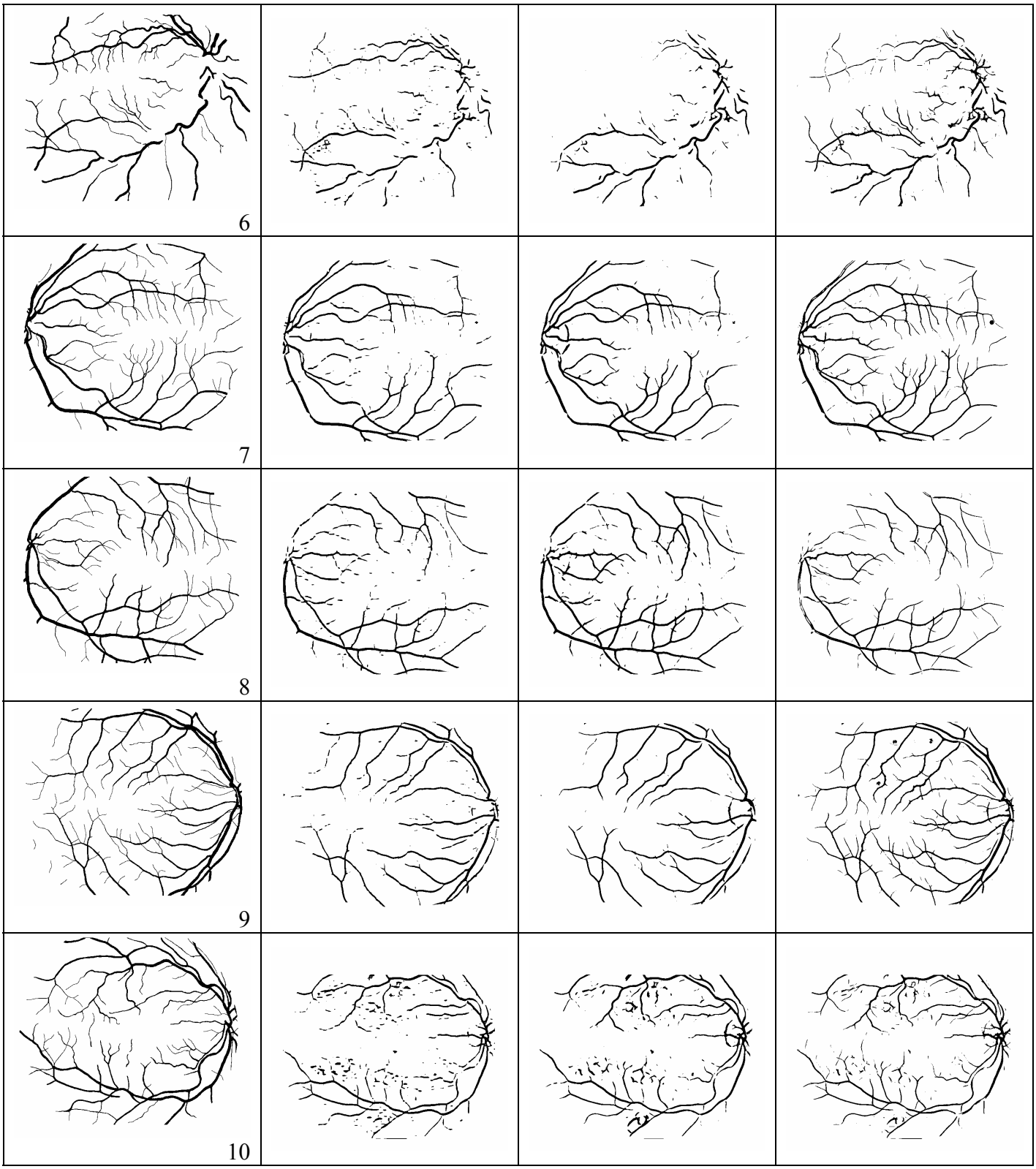

All Rights Reserved - Library of University of Jordan - Center of Thesis Deposit

المنارة للاستشارات
www.manaraa.com

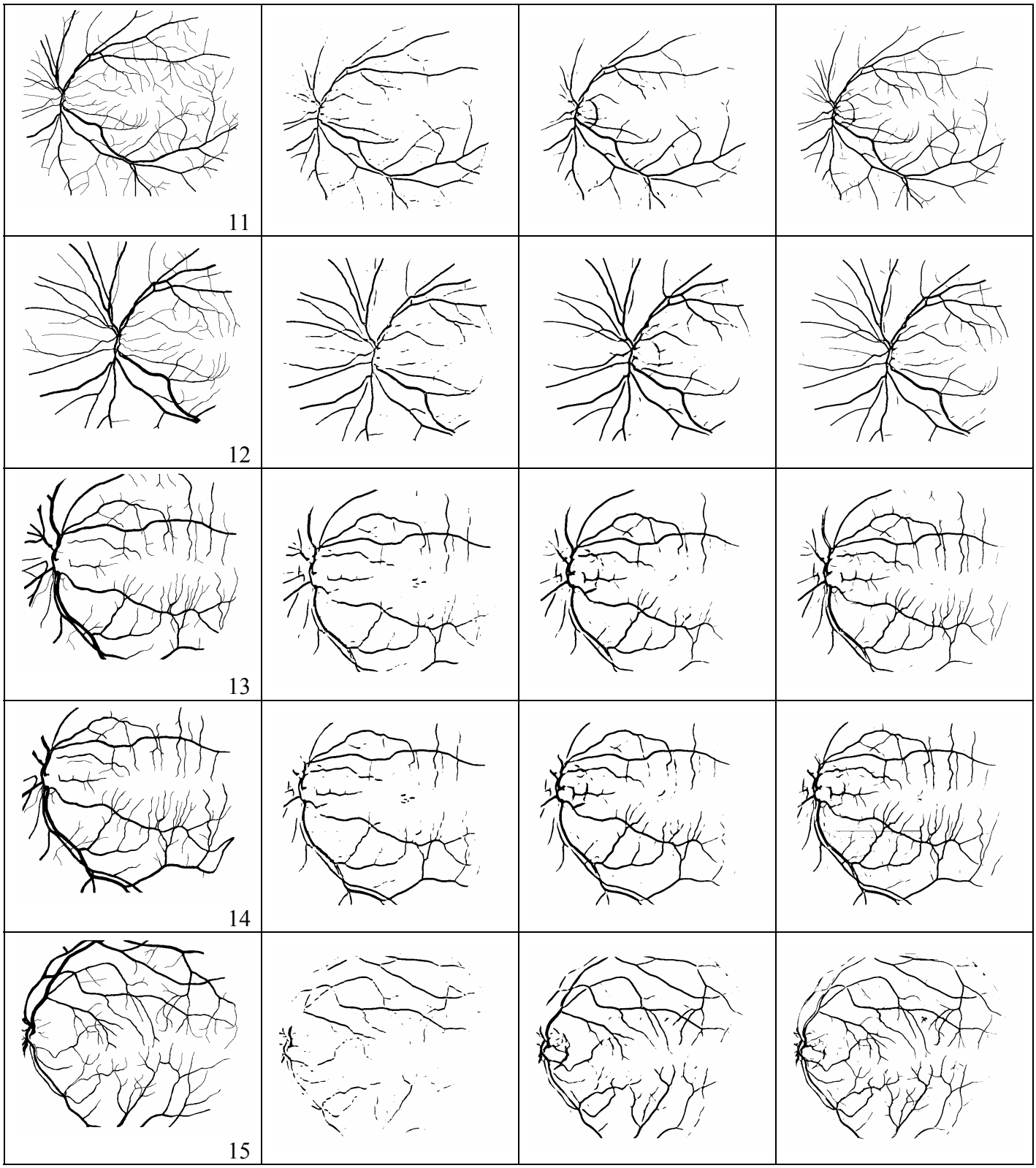

All Rights Reserved - Library of University of Jordan - Center of Thesis Deposit

www.manaraa.com

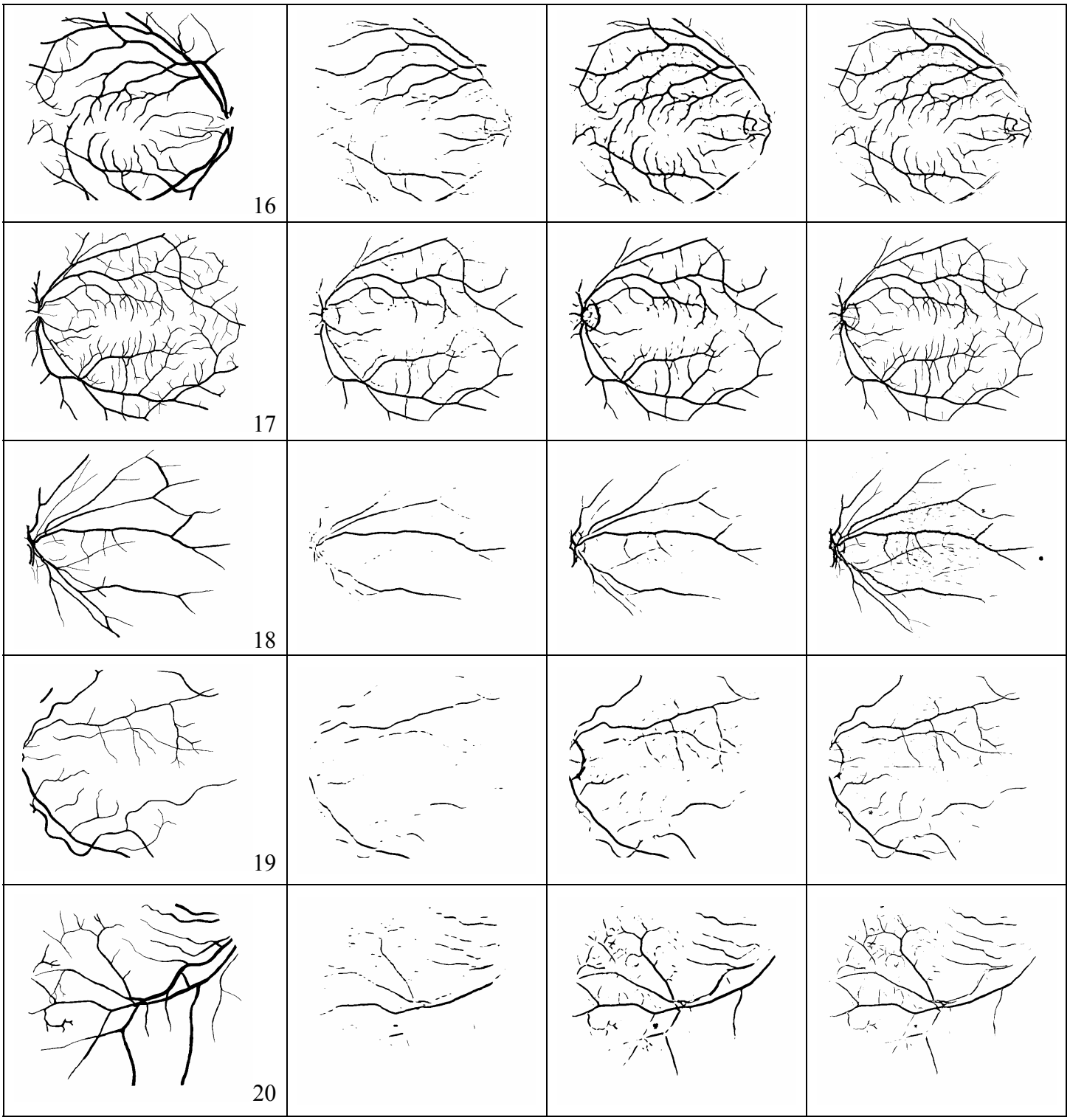

Figure 25 *The First column is the Hand labeled images and the second, third, and fourth columns are the segmented images using GMF, OGMF, and GAMF(Filter 1) respectively where each image is thresholded at the best threshold for the 20 image in the Hoover database.*

All Rights Reserved - Library of University of Jordan - Center of Thesis Deposit

www.manaraa.com

GAMF(Filter 6) at the best threshold	GAMF (Filter 6) at the best average threshold (0.4125)	GAMF(Filter 6) at the best threshold	GAMF (Filter 6) at the best average threshold (0.4125)
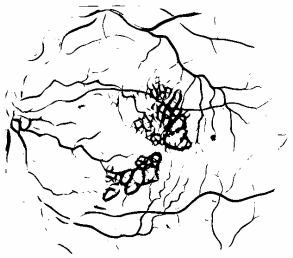 1	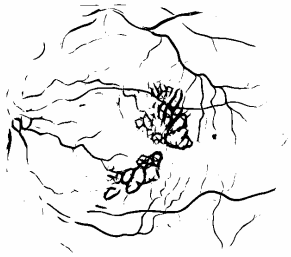 1	6	6
2	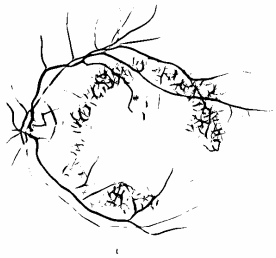 2	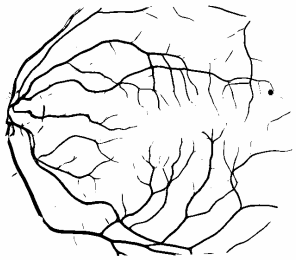 7	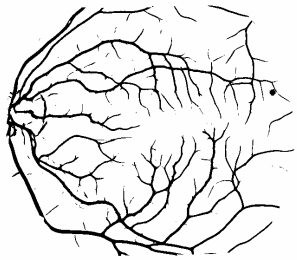 7
3	3	8	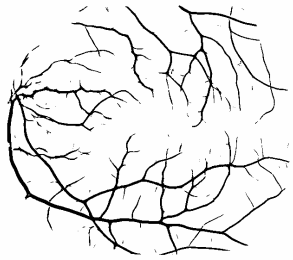 8
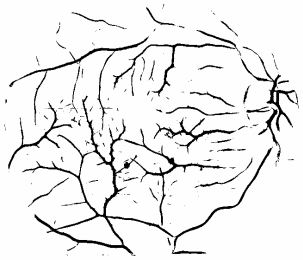 4	4	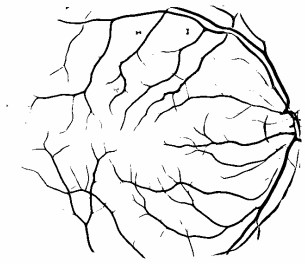 9	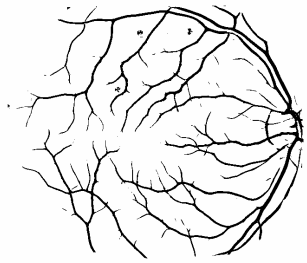 9
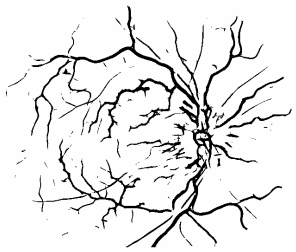 5	5	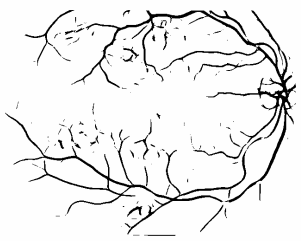 10	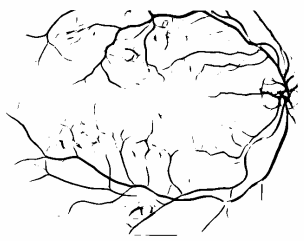 10

All Rights Reserved - Library of University of Jordan - Center of Thesis Deposit

المنارة للاستشارات
www.manaraa.com

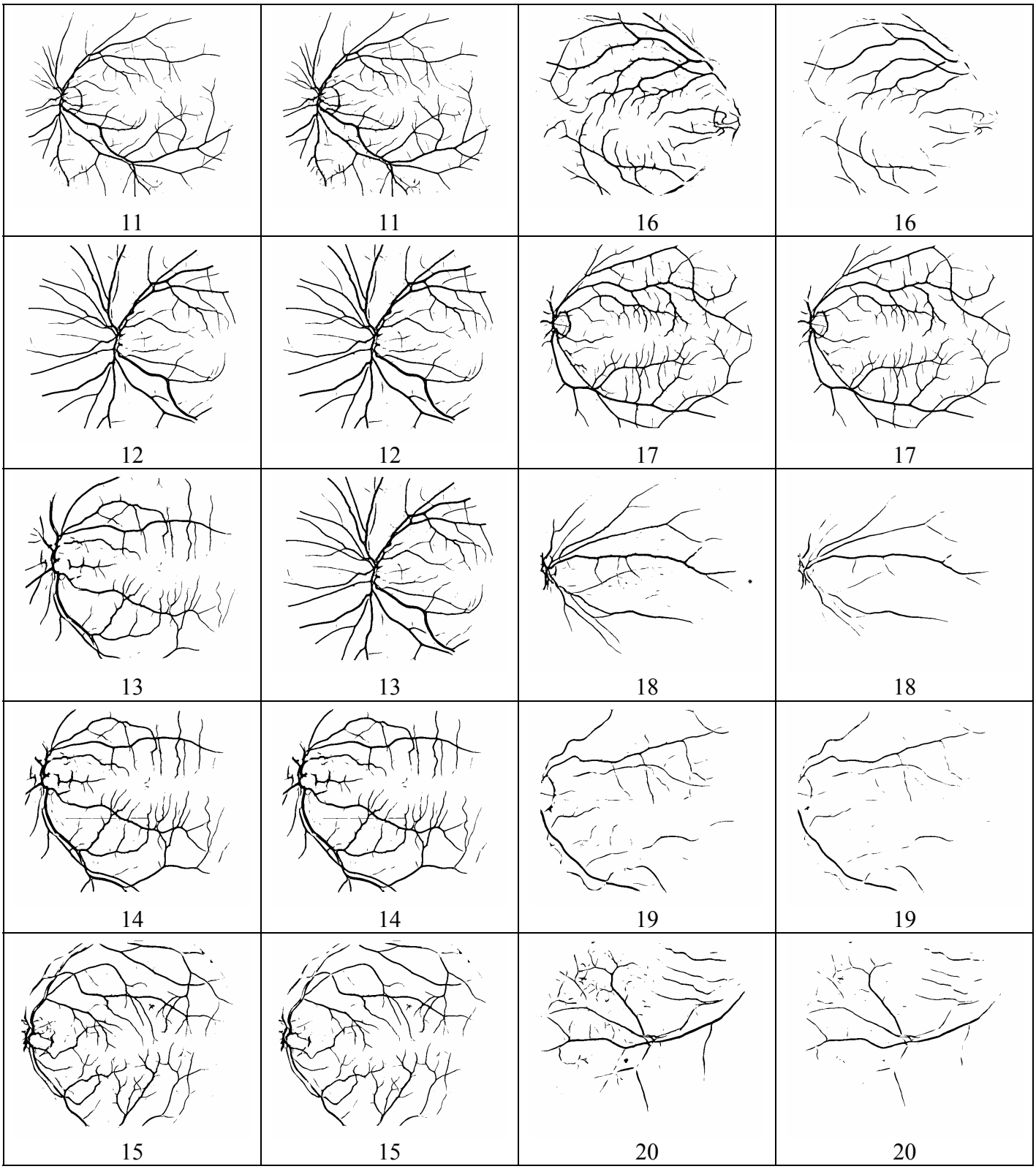

Figure 26 *The first and the third columns are the segmented images by GAMF(Filter 6) at the best thresholds, and the second and fourth columns are the segmented images using GAMF(Filter 6) at the best average threshold (0.4125) for the Hoover database.*

All Rights Reserved - Library of University of Jordan - Center of Thesis Deposit

www.manaraa.com

استخدام الخوارزمية الجينية للحصول على فلتر المطابقة لاستنباط الأوعية الدموية من الصور الرقمية لشبكية العين

إعداد

هدى عبد الرحيم كراجه

المشرف

الدكتور محمد الراوي

ملخص

التشخيص الآلي والتقني لصور شبكية العين أصبح عملية ضرورية و مهمة في طب العيون في عصرنا الحاضر، لذلك فإن هنالك الكثير من الأبحاث والجهود التي قد سعت لتحقيق هذه الغاية. إن استنباط الأوعية الدموية من شبكية العين يعتبر المهمة الأولية في هذا النظام الآلي حيث إن متابعة هذه الأوعية الدموية من حيث التغيرات في أشكالها، كتضيقها أو توسعها أو وجود نمو زائد فيها يساعدنا في تشخيص و متابعة الكثير من أمراض الشبكية. ولذلك فنحن بحاجه إلى طريقة موثوق بها لاستنباط هذه الأوعية الدموية من شبكية العين لكي تعطينا القياسات بدقة عالية.

طبقت كثيراً من الطرق لهذا الهدف في السنوات الأخيرة. فلتر المطابقة هو أكثر الطرق استخداما لهذه الغاية واستخدم من قبل الكثير من الأنظمة الموجودة. ولذلك تطوير استجابته لهذه

All Rights Reserved - Library of University of Jordan - Center of Thesis Deposit

المنارة للاستشارات

www.manaraa.com

العملية هي عملية مرغوب بها. والمشتقة الثانية من فلتر المطابقة هو أيضا يستخدم لاستنباط الأوعية الدموية، وكلاهما يعطي نتائج مختلفة لعملية الاستنباط تبعاً لإختلاف المتغيرات المستخدمة (Parameters).

في هذه الرسالة، تم تحسين فلتر المطابقة و مشتقته الثانية بهدف زيادة دقة الإستنباط لهذه الأوعية. وهذا التحسين قد تحقق بإيجاد متغيرات أفضل (Parameters) من التي استخدمت في السابق. وقد تم التوصل لهذه المتغيرات باستخدام الخوارزمية الجينية، وذلك لأنها تمثل الحل المثالي للمشاكل التي تحتاج إلى تحسين وتطوير بإعتمادها على الاختيار الأمثل للحل من خلال مجال اكبر للبحث. والمساحة تحت المنحنى (Receiver Operating Curve) أو الدقة الأعلى (Maximum Accuracy) يستخدمان كهدف للخوارزمية الجينية التي تسعى لزيادتهما واللذان أيضا يعتبران كمقياس لتقييم فلتر المطابقة المطوّر وذلك بعد إيجاد أفضل متغيرات له.

تعتبر الصورة الأولى من قاعدة البيانات الصورية والتي تسمى ب(DRIVE) كوحدة إدخال للخوارزمية الجينية ومن ثم يفحص فلتر المطابقة و مشتقته الثانية باستخدام المتغيرات الناتجة من الخوارزمية الجينية على قاعدتين من البيانات الصورية هما: DRIVE و Hoover، حيث تستخدم عشرون صورة من قاعدة بيانات DRIVE كمقياس لهذا الفلتر و مشتقته الثانية المطوّرين، وقد حقق هذا الفلتر المطوّر معدل مساحة تحت المنحنى 0.9609 ومعدل أعلى دقة بنسبة 0.943 وتعتبر هذه النتائج أفضل بكثير من التي تحققت باستخدام الفلتر الأصلي بمتغيراته السابقة، ومتقاربة إلى حدٍ ما مع الطرق الأخرى الجيدة لاستنباط الأوعية الدموية آلياً والتي قد تحتاج إلى طرق معقدة على النقيض من فلتر المطابقة.

All Rights Reserved - Library of University of Jordan - Center of Thesis Deposit

المنارة للاستشارات
www.manaraa.com